AD-A113 554 COLORADO UNIV AT BOULDER F/G 20/6
A PROGRAM OF RESEARCH IN RADIATIVE COLLISIONS.(U)
DEC 80 J COOPER N00014-76-C-0611
UNCLASSIFIED CU-153-1120 NL

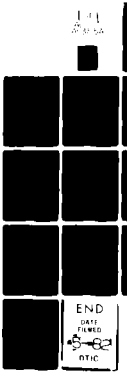

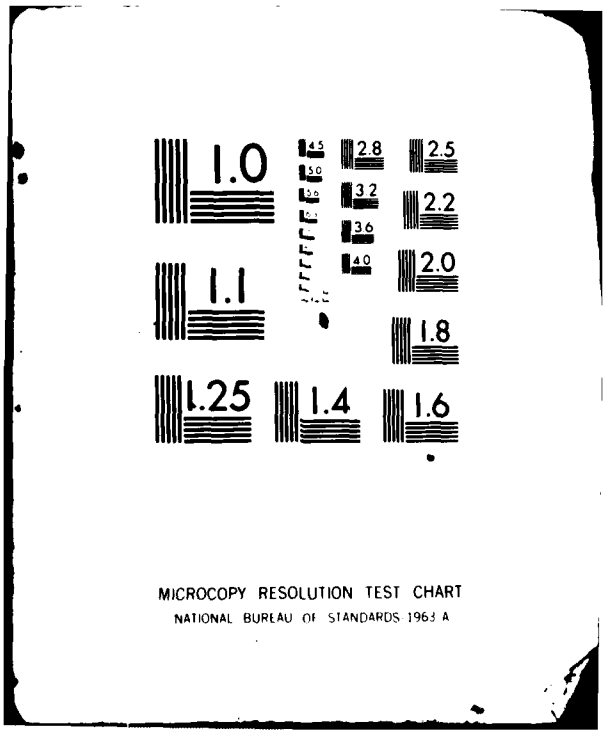
1.0
1.1
1.25
1.4
1.6
1.8
2.0
2.2
2.5
2.8
3.2
3.6
4.0
4.5
5.0
MICROCOPY RESOLUTION TEST CHART
NATIONAL BUREAU OF STANDARDS 1963 A

FINAL REPORT to Office of Naval Research

Contract N00014-76-C-0611 (modification P00003)

A program of research in radiative collisions

(University of Colorado #CU 153-1120)

Report prepared by J. Cooper

This contract covered the period 1 January 1976 through 12 December 1980. The period 1 January 1980 to 12 December 1980 represented a no cost extension.

During 1980, we completed the proposed studies of collisional redistribution in the thallium-argon system. The work included experimental and theoretical studies of both spontaneous and stimulated light scattering by atoms in a collisional environment. The principal work included studying the effects of radiative trapping on the shape of the spontaneous redistribution line profile, and developing and applying a theoretical model[6] to the data previously obtained on stimulated Raman scattering (SRS) and stimulated collision-induced fluorescence (SCF). The major results on Tl-Ar summarized here are discussed in detail in the Ph.D. thesis of M. Raymer.[1]

Previously we had published[5] the first quantitative comparison between a collisional redistribution profile and an emission profile (conventional line broadening study of B. Cheron, R. Scheps, and A. Gallagher, Phys. Rev. A 15, 651 (1977)). For redistribution in thallium we found generally good agreement between the shapes of the profiles obtained by the two experimental methods, but an uncertainty remained as to the absolute scale (or calibration) of our

method. [As indicated at the end of this report, good agreement is to a large extent unique for thallium which has an $S_{1/2}$ upper state. We now know that in general scattered profiles and emission profiles are only the same under quite restrictive circumstances (like angular and polarization averaging).] The uncertainty in absolute scale resulted from the presence of radiative trapping. We observed as our signal photons emitted at 535.0 nm to the $^2P_{3/2}$ level of thallium. Since many ground-state thallium atoms were in the line-of-sight of our detection optics (along the laser beam, in the backward direction), photons which were initially emitted at 377.6 nm could be reabsorbed (trapped) and subsequently emitted at 535.0 nm, thus causing our detected signal at 535.0 nm to be anomalously large. This effect could give rise to at most an increase by a factor of two, since the two resonance lines have nearly equal oscillator strengths. After further experimentation we discovered that optical pumping by the laser caused a significant population in the $^2P_{3/2}$ level, which tended to reduce the detected signal at 535.0 nm by radiative trapping. The competition between these two trapping effects was studied by observing emission in both the backward and side directions, and it was concluded that the two effects largely cancelled each other, and that the good (30%) reported[5] agreement between the redistribution and emission profiles was somewhat fortuitous, though understandable.

In our research on stimulated scattering, we made progress in the analysis of existing data on SRS and SCF. We further developed the theory of stimulated scattering by pulsed laser sources to account for these data. The theoretical work was initiated to explain a discrepancy reported earlier[3] in the SCF turn-on behavior, associated with the transient nature of the excitation. The theoretical model which was developed proved to be capable of explaining several other important aspects of the stimulated scattering,

including argon buffer gas pressure, laser detuning, thallium number density, and laser bandwidth. [Again, details of these studies are described in M. Raymer's thesis.[1]]

During 1980, when the final stages of this contract were being completed, work by the co-principal investigator (K. Burnett, J. Cooper, R. Ballagh and E. W. Smith, Phys. Rev. A 22, 2005 (1980); K. Burnett and J. Cooper, Phys. Rev. A 22, 2027 (1980), and Phys. Rev. A 22, 2044 (1980)) indicated that the analysis of redistribution experiments in terms of absorption (or emission) profiles as performed earlier in this contract (refs. 2 and 5, in particular) can often be erroneous and is at best misleading. Effects of Zeeman-degeneracy mean that the polarization and angular distribution of the scattered radiation is very complicated and the concept of profiles has to be generalized. (This has recently been confirmed experimentally for the Sr-Ar system — P. Thomann, K. Burnett and J. Cooper, Phys. Rev. Lett. 45, 1325 (1980)). Fortunately, for the thallium-argon system the upper state is an $S_{1/2}$ state and isotropic scattering and a unique comparison with the absorption profile is in this case possible (but not for non-S-states!).

Thus, although the major work on Tl-Ar was completed, the final period of the contract was devoted to a further study of Zeeman degeneracy effects (especially for high power lasers following J. Cooper, R. J. Ballagh and K. Burnett, Phys. Rev. A 22, 535 (1980)). The results of this work (see ref. 8) showed that the scattering was a triplet for polarizations parallel to the laser but a doublet for polarizations perpendicular to the laser — not just a triplet as initially supposed.[3]

The ultimate conclusion is that in the future in order to understand radiative collisions, in particular, and the effects of laser interactions with atomic systems, in general, we will need to know much more detail concerning Zeeman degeneracy and specific interatomic interactions.

WORK SUPPORTED BY CONTRACT:

1. M. G. Raymer, Ph.D. Thesis (1979), University of Colorado.

2. J. L. Carlsten, A. Szoke and M. G. Raymer, Phys. Rev. A 15, 1029 (1977).

3. M. G. Raymer and J. L. Carlsten, Phys. Rev. Lett. 39, 1326 (1977).

4. G. Pichler and J. L. Carlsten, J. Phys. B 11, L483 (1978).

5. M. G. Raymer, J. L. Carlsten and G. Pichler, J. Phys. B 12, L119 (1979).

6. M. G. Raymer, J. Mostowski and J. L. Carlsten, Phys. Rev. A 19, 2304 (1979).

7. M. G. Raymer and J. Cooper, Phys. Rev. A 20, 2238 (1979).

8. P. D. Kleiber, K. Burnett, and J. Cooper, Phys. Lett. 84A, 182 (1981).

PHYSICAL REVIEW A VOLUME 15, NUMBER 3 MARCH 1977

Collisional redistribution and saturation of near-resonance scattered light*

J. L. Carlsten, A. Szöke,† and M. G. Raymer‡
Joint Institute for Laboratory Astrophysics, University of Colorado and National Bureau of Standards, Boulder, Colorado 80309
(Received 9 September 1976)

This paper reports on our studies of near-resonant scattering of laser light in a collisional environment. A pulsed dye laser with a peak power of 55 MW/cm² was tuned near the 460.73-nm resonance line of strontium and the side emission was observed from an oven containing both strontium vapor and argon buffer gas. The emission was composed of three spectral components: Rayleigh scattering at the frequency of the laser ω_L, fluorescence at the resonance frequency ω_0 of strontium, and a third component at $2\omega_L-\omega_0$. These three components have been studied as a function of the frequency and intensity of the laser and also as a function of the argon buffer gas pressure. While the Rayleigh emission was found to vary as Δ^{-2} ($\Delta=\omega_0-\omega_L$), the fluorescence component, which was produced by Sr-Ar collisions, was found to be asymmetric with the sign of Δ as predicted by line-broadening theory. By measuring the ratio of the intensities of the fluorescence and Rayleigh components, we were able to measure directly the collisional redistribution function, important in the study of radiative transfer in stellar and planetary atmospheres. At high laser intensities all three components were found to saturate. The results were compared with the theoretical predictions of Mollow's steady-state theory. Theoretical fits for the high-intensity results were obtained when the collisional cross sections were taken to be considerably smaller than in our low-intensity measurements. We believe the discrepancy lies in the use of a steady-state theory for a transient experiment. Effects of radiative trapping and spatial averaging are also discussed.

I. INTRODUCTION

In two previous Letters[1,2] we reported on the first observation of the spectral resolution of light scattered by an atomic vapor near a resonance line, and on the first experimental study of the spectral redistribution of light by collisions as a function of the detuning of the incident light. This paper is a summary and extension of these studies, giving details of the previous measurements and reporting later studies of saturation behavior. Basically, in all of our measurements we illuminate a cell containing Sr vapor (10^{-4}–10^{-1} Torr) and Ar buffer gas (10–500 Torr) with a pulsed, tuneable dye laser whose wavelength is near the 460.73-nm ($^1P_1^\circ-{}^1S_0$) resonance line of Sr, and we analyze the spectrum of scattered light. In this Introduction we would like to put our measurements into perspective by pointing out their relation to other studies.

When a monochromatic light wave impinges on an atom near one of its resonance (absorption) lines, part of the light is scattered. In the absence of collisions and at low intensities, the spectrum of the scattered light is a single line centered on the incident wavelength, known as Rayleigh scattering. If the lower state is the ground state, the scattered light is monochromatic for a stationary atom[3] and Doppler-shifted for a moving atom.[4] If the lower state decays, the spectrum of the scattered light is broadened.[5–8] If the atom that scatters the light collides with other atoms, the scattered light has a second component emitted near the resonance frequency that is known as fluorescence. In a simple-minded description this component is due to the absorption of the incident light in the collision-broadened wing of the absorption line and its subsequent emission near line center. The theory of collisional redistribution has been developed from basic principles (the Kramers-Heisenberg dispersion formula, and collision dynamics) by Omont, Smith, and Cooper[8] and Huber[9] and is applicable in the central, impact region of the spectrum. No explicit theory for redistribution exists outside this region. The knowledge of the spectral and spatial redistribution of light scattered by atoms in the presence of collisions is of fundamental importance in the study of radiation transfer in stellar and planetary atmospheres.[4,10] In fact we found it quite surprising that no direct measurements of the redistribution function had been made earlier.

Low-intensity absorption and emission measurements have been done for many years in atomic vapors broadened by a foreign gas. In fact, both the impact and the quasistatic theories of line broadening[11–13] were developed to deal with these absorption[14] and emission[15] spectra. It is intuitively clear that the "excitation functions" (i.e., the dependence of the intensities of the various spectral components of scattered light on the incident frequency) are related to the absorption and emission spectra. In the impact region this relation can be shown explicitly from the general theory,[8,9] and outside the impact region our experimental results suggest a similar connection.

When the incident light is strong, even for a noncolliding stationary atom and monochromatic incident field, three components appear. This was predicted first by Mollow[16] and studied since theoretically by many[6,7,17-22] who obtained essentially the same results. These components were observed in atomic beam experiments using very narrow cw dye lasers,[23-25] and recent results agree[24] with the theory. In addition to the Rayleigh component mentioned above, there is a "three-photon" component that corresponds to absorption of two incident photons and the emission of another photon (a resonant Raman effect). Conservation of energy then requires the emission of one "fluorescence" photon on resonance. As the intensity is raised, all three components eventually saturate.

Scattering at high light intensity including the effects of collisions has been studied using several theoretical approaches. Mollow[26,27] introduced phenomenological damping terms into his treatment of the collisionless atom scattering in a strong steady-state light field. This procedure is expected to give correct results if the "optical" cross section, which is related to the transition probability per incident photon, is independent of the (strong) incident flux. Another approach, to some extent complementary, was taken by Yakovlenko and co-workers,[28-30] who studied the dynamics of atomic collisions in the presence of a classical (strong) incident field. They show that for weak fields the absorption reduces to the impact or quasistatic limits, implying a constant (in intensity) but frequency-dependent optical cross section. For high intensities they predict a change of the optical cross section. A similar study was done by Kroll and Watson[31] and Lau.[32]

There is yet another point of view of the scattering process that unifies and simplifies many calculations: that of the dressed atom and dressed molecule.[22,33] The dressed atom state is the (adiabatic) eigenstate of the atom in a strong, single-mode external field—in the rotating-wave approximation. Light scattering can be viewed as spontaneous emission causing transitions among the various states.[22,34] The absorption process during collisions can be viewed as a simple transition among these states: the ground state of the absorber before the collision and its excited state with one less photon in the field after the collision. A similar view, put forward originally by Yakovlenko *et al.*[28-30] provides a unified picture of absorption, collision-induced absorption, and radiative ("optically induced", "switching") collisions.[28-30,35,36]

A number of recent experiments indicate the importance of collisional redistribution of light. Rousseau *et al.* have seen two different time dependences in their pulse-excited Raman spectra in iodine.[37-39] Several authors have analyzed this experiment.[34,40-42] Recently Liran[13] found that indeed the shifted (Raman) component follows the laser pulse in time and the fluorescence component decays with the lifetime of the upper state, as predicted.[31,42] Collisional redistribution has been observed in resonance scattering from sodium in high-pressure helium,[41] from sodium in a dense high-temperature plasma,[15] and also from strontium vapor.[16] Collisional redistribution has been studied as an excitation mechanism in cesium–rare-gas mixtures.[17] In two-photon absorption, a "fast" off-resonance component and a "slow" on-resonance component were studied by Grischkowsky.[18] The formation of molecules that occurs during collisional absorption of light has been utilized for spectroscopy by Gallagher[15] and others[19] for many years.

In Sec. II we review the relevant theory as it exists. The experiment is described in Sec. III, and the results are analyzed in Sec. IV. Basically we studied the three emission components as a function of laser frequency, laser intensity and buffer gas pressure. There are also separate sections on our "auxiliary" experiments: studies of radiation trapping, measurements of absorption and emission spectra, and the measurement of the laser spatial profile. Section V presents a brief summary and discussion.

II. THEORY

A. Low laser intensities: collisional regime

Consider an atom and an incident monochromatic laser field, which, at the position of the atom, is

$$\vec{E}(t) = \hat{\epsilon}_L E \cos(\omega_L t), \tag{1}$$

where $\hat{\epsilon}_L$ is the polarization vector, ω_L is the incident frequency, and E is the electric field amplitude. The incident intensity of the laser in units of photons $cm^{-2}\,sec^{-1}$ is

$$I_L = cE^2/8\pi\hbar\omega_L. \tag{2}$$

The incident light frequency ω_L is taken to be near the atomic resonance frequency ω_0, and the detuning Δ is defined by

$$\Delta = \omega_0 - \omega_L. \tag{3}$$

We now define the Rabi frequency on resonance:

$$\Omega = dE/\hbar, \tag{4}$$

where $d = e\langle 1|\hat{\epsilon}_L \cdot \vec{r}|2\rangle$ is the electric dipole matrix element between the two relevant atomic states. Thus the laser intensity is proportional to the square of the Rabi frequency, $I_L \propto \Omega^2$. We make

the unrealistic assumption that both states are nondegenerate. When a $^1S_0$ state is coupled by linear polarized radiation to a $^1P_1^0$ state (as in our studies) this is a good approximation in the absence of collisions. In presence of collisions the picture has to be modified.[50] We also assume that the lower of these states $|1\rangle$ is the ground state, and the upper state $|2\rangle$ has a total damping rate γ (half width at half maximum) given by

$$\gamma = \gamma_N + \gamma_E + \gamma_I . \tag{5}$$

The unit of γ is rad/sec. The rate γ_N is due to the natural radiative decay of the excited state, while γ_E and γ_I result from elastic and inelastic collisions, respectively.

These damping processes are shown schematically in Fig. 1. The driving laser field is represented by the solid lines, spontaneous decay by the wavy line, and collisions by double lines. Elastic collisions are usually viewed as collisions which interrupt the phase of the emitted wave train. However, in the context of our work an elastic event can also be considered as a collision which transfers populations from the laser-excited virtual level to the real level. In this sense these events are actually "quasielastic" since the collisions must provide or absorb the energy difference $\hbar\Delta$. In contrast to this, inelastic collisions (quenching collisions) are those events which cause a net population transfer from the excited state to the ground state in a two-level system or to nearby levels in a multilevel system.

The theory has been worked out in detail for the impact region of the spectrum.[8,9,40,41] The impact theory is valid only for pressures low enough that the duration of the collision is small compared to the time between collisions. In addition, it is applicable only for the frequency region close to line center. Mihalas[4] has shown that the boundary frequency Δ_s, beyond which the impact approximation fails, is given (for a Van der Waals interaction) by

$$\Delta_s \approx 1.65 v^{3/2} N_p^{1/2} \gamma_E^{1/2} , \tag{6}$$

where N_p is the density of the perturbers (in our case the argon atoms), γ_E is the half width at half maximum (HWHM) of the broadening due to elastic collisions, and v is the mean relative velocity of the emitting and perturbing atoms. The collisional linewidth is usually determined by experiment, or by specific theoretical calculations. For example, in Van der Waals broadening[4]

$$\gamma_E = N_p \sigma_E v , \tag{7}$$

where

$$\sigma_E = 4.04 (C_6/v)^{2/5} . \tag{8}$$

Here C_6 is the Van der Waals interaction constant.

Inside the impact region, for stationary atoms excited from their ground state by weak monochromatic light, the intensity distribution of the scattered light integrated over all angles and summed over polarizations, in steady state, in units of photons cm^{-3} sec^{-1} is given by Huber's Eq. (4.8),[9]

$$I(\omega)\, d\omega = \left(\frac{\omega}{\omega_0}\right)^3 N \frac{(\gamma_N/2)\Omega^2\, d\omega}{\Delta^2 + \gamma^2} \times \left[\delta(\omega - \omega_L) + \frac{\gamma_E}{\gamma_E + \gamma_I} \frac{\gamma/\pi}{(\omega_0 - \omega)^2 + \gamma^2}\right] , \tag{9}$$

where N is the density of scatterers (in our case the strontium atoms), and the symbols are defined above.

The first term in this equation, which occurs at the incident frequency ω_L, is known as Rayleigh scattering and corresponds to the process shown in Fig. 2(b). The incident light is elastically scattered off a virtual state produced by the laser (shown as a broken line). Since the ground state has no natural width, the Rayleigh scattering has the same spectral profile as the excitation source.

The second term in Eq. (9) is the collision-induced fluorescence and corresponds to the process shown in Fig. 2(d). The laser-induced virtual state is collisionally transferred to the real excited state which then fluoresces with a Lorentzian profile centered at ω_0 and has a width equal to the sum of the natural and collisional widths. In the absence of collisions, the fluorescence vanishes and the scattered light maintains the profile of

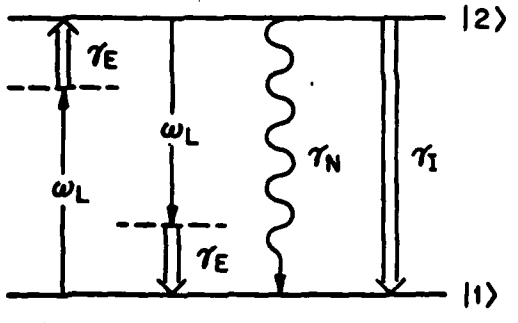

FIG. 1. Two-level atom with driving frequencies and damping rates. The straight arrows represent the laser field at frequency ω_L, while the wavy arrow represents radiation damping of the upper level at the spontaneous rate γ_N. The double arrows represent collisional damping: elastic collisions take the atom from the virtual level (dashed line) to the real level at a rate γ_E, while inelastic (quenching) collisions take the atom from level $|2\rangle$ to level $|1\rangle$ at a rate γ_I.

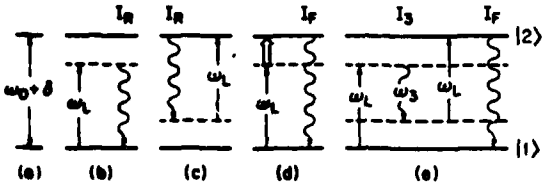

FIG. 2. (a) Two atomic levels separated by the unperturbed resonant frequency ω_0 plus the laser-induced Stark shift δ; (b) Rayleigh scattering from the ground state at the laser frequency ω_L; (c) Rayleigh scattering from the excited state; (d) collision-induced fluorescence at $\omega_0+\delta$; (e) "three-photon" scattering at $\omega_3=2\omega_L-(\omega_0+\delta)$ and consequent fluorescence at $\omega_0+\delta$.

the incident light, even if the excitation source is narrower than and tuned inside the natural width of the resonance line.[3,51]

In an atom whose upper and lower levels have spatial degeneracy, the angular distribution of the radiation and its polarization properties are complicated (cf. Omont *et al.*[8]). In our experiments the lower level is a $^1S_0$ state, and the upper one is $^1P_1$; therefore, the Rayleigh scattering has a classical dipole distribution, but the resonance fluorescence distribution depends on the details of the depolarization due to collisions.[50] In our experiment this is further complicated by the fact that our sample is optically thick on resonance; therefore the light that reaches our detector is multiply scattered. We have not studied these depolarization effects.

When the laser is tuned far off resonance, $|\Delta| \gg \gamma$, the two components can be resolved and the spectrally integrated intensities of the Rayleigh scattering I_R and collisionally induced fluorescence I_F are

$$I_R = N\left(\frac{\omega_L}{\omega_0}\right)^3 \frac{(\gamma_N/2)\Omega^2}{\Delta^2}, \tag{10}$$

$$I_F = N\left(\frac{\gamma_E}{\gamma_N+\gamma_I}\right)\frac{(\gamma_N/2)\Omega^2}{\Delta^2}. \tag{11}$$

Thus in the impact region, the integrated intensities of both the Rayleigh scattering and fluorescence behave as Δ^{-2}.

Note that Eq. (11) predicts that the integrated fluorescence signal I_F should be linear in laser intensity and also linear in the density of perturbers N_p ($\gamma_E \propto N_p$). However, the linearity holds only at low laser intensity and low pressure. In Sec. IV we will see that at higher laser intensity or at high pressure, saturation occurs.

As $|\Delta|$ becomes larger than Δ_c, the impact approximation fails. Theories for the redistribution function outside the impact region have not been conveniently developed. (Huber[9] has written down the integrals in terms of the time development operator, but they have not been solved.) However, since for $|\Delta| \gg \gamma$, collisions of the scattering atom do not change the Rayleigh intensity, we expect Eq. (10) to hold outside the impact region. Indeed far from line center, it goes over to the well-known Rayleigh scattering formula.[52]

While collisions do not affect the Rayleigh intensity far from resonance, the fluorescence component depends heavily on the collision dynamics. Basically it depends on the ability of the collisions to supply (or absorb) the energy difference between the laser photon and the scattered photon. Indeed, far from resonance, the collision can no longer provide this energy difference efficiently and the cross section is expected to drop off.[12] Even before the fall-off, non-Lorentzian shapes similar to those seen in emission and absorption experiments are expected. Accordingly, we will replace γ_E in Eq. (11) by the "empirical" elastic collision rate $\gamma_E(\Delta)$, which is a function of the detuning and will be indicative of a non-Lorentzian line shape. The cross section in Eq. (7) also becomes a function of detuning, denoted by $\sigma_E(\Delta)$.

Lisitsa and Yakovlenko[30] have shown the connection between $\sigma_E(\Delta)$ and the static theory of line broadening. It should be emphasized that the optical cross section $\sigma_E(\Delta)$ is not a cross section in the usual sense (although it does have dimensions of cm^2). The actual rate of production of excited atoms is described by the quantity $\sigma_E(\Delta)\Omega^2/\Delta^2$. Therefore it is proportional to the incident laser flux in dimensionless units.

B. High laser intensity; collisionless regime

We now discuss the distribution of scattered light when the laser intensity is allowed to become large, but when no collisions are present and Doppler broadening has been neglected. Recently there has been considerable theoretical interest in the spectrum of scattered light at high incident intensities.[6,7,16-22] When $\Omega^2+\Delta^2 \gg \gamma_N^2$, the intensity (photons cm^{-3} sec^{-1}) in steady state for monochromatic incident light is given by Mollow[16] as

$$I(\omega)\,d\omega = \frac{N(\gamma_N/2)\Omega^2\,d\omega}{\Delta^2+\Omega^2/2}\left[\frac{\Delta^2+\gamma_N^2}{\Delta^2+\Omega^2/2}\,\delta(\omega-\omega_L) + \frac{\Omega^4/4}{(\Delta^2+\Omega^2)(\Delta^2+\Omega^2/2)}\left(\frac{s/\pi}{(\omega-\omega_L)^2+s^2}\right)\right.$$
$$\left. + \frac{\Omega^2/4}{(\Delta^2+\Omega^2)}\left(\frac{\xi/\pi}{[\omega-\omega_L+(\Delta+\delta)]^2+\xi^2} + \frac{\xi/\pi}{[\omega-\omega_L-(\Delta+\delta)]^2+\xi^2}\right)\right], \tag{12}$$

where the widths of the Lorentzian emission profiles are given by

$$s=\gamma_N\left(\frac{\Omega^2+2\Delta^2}{\Omega^2+\Delta^2}\right),\quad \xi=\gamma_N\left(\frac{\frac{3}{2}\Omega^2+\Delta^2}{\Omega^2+\Delta^2}\right), \tag{13}$$

and the other terms are defined in Sec. II A with the exception of δ which is the ac Stark shift given by

$$\delta=\Delta\{[1+(\Omega/\Delta)^2]^{1/2}-1\}. \tag{14}$$

Note that at low intensities the shift becomes

$$\delta=\tfrac{1}{2}\Omega^2/\Delta\quad(\Omega\ll|\Delta|), \tag{15}$$

which is the well-known result derived from second-order perturbation theory.[53]

There are four components in the emission spectrum given by Eq. (12). The first two terms are centered at the frequency of the incident laser. These terms are identified as the coherent and incoherent parts of the Rayleigh scattering, respectively, and are shown at ω_L in Fig. 3. The incoherent Rayleigh component is unimportant at low intensities but becomes dominant at high laser intensities. The third and fourth terms are centered at $\omega=\omega_L-(\Delta+\delta)$ and $\omega=\omega_L+(\Delta+\delta)$. These "side bands," which have recently been observed experimentally by a number of researchers,[1,23-25] are due to higher-order photon interactions. The process leading to these side bands is depicted in Fig. 2(e). With the laser tuned to $\omega_L\neq\omega_0$, two laser photons are absorbed, a photon is emitted and an excited state produced. This "three-photon" component is given by the third term and is shown as the profile at ω_3 in Fig. 3. Since an excited state is produced for every photon generated at ω_3, there will also be emission at $\omega_0+\delta$ from the excited atom. This is the origin of the other side band which is shown as the *broken* profile at ω_0 in Fig. 3. Thus the two side bands have equal intensities. When the excitation laser is tuned to resonance, these two peaks occur as side bands located at $\omega_L+\Omega$ and $\omega_L-\Omega$. Therefore when the laser is tuned to resonance, one sees the Rayleigh emission at ω_L with two side bands each shifted by the Rabi frequency from the resonance. At this point it is useful to think of the side bands as resulting from the modulation of the resonance frequency ω_0 by the Rabi frequency Ω.[22]

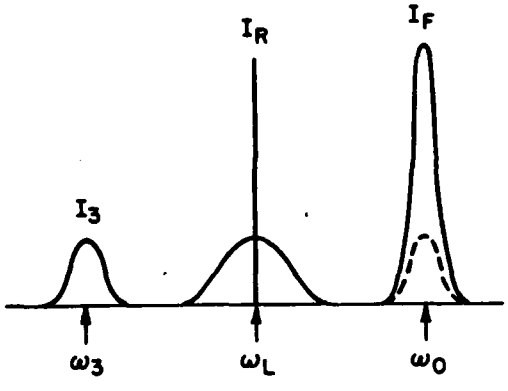

FIG. 3. Sketch of the emission spectrum of a two-level atom strongly driven near resonance by a monochromatic excitation source at frequency ω_L. In the presence of collisions, the spectrum consists of the four components shown by solid lines: coherent (narrow) and incoherent (broad) Rayleigh scattering at ω_L, "three-photon" emission at ω_3 and resonance fluorescence at ω_0 produced by both elastic collisions and the "three-photon" process. In the absence of collisions the fluorescence (broken line) has the same magnitude as the component at ω_3.

Having discussed the higher-order photon interactions, we can now understand the dependence of the two Rayleigh components on laser intensity. The coherent Rayleigh scattering, linear in laser intensity, is scattering off the ground state by a single laser photon. The incoherent Rayleigh scattering, cubic in laser intensity, indicates the following process: Two laser photons are absorbed to give an excited state as in Fig. 2(e) which Rayleigh scatters a third laser photon as in Fig. 2(c). As the excited state has a width, this gives rise to the width s of the incoherent Rayleigh scattering.[22,54]

When $\Omega^2+\Delta^2\gg\gamma_N^2$ the side bands can be resolved from the central Rayleigh scattering and Eq. (12) can be integrated over ω, giving the integrated Rayleigh intensity I_R (the sum of the coherent and incoherent components) and the integrated side bands I_3 and I_F, due to the "three-photon" scattering and the subsequent fluorescence, where

$$I_R=N\frac{(\gamma_N/2)\Omega^2}{\Delta^2+\Omega^2} \tag{16}$$

and

$$I_3=I_F=N\frac{(\gamma_N/8)\Omega^4}{(\Delta^2+\Omega^2)(\Delta^2+\Omega^2/2)}. \tag{17}$$

As before, the Rayleigh scattering can be viewed as emission from the laser-excited virtual level. At low intensities when the excited state population is small, we can associate a population $(N/2)[\Omega^2/(\Delta^2+\Omega^2)]$ with this virtual level. If we let this "state" radiate at a rate γ_N, we obtain Eq. (16). An analogous argument can be made at higher laser intensities by including scattering off the excited state.

Equation (16) predicts that at high intensities the Rayleigh intensity I_R will saturate. This process can be viewed as an equalization of the population in the virtual and real states. It is a manifestation of the limitation on the spontaneous scatter-

ing intensity by the coupling constant to the vacuum, γ_N.

Equation (17) shows that at low intensities, the "three-photon" scattering and resulting fluorescence are proportional to the square of the laser intensity. At higher intensities, these components also saturate due to population equalization of the ground and excited states. Note that since the three-photon process corresponds to the generation of a photon and an excited atom, the process is a type of Raman scattering and therefore will have positive gain for a noninverted system. Stimulated emission of the component at ω_3 has been predicted[55-59] and observed.[60-63] Also, the emission of I_3 and I_F, the absorption of two laser photons and the return of the atoms to the ground state is a four-photon parametric process that has been discussed in the literature.[64]

C. High laser intensity: collisional regime

In this section, we consider the effects of high laser intensities when collisions are also present. A number of papers have treated collisions through phenomenological relaxation terms, extending the treatment of the collisionless atom interacting with radiation.[26,27,34,42,65] In all these treatments it was assumed that a strong incident electromagnetic field has no direct influence on the rate of collisions, γ_E; the main effect is to saturate the fraction of virtual levels and the population difference in the two-level system. Recently, collisions of atoms in the presence of the incident field were treated more accurately, and it has been pointed out that when the fields get strong they can directly influence the collision rates.[28-32] However the emission spectrum was not explicitly computed. Therefore we have chosen to treat the relaxation constant γ_E in Mollow's treatment[26,27] as a free parameter.

Since we are primarily concerned with scattering at optical frequencies, the major collisional effect is due to elastic collisions. Inelastic collisions also have to be considered but are generally less frequent as they require large momentum transfers. At optical frequencies inelastic collisions that transfer the atom from the ground state to the excited state are usually negligible, since $\hbar\omega_0/kT$ is large.

We quote the results of Mollow's calculation,[26,27] in which he added phenomenological relaxation terms to the equations of a strongly driven two-level system. The use of phenomenological relaxation terms gives rise to Lorentzian line shapes and is therefore only applicable in the impact region of the spectrum [cf. Eq. (6)]. When $\Omega^2+\Delta^2 \gg \gamma^2$, the scattered spectrum (in photons cm^{-3} sec^{-1}) in steady state is

$$I(\omega)\,d\omega = \frac{N(\gamma_N/2)\Omega^2\,d\omega}{\Delta^2+\eta\Omega^2}\left[\frac{\Delta^2+\gamma^2}{\Delta^2+\eta\Omega^2}\delta(\omega-\omega_L)+\frac{\Omega^2[(2\eta-1)\Delta^2+\eta^2\Omega^2]}{(\Delta^2+\Omega^2)(\Delta^2+\eta\Omega^2)}\left(\frac{s_1/\pi}{(\omega-\omega_L)^2+s_1^2}\right)\right.$$
$$+\frac{1}{2}\frac{(\Omega'-\Delta)[\eta(\Omega'-\Delta)+\Delta]}{(\Delta^2+\Omega^2)}\left(\frac{\xi_1/\pi}{(\omega-\omega_L+\Omega')^2+\xi_1^2}\right)$$
$$\left.+\frac{1}{2}\frac{(\Omega'+\Delta)[\eta(\Omega'+\Delta)-\Delta]}{(\Delta^2+\Omega^2)}\left(\frac{\xi_1/\pi}{(\omega-\omega_L-\Omega')^2+\xi_1^2}\right)\right], \tag{18}$$

where the parameter η is defined as

$$\eta=(\gamma_N+\gamma_I+\gamma_E)/(2\gamma_N+2\gamma_I). \tag{19}$$

The detuning parameter is defined as

$$\Omega'=\Delta+\delta, \tag{20}$$

and the widths of the profiles are

$$s_1=(\gamma_N+\gamma_I)\left(\frac{2\eta\Omega^2+2\Delta^2}{\Omega^2+\Delta^2}\right),$$
$$\xi_1=(\gamma_N+\gamma_I)\left(\frac{(1+\eta)\Omega^2+2\eta\Delta^2}{\Omega^2+\Delta^2}\right). \tag{21}$$

The four terms in Eq. (18) are analogous to the terms given in Eq. (12) for the collisionless case. Therefore we will refer to these terms as coherent Rayleigh scattering, incoherent Rayleigh scattering, "three-photon" scattering, and fluorescence, respectively. One effect of the collisions is to increase the widths of the Lorentzian profiles. However, the intensities of the various components are also affected. The largest change occurs in the fluorescence which can now occur both by the three-photon process and by direct collisional transfer from the laser excited virtual level. Thus it is always larger than the three-photon component, as shown in Fig. 3.

We can now see from Eq. (18) that the condition of "weak excitation" can be precisely stated as

$$\eta\Omega^2 \ll \Delta^2. \tag{22}$$

When the laser is "weak" and the collision rates are low, the spectrum given by Eq. (18) reduces to the low intensity limit given by Eq. (9). When $\Omega^2+\Delta^2 \gg \gamma^2$, the components can be resolved and the integrated Rayleigh intensity I_R is again given by Eq. (16). While the collisions affect the coherent and incoherent Rayleigh intensities separately, the sum I_R is unaffected because Rayleigh scat-

tering can occur off ground or excited states; thus collisions do not affect the number of scattering centers. The integrated side bands I_3 and I_F are given by

$$I_3 = \frac{N(\gamma_N/4)\Omega^2(\Omega'-\Delta)[\eta(\Omega'-\Delta)+\Delta]}{(\Delta^2+\Omega^2)(\Delta^2+\eta\Omega^2)}, \quad (23)$$

$$I_F = \frac{N(\gamma_N/4)\Omega^2(\Omega'+\Delta)[\eta(\Omega'+\Delta)-\Delta]}{(\Delta^2+\Omega^2)(\Delta^2+\eta\Omega^2)}. \quad (24)$$

When η depends on the detuning, as will be the case outside the impact regime, the theory has not been worked out. We expect that the integrated intensities will be given by Eqs. (23) and (24), but that the line shape will not be Lorentzian. In fact, we expect that as long as the strong laser intensity has no direct influence on the collision rate, $\eta(\Delta)$ can be obtained from low-intensity measurements of $\sigma_E(\Delta)$.

It should be noted that a simple theory,[31] using dressed states gives all the results for integrated intensities correctly and also is valid in the transient regime.

III. EXPERIMENTAL APPARATUS

The strontium resonance line ($5s5p\ ^1P_1^o$-$5s^2\ ^1S_0$) is located at 460.73 nm (21 698.482 cm^{-1}). The oscillator strength of this transition is $f=1.94$ corresponding to a radiative lifetime of 4.68 nsec.[66] Since strontium is predominantly an even-even nucleus (93%), there is no hyperfine structure. Therefore, in the absence of collisions, this system will respond to a linearly polarized laser beam as a two-level system.

A nitrogen-laser-pumped dye laser was tuned near this 460.73-nm resonance line as shown in Fig. 4 and focused into an oven containing strontium vapor and argon buffer gas. A schematic of the experimental apparatus is shown in Fig. 5. The oven was generally run with a buffer gas pressure of 10–500 Torr and in a temperature range of 400–500 °C. At 500 °C the vapor pressure of strontium is ~8×10^{-3} Torr and the Doppler width (half width at e^{-1} height) of the 460.73-nm resonance line is 2.8×10^{-2} cm^{-1} (5.9×10^{-4} nm). The side emission from the excited region in the oven was spectrally analyzed. Details of the apparatus are discussed below.

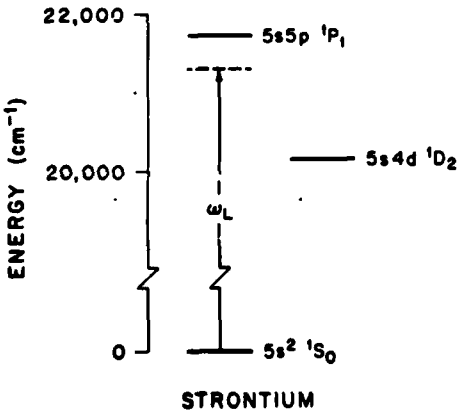

FIG. 4. Simplified energy levels for Sr. The laser, with frequency ω_L, is tuned near the $5s^2\ ^1S_0 - 5s5p\ ^1P_1$ resonance line located at 21 698.482 cm^{-1} (460.73 nm).

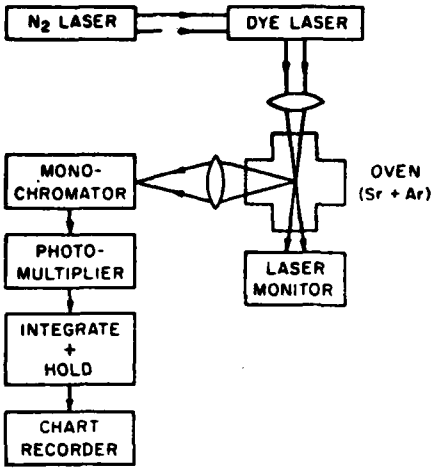

FIG. 5. Schematic diagram of experimental apparatus.

A. Dye laser

The dye laser was pumped by a modified version of an N_2 laser described by Woodward *et al.*[67] in the standard transverse pumping arrangement with a ×10 beam expander and an Echelle grating (316 lines/mm). The N_2 laser output was focused into the dye cell with a simple quartz lens (18 cm focal length). The dye cell was a variation of a basic design by Drullinger[68] and consisted of a stainless-steel block fitted with a quartz entrance window and two 30′ wedged side windows which were canted at 5° to prevent multiple reflections. All three windows were sealed to the stainless cell with Teflon O rings. The dye was flowed through the cell with a system containing parts made of stainless steel, Teflon, and polyethylene and including a Millipore filter. The output of the dye laser was almost totally linearly polarized with a linewidth of 1.4 cm^{-1} (0.03 nm) and a half-angle beam divergence of 1 mrad. The laser had a 5 nsec pulse length and an energy of ~0.2 mJ at the oven entrance. The dye laser beam was focused into the oven with a ×5 beam contractor.

B. Oven

The vapor cell oven was made from 2-in.-diam stainless-steel tubing in the shape of a cross with 20-cm legs and with asbestos-insulated nichrome heater wire wound around the legs. Each leg of the cross was fitted with a window. Thermocouples and a temperature controller were used to maintain the temperature to within ±2 °C. The strontium was held in a stainless-steel boat with 5 mm holes in each end to allow passage of the laser and 3 × 10 mm slits in the sides to allow the side emission to be studied. Since we were looking at Rayleigh emission with the same frequency as the laser, spurious scatter had to be carefully avoided. To facilitate this, the windows through which the laser passed were set at an angle to avoid back reflections. To protect the windows in the oven, water cooling coils were attached to the stainless cross near the windows. In addition, a buffer gas of Ar of at least 10 Torr kept the windows from being coated with Sr.

C. Detection system

The side emission was studied with an $f/10$ detection system. By using a periscope the excitation region, which was approximately a cylinder of 110 μm diameter, was imaged parallel onto the slit of a 0.3-m McPherson model 218 monochromator using two camera lenses. By scanning one of the lenses in the detection optics, we measured the spatial profile of the Rayleigh scattering at low intensities. Using this profile, we estimated the peak power of the laser at the center of the excitation region to be 55 MW/cm². The resolution of the monochromator was 0.03 or 0.06 nm depending on the grating installed. The output of the RCA 7326, S-20 photomultiplier, which was placed at the exit of the monochromator, was fed into a gated (10 μsec) analog integrate-and-hold circuit and recorded on a chart recorder with a 1.5-sec time constant. The monochromator measured the wavelength to a resettable accuracy of 0.01 nm.

IV. EXPERIMENTAL STUDIES

When the dye laser was tuned near the $^1P_1^0$-$^1S_0$ resonance transition at 460.73 nm, three components were observed in the side emission as predicted by the theoretical discussion of Sec. II. Figure 6 shows the spectral distribution of the side emission for two different laser intensities with the laser tuned to 460.56 nm ($\Delta = -8.0$ cm^{-1}), the blue side of the resonance. The central component, which occurs at the excitation frequency ω_L, is the Rayleigh scattering. The width of this component is 0.07 nm which is determined primarily by the resolution of the monochromator.

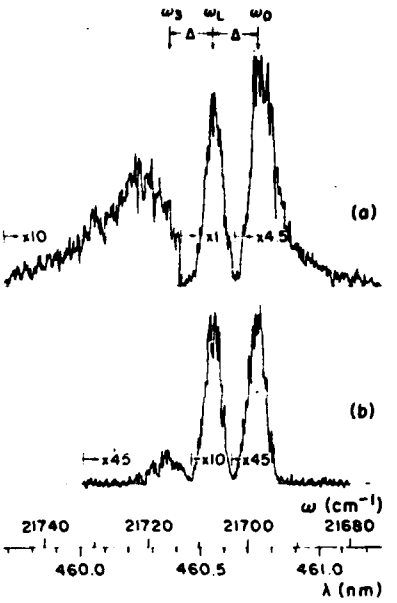

FIG. 6. Emission spectra for the laser tuned to the blue side of resonance ($\Delta = -8.0$ cm^{-1}). (a) Full laser intensity, (b) laser attenuated by a factor of 50. The factors give the detection sensitivity. Observed are the Rayleigh scattering at ω_L, the resonance fluorescence at ω_0 and the "three-photon" scattering at ω_3.

The component near $\omega_3 = \omega_L - \Delta$ is due to three-photon scattering. Note that at high laser intensity it is considerably shifted due to the ac Stark effect. Since our laser is pulsed, this effect shows up both as a shift and a broadening as seen previously by others.[69,70] The fluorescence component is located near the resonance frequency ω_0. This component is a result of both three-photon scattering and collisional redistribution. At high laser intensity this component is also shifted and broadened. Since the lifetime of the excited state is comparable to the laser pulse length, only part of the fluorescence is emitted during the time the laser is on. Thus the shift and broadening of the fluorescence due to the ac Stark effect are not as large as those of the three-photon component, which is emitted only during the laser pulse.

We studied these emission components as a function of argon pressure, laser detuning, and laser intensity. All the data to be presented will be given as the integrated intensities of the resolved spectral components: I_R, I_F, and I_3. These values were obtained by graphically integrating scans such as those in Fig. 6 and are thus limited in precision by noise in the apparatus. We estimate the precision of these measurements to be ±20%.

A. Emission versus detuning at low laser intensities

We studied the effect of detuning on the integrated Rayleigh emission I_R and integrated fluorescence I_F at low laser intensities over a large range of Δ. The oven was run at a temperature of 530 °C and an argon buffer gas pressure of 50 Torr. At this temperature the number density of strontium was estimated to be 9.7×10^{13} cm^{-3} from vapor pressure data.[71] In making the measurements, the linearity with laser intensity was checked for each point. This check eliminated the possibility of multiphoton and saturation effects and guaranteed that we were in the low intensity regime. In particular it guaranteed that the fluorescence was due only to collisional transfer from the virtual level and not to the higher-order three-photon process.

1. Rayleigh emission versus detuning

Since we were always in the region where $|\Delta| \gg \gamma$, we expected from Eq. (10) that the Rayleigh intensity should fall off as Δ^{-2}. The results are shown in Fig. 7 for detunings on both sides of resonance. The dashed curve shows the predicted Δ^{-2} dependence adjusted for the overall gain of the detection system. We see that for two decades of detuning, the integrated Rayleigh intensity goes as Δ^{-2}. Note that Δ was never large enough for the quadrupole allowed $^1S_0 - {}^1D_2$ transition (cf. Fig. 4) to affect the Rayleigh scattering. In Fig. 7 scattering from the surface of the oven (of the order of I_R at $\Delta = 200$ cm^{-1}) was subtracted. We were not able to measure the Rayleigh scattering at $\Delta \approx +5$ cm^{-1} since the red absorption wing of the atoms surrounding the excitation region attenuated the Rayleigh intensity. The effect of ground-state atoms surrounding the excitation region and the resulting radiative trapping will be more fully discussed in the next section when we consider the fluorescence component.

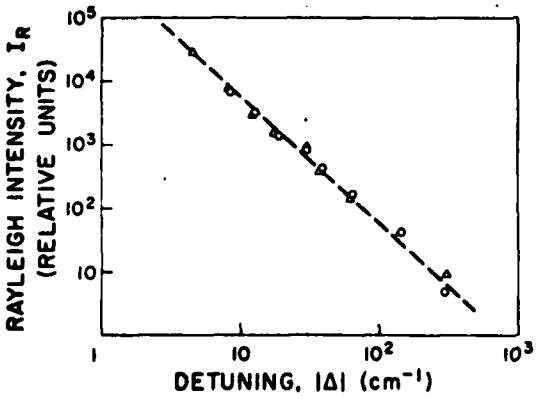

FIG. 7. Rayleigh scattering (spectrally integrated) versus detuning of the laser from resonance at low laser intensity. Detunings to the blue and red sides of resonance are shown by triangles and circles, respectively. The broken line shows the expected Δ^{-2} Lorentzian fall-off.

2. Fluorescence versus detuning

In our experiment, the impact approximation is expected to be valid only for $|\Delta| < 4.6$ cm^{-1}. This was determined using the measurements of Penkin and Shabanova[72] and our Eq. (6). Thus we expect that for $|\Delta| > 4.6$ cm^{-1}, the impact approximation will fail and the collision-induced fluorescence will no longer be Lorentzian. Experimentally we find that indeed the fluorescence is strongly frequency dependent and asymmetric. The composite spectral scans of Fig. 8 show that the fluorescence component, near ω_0 (slightly displaced by the ac Stark effect) is an order of magnitude larger when the laser is tuned to the red side of the resonance than when tuned to the blue.

Figure 9 shows experimental curves for the integrated intensity of collision-induced fluorescence as a function of Δ. The data at 5-cm^{-1} border the impact region. The units of I_F are relative to I_R of Fig. 7. The vertical error bars were determined by the scatter of several experimental readings for each point, while the horizontal bars simply show the 1.4 cm^{-1} uncertainty in frequency due to the laser linewidth. Also drawn is a broken curve for a Lorentzian fall-off corresponding to a constant γ_E in Eq. (11), where γ_E is taken from the pressure-broadening measurements.[72] The broken

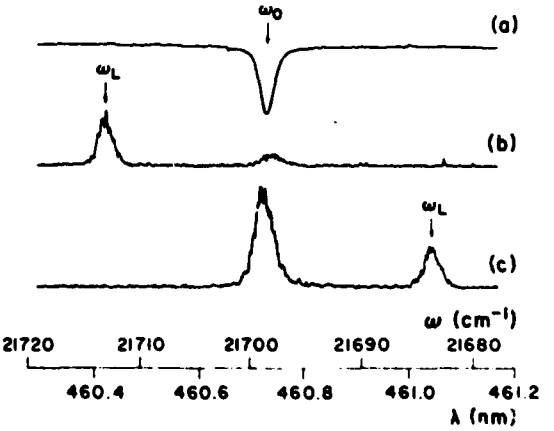

FIG. 8. Spectra showing asymmetry of fluorescence, at ω_0, as a function of the laser frequency ω_L. (a) White light absorption profile showing location of resonance. (b) and (c) show the laser detuned from resonance by plus and minus 15 cm^{-1}, respectively. While the Rayleigh emission is symmetric with detuning, the collision-induced fluorescence is highly asymmetric.

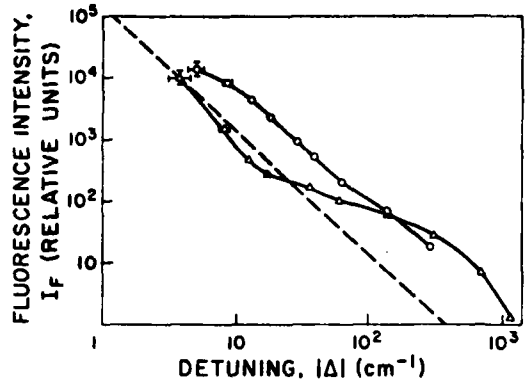

FIG. 9. Collision-induced fluorescence (spectrally integrated) as a function of detuning of the laser from resonance. Detunings to the blue and red sides of resonance are shown by triangles and circles, respectively. The broken line shows the Δ^{-2} dependence, valid in the impact region, extended to large detunings. Impact approximation is only valid for $|\Delta| < 4.6$ cm^{-1}.

curve was corrected for self-absorption of the sample (see Sec. IV A 3 on radiative trapping).

It is seen from Fig. 9 that γ_E is strongly frequency dependent, as discussed in Sec. II A. In particular, when the laser is tuned to the red side of resonance, the fluorescence is initially much larger than when the laser is tuned to the blue. This "red wing" is very similar to the results found in absorption and emission experiments. This similarity is due to the fact that all these experiments effectively measure the collisional line shape of the transition. In particular, our experiment can be viewed as an absorption event followed by an emission event.

The origin of the red wing can be understood from very basic ideas involving potential curves. Figure 10 shows a schematic representation of the potential curves for the strontium-argon collision. Since the $Sr(^1P)$ level is more polarizable than the $Sr(^1S)$, the potential curve for the $Sr(^1P)$-$Ar(^1S)$ collision will be more attractive than the potential curve for the $Sr(^1S)$-$Ar(^1S)$ collision. When the laser is tuned to the red side of the resonance, the frequency of the laser will be equal to the difference potential at some internuclear separation and there will be a large overlap between the upper and lower state wave functions. Thus, according to the Franck-Condon principle, a transition will be induced. This side of resonance is referred to as the quasistatic wing.[13] On the other hand, when the laser is tuned to the blue side of resonance, the overlap is less so that the collision-induced fluorescence is smaller. This side of resonance is referred to as the antistatic wing.[13] When the laser is tuned far off resonance the repulsive parts of the curves will become important.

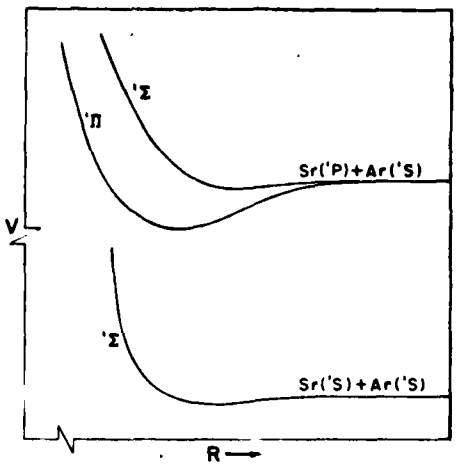

FIG. 10. Schematic drawing showing the general behavior of the potentials for a collision between the strontium (^1P or ^1S) atom and the ground-state argon atom.

For instance as seen from the schematic of Fig. 10, when the laser is tuned far off resonance to the blue, the $^1\Sigma$ upper curve and the $^1\Sigma$ lower curve run parallel so that the difference potential is constant and the transition probability increases. In our experiment this is probably the reason why the blue wing becomes more significant for large detunings.

In order to bring out the dependence on Δ more clearly, the quantity $\sigma_E(\Delta)$ is plotted versus Δ in Fig. 11. This was determined by the ratio of I_F/

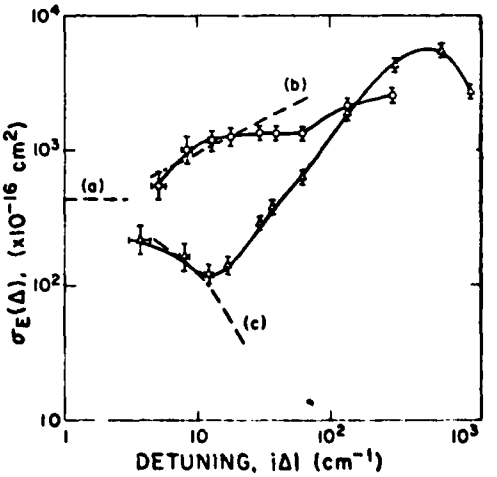

FIG. 11. Cross section σ_Δ for collision-induced fluorescence as a function of detuning at 530 °C. Detunings to the blue and red sides of resonances are shown by triangles and circles, respectively. The dashed curves show the prediction of the theory of Szudy and Baylis (Ref. 13) using a Van der Waals interaction constant $C_6 = 9.8 \times 10^{-31}$ $cm^6 sec^{-1}$: (a) the impact region, (b) the quasistatic region, and (c) the antistatic region.

I_R from Figs. 7 and 9. Account was also taken of the attenuation due to radiative trapping as discussed in the next section. The rate of collisional quenching was determined self-consistently from the measurements of Sec. IV B to be $\gamma_i = 0.29\gamma_R$.

We have compared our results with the predictions of the line-shape theory of Szudy and Baylis.[13] Using their predictions for the line shape from a R^{-6} Van der Waals potential, we obtained the dashed curves for the (a) impact region, (b) quasistatic region, and (c) antistatic region when we used a value of $C_6 = 9.8\times10^{-31}$ cm^6 sec^{-1}. As can be seen in Fig. 11 the value of σ_E in the impact region ($|\Delta| < 4.6$ cm^{-1}) is then predicted to be 4.4×10^{-14} cm^2 for 530 °C. This is higher than that obtained at 530 °C from the data of Penkin and Shabanova[72] (2.3×10^{-14} cm^2) and also Farr and Hindmarsh[73] (3.6×10^{-14} cm^2). The differences are within the expected uncertainty.

Under our experimental conditions we found that the broadening was entirely due to Sr-Ar collisions and not Sr-Sr collisions. This was expected in the impact region from measurements of collisional widths for Sr-Sr collisions and Sr-Ar collisions. The values[72,74] of these widths at 530 °C and 50 Torr of argon are γ_E(Sr-Sr) = 5.6×10^7 rad sec^{-1} and γ_E(Sr-Ar) = 1.2×10^9 rad sec^{-1}. This expectation was confirmed by repeating the experiment with the strontium density lowered by a factor of 8 and observing no change in the shape of the profiles in Fig. 9. This is consistent also with our data on fluorescence versus argon pressure at a detuning of 9.4 cm^{-1} (see Sec. IV B).

For large detunings, a question arose as to the mechanism responsible for populating the excited state. Since our laser had a spectral width of 0.03 nm, the possibility of excitation by the spectral wings[75-79] needed to be considered. In addition, the spectral wings of the laser can produce a continuum of excited states between $\hbar\omega_L$ and $\hbar\omega_0$ which could be collisionally transferred to the excited state. When the laser is tuned very far from resonance, this "cumulative wing effect" could dominate the "normal" collision-induced fluorescence arising from the virtual state at $\hbar\omega_L$. Direct excitation by spectral components at the transition frequency was expected to be negligible because the oven had an optical depth of ~800, thus absorbing all components within the absorption line before reaching the excitation region. To verify this expectation and to show also that the "cumulative wing effect" was negligible under our conditions, we placed a 0.03-nm bandpass monochromator in the laser beam to filter out any spectral wings. When the fluorescence versus detuning data of Fig. 9 were taken again with the filter in, no differences were seen. Thus the collision-induced fluorescence could be considered to arise entirely from collisional transfer from the virtual level at $\hbar\omega_L$ to the excited state, where the location of the virtual level is known only to within the line width of the laser.

3. Radiative trapping

The small cylindrical region of Sr atoms that is excited by the laser is surrounded by unexcited Sr atoms. Most of our experiments were done at densities where this unexcited region is many absorption lengths deep (~800). The simplest way to estimate the number density of strontium atoms and therefore the optical depth is by measuring the equivalent width of the absorption line.[80] This measurement can also be checked with vapor-pressure curves. As a result of the radiative trapping, the fluorescence component of the scattered intensity was heavily attenuated. The loss of intensity comes from two separate sources: first, radiative trapping lengthens the lifetime of the excitation so that any quenching mechanism that is present becomes more effective; second, because of the diffusion of the radiation, the size of the radiative region increases, therefore that part of the emission that is collected on the slit of the monochromator decreases.

In order to verify that the trapping did not change the shape of the curves in Fig. 9, but only the overall gain, we checked the linearity of the fluorescence signal in laser intensity at every data point by inserting a neutral density filter into the laser beam and observing the appropriate linear drop in fluorescence signal. At *high* laser intensities and *small* detunings, the ac Stark shift by the laser can be large enough to shift the emission frequency outside the absorption equivalent width, reducing the amount of trapping and leading to an increase in fluorescence signals. The linearity check justified our using a higher laser intensity to produce signals at *large* detunings and then normalizing all the points in Fig. 9 to some fixed laser intensity. That the fluorescence was linear in laser intensity indicated that no significant Stark effects were occurring for these measurements.

It was mentioned in the previous section that the broken line in Fig. 9 was corrected for self-absorption of the sample. This was done by multiplying Eq. (11) by a constant attenuation factor determined as follows. By lowering the oven temperature to 400 °C (strontium density $\approx5\times10^{11}$ cm^{-3}), we substantially reduced the amount of trapping. At this low density, however, fluorescence could be observed only at small detunings. When the emission was observed at both plus and minus 5 cm^{-1} detuning, which borders the impact region, the fluorescence relative to the Rayleigh scatter-

ing was within a factor of 3 of that predicted by Eqs. (10) and (11), indicating an absence of trapping. Thus we used the ratio of the relative fluorescence signals with and without trapping as our attenuation factor.

4. *Comparison of redistribution line shape with absorption and emission experiments*

Absorption experiments measure the extinction coefficient which is the attenuation of a well-collimated monochromatic light beam at frequency ω_L. On the other hand, in emission experiments, the atoms are excited near line center by monochromatic light, and the fluorescence spectrum is measured off line center. Equation (9) shows that in the impact region of the spectrum the line shapes measured in absorption and emission should be the same as the profile determined by the scattering experiment described in this paper. Outside the impact region, the theory has not been explicitly developed. We have done two crude experiments to determine if any major differences exist between these various experiments in the quasistatic and antistatic region.

Figure 12(a) shows a scan of the absorption profile of the 460.73-nm resonance line of strontium. In order to see the spectral wings we operated at a temperature of 580 °C and 595 Torr of argon. The scan was obtained with a dc broadband light source passing through the oven and focused onto the monochromator slit. As in our redistribution experiments, we see a large red wing. Figure 12(b) shows a scan of the emission profile for the same temperature and pressure conditions when the laser was tuned to 459.9 nm. The Rayleigh emission is seen at the laser frequency as expected, and is as narrow as our resolution. As in both the redistribution experiment (Fig. 9) and the absorption experiment [Fig. 12(a)], the fluorescence line shape again has a strong red wing. Note that for this higher temperature and pressure the radiative trapping is evident from the dip in the fluorescence near ω_0. We have determined the absorption profile $[-\log(I/I_0)]$ from Fig. 12(a) and also the emission profile from Fig. 12(b) and find that the shape of the profiles is the same as the redistribution profile shown in Fig. 9 to within a factor of 2.

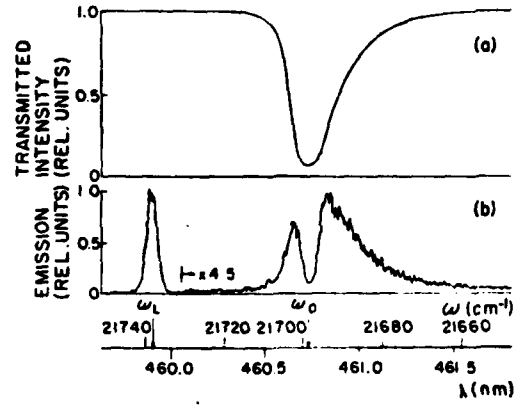

FIG. 12. (a) Scan of the absorption profile of the 460.73-nm line in strontium at 580 °C and 595-Torr argon. (b) Emission profile for the same experimental conditions with the laser tuned to 459.9 nm. Both profiles show a large red wing as do the redistribution results (Fig. 9). The factor gives the increase in detector sensitivity.

B. Emission versus argon pressure

We have studied the fluorescence component as a function of argon buffer gas pressure with the laser tuned to 460.93 nm ($\Delta = 9.4$ cm^{-1}). The study was done at a temperature of 400 °C so that effects of radiative trapping were minimal. Agreement with theory was obtained when the inelastic rate γ_I was taken to be linear in argon pressure. Experimental and theoretical curves showing the fluorescence versus Ar pressure at three different laser intensities are shown in Fig. 13.

The theoretical curves were computed from Eq. (24) with two adjustable parameters: γ_I and Ω^2 (laser intensity for curve a). The laser intensities for the lower curves were determined by the

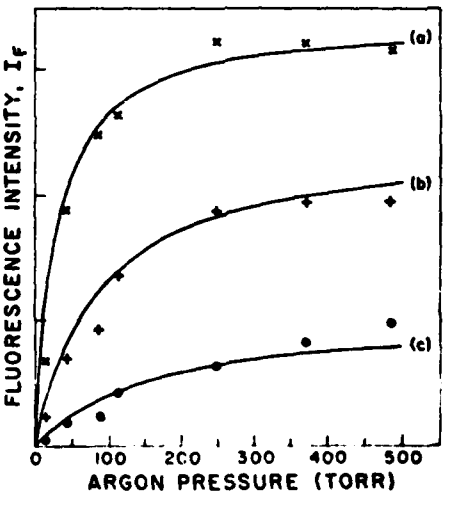

FIG. 13. Collision-induced fluorescence (spectrally integrated) as a function of argon buffer gas pressure for three different laser intensities. (a) Full laser intensity, (b) laser attenuated by 4.5, (c) laser attenuated by 20. The solid curves were computed from Eq. (24) with two common parameters: the quenching rate γ_I and the laser intensity for curve (a).

known attenuations of the neutral density filters used in the experiment. The value of γ_I determined by this fitting technique is $\gamma_I/\gamma_E = 0.007 \pm 0.002$. The value of Ω^2 was determined to be $\Omega^2/\Delta^2 = 0.1 \pm 0.03$ (0.5 MW/cm^2). The radiative decay rate γ_N was taken[66] to be 1.07×10^8 rad sec^{-1} and the elastic collision rate γ_E was determined self-consistently from the data in Fig. 11.

The general form of the curves for low laser intensity can be understood *qualitatively* by considering the rate scheme shown in Fig. 1. Following Eq. (17) it was pointed out that the "population" in the upper virtual level can be taken as $(N/2)(\Omega^2/\Delta^2)$. This "population" is then transferred to the upper state at a rate γ_E due to elastic collisions. Thus the transfer rate from the lower state to the upper state is $\gamma_T = (\gamma_E/2)(\Omega^2/\Delta^2)$. There is also a route for laser-induced collisional depopulation of the excited state. Thus we expect that the curves should be linear at low Ar pressure with the slopes increasing with increasing laser intensity and that each curve should saturate to some maximum fluorescence level, due to equalization of the excited and ground state populations. In the absence of quenching, all curves would saturate to the same level. This is because the transfer rate γ_T will eventually dominate the radiative decay rate γ_N. However, in the presence of quenching, there is a competition between the quenching rate γ_I and the transfer rate γ_T between levels so that each curve saturates to a different intensity as seen in Fig. 13. In fact, if the fluorescence is taken to be given by the decay rate γ_N times a steady-state population, we obtain $I_F = N\gamma_N[\gamma_T/(\gamma_I + \gamma_N)]$. It is interesting to note that Eq. (24), which was used to compute the curves in Fig. 11, reduces to this expression at low laser intensities.

C. Emission versus laser intensity

We studied the saturation of the three emission components at high laser intensities. The oven was run at 490 °C with an argon buffer gas pressure of 10 Torr. Thus, the number density of argon was $N(\mathrm{Ar}) = 1.3 \times 10^{17}$ cm^{-3} and the number density of strontium was $N(\mathrm{Sr}) = 2.5 \times 10^{13}$ cm^{-3}.

In our initial comparisons with the theoretical predictions given by Eqs. (16), (23), and (24), we assumed the laser intensity was constant spatially. However, we found that at high degrees of saturation, there were deviations from the theory due to the nonlinear effects of the spatial wings of the laser. Therefore, we decided to average the theoretical predictions over the spatial profile of the laser. The method used for the spatial averaging is discussed below.

1. Spatial average

In the coordinate system shown in Fig. 14, the laser beam travels along the z direction (out of the page) and the detection system is along the x direction. For an emission profile $\epsilon(r)$, where r is the radial distance, the observed intensity profile is

$$I(y) = 2\int_0^\infty \epsilon(r)\,dx = 2\int_y^\infty \frac{r\epsilon(r)\,dr}{(r^2 - y^2)^{1/2}}. \tag{25}$$

By using the Abel inversion,[81] $\epsilon(r)$ can be obtained:

$$\epsilon(r) = -\frac{1}{\pi}\int_r^\infty \frac{\{dI(y)/dy\}\,dy}{(y^2 - r^2)^{1/2}}. \tag{26}$$

To determine the laser profile $I_L(r)$ in the interaction region, we scanned the collection lens in the y direction while the monochromator observed the Rayleigh emission. The laser was run at low intensities so the Rayleigh emission was linear in laser intensity. Then by using Eq. (26) we found that the laser profile $I_L(r)$ (photons cm^{-2} sec^{-1}) could be approximated by

$$I_L(r) = I_L\left(\frac{r_0^2}{r^2 + r_0^2}\right)^{3/2} \tag{27}$$

over the range of $r \leq 700$ μm. Outside this range our signal was in the noise. Here $I_L = I_L(r=0)$, and r_0 was found to be 110 μm. The spatial profile of the laser beam was then folded into Eqs. (16), (23), and (24) using Eq. (25). In this way, theoretical predictions for the three emission components as a function of laser intensity I_L were obtained, as presented in the following sections.

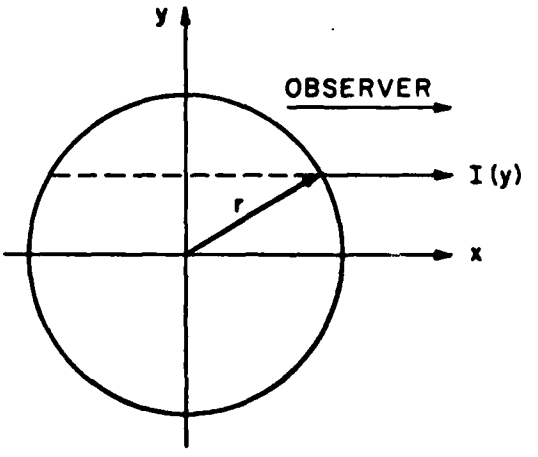

FIG. 14. Coordinate system for spatial averaging. The laser beam travels along the z axis (out of the page) and the detection system is in the x direction.

2. Rayleigh component

The dependence of the spectral integrated Rayleigh intensity on the incident laser intensity is given by Eq. (16). This equation shows that at low laser intensities, the dependence is linear in laser intensity. However, when $\Omega^2 \approx \Delta^2$, saturation begins to occur and the Rayleigh intensity falls below the linear dependence, eventually becoming constant.

We studied the saturation effect of the Rayleigh scattering at several detunings of the laser on both sides of resonance. The results are shown in Fig. 15 where it is seen that the saturation is less rapid when the laser is tuned far from resonance than when it is tuned near to resonance. The theoretical curves shown by the broken lines were obtained assuming a rectangular spatial profile for the laser and are therefore plots of Eq. (16) with two free parameters—the incident laser intensity and the overall detection sensitivity. All three curves use the same values for these parameters; only Δ was changed as measured experimentally. The fit was obtained with an incident laser intensity of 35 MW/cm^2. When a spatial average was taken as described in Sec. IV C 1, the theoretical curves shown by the solid lines were obtained. The fit was obtained with a laser intensity of 105 MW/cm^2 at the center of the excitation region. The deviation of the fit with and without spatial averaging is comparable to our experimental error. Note that for $|\Delta| = 0.75$ nm, spatial averaging does not change the theoretical curve.

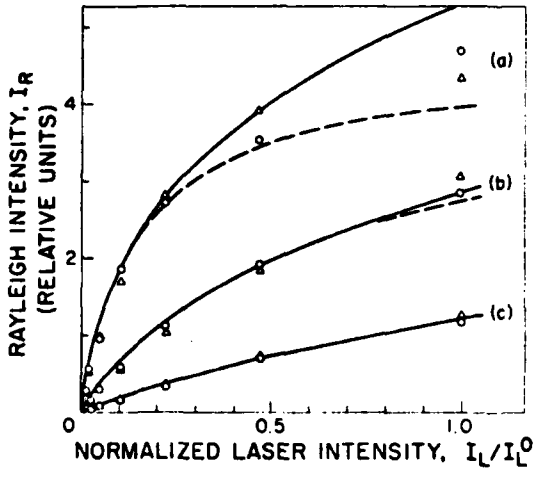

FIG. 15. Rayleigh scattering (spectrally integrated) versus laser intensity for several detunings. Detunings to the blue and red sides of resonance are shown by triangles and circles, respectively. (a) $\Delta = \pm 0.17$ nm, (b) $\Delta = \pm 0.36$ nm, (c) $\Delta = \pm 0.75$ nm. Near resonance, saturation is seen. The theoretical curves were obtained from Eq. (16) assuming a rectangular spatial profile (broken curves), and using the measured spatial profile given by Eq. (27) (solid curves). See Sec. IV C 2 for discussion.

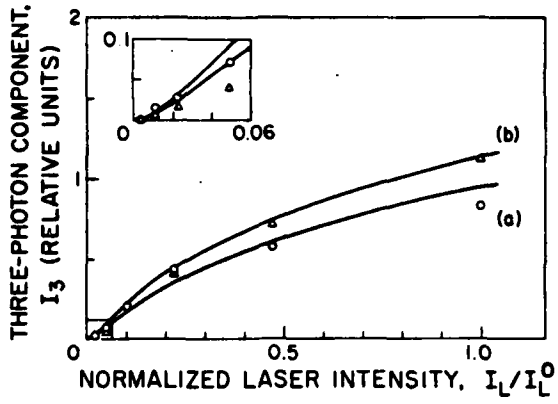

FIG. 16. Three-photon scattering (spectrally integrated) versus laser intensity for a detuning of 0.17 nm on the red side (a) and the blue side (b) of resonance. Solid curves are theoretical predictions using Eq. (23) with no free parameters. The insert shows the region at low intensity expanded by five. The intensity of the three-photon component is predicted to be quadratic in the region below a normalized laser intensity of 0.01. See Sec. IV C 3 for further discussion.

3. Three-photon component

Theory predicts that at low intensities the three-photon component is quadratic in laser intensity but eventually saturates and levels off as does the Rayleigh intensity. As can be seen from Eq. (23), the integrated intensity I_3 of the three-photon component not only depends on the detuning and intensity of the laser, but also to a small degree on the collisional rates.

We have observed this three-photon component at the predicted position for both positive and negative values of the detuning Δ and for various laser intensities. In particular at $\Delta = \pm 0.17$ nm we have measured the intensity dependence of this component. The results are shown in Fig. 16. The vertical scale is the same relative scale used in plotting the Rayleigh intensity in Fig. 15. The curves shown in Fig. 16 are *zero* parameter predictions for the integrated intensity I_3 of the three-photon component using Eq. (23) and the values for the fixed parameters determined as follows. The overall sensitivity of the detection system, spatial average and incident laser intensity are the same as used to fit the Rayleigh saturation data in Fig. 15. Also γ_I was determined from our data presented in Sec. IV B. Finally, γ_E was determined from our low intensity data on the fluorescence (Fig. 11). We see that this zero parameter fit is within our 20% experimental accuracy.

4. *Fluorescence component*

We studied the laser intensity dependence of the spectrally integrated fluorescence at various detunings on both sides of resonance. Data at $\Delta = \pm 0.17$ nm are shown in Fig. 17. The relative units of the vertical scale of Fig. 17 are the same as in Fig. 15 for the Rayleigh intensity.

The solid curves in Fig. 17 are theoretical predictions using Eq. (24) with the spatial averaging procedure discussed in Sec. IV C 1. The fits were obtained using the elastic collision rate σ_E as a free variable. All other parameters were determined by previous data as for I_3. The best fit to the data on the red side of resonance was obtained with $\sigma_E = 320 \times 10^{-16}$ cm^2. This is about a factor of 3 smaller than expected from our low-intensity measurements of the fluorescence shown in Fig. 11. On the blue side of resonance the best fit was for $\sigma_E = 18 \times 10^{-16}$ cm^2 which is a factor of 8 smaller than our low-intensity measurement.

The reason for this discrepancy probably lies in the fact that we have applied a steady-state theory to a pulsed experiment. Unlike the Rayleigh and three-photon components, which are only emitted during the laser pulse, the fluorescence decays exponentially after the laser has turned off. As discussed in Sec. IV A 3 there is considerable radiation trapping due to the surrounding strontium atoms. At high laser intensities and small detunings, the ac Stark effect is large enough that the fluorescence emitted during the laser pulse is essentially untrapped. However, the fluorescence emitted after the laser pulse is heavily trapped, so that the total fluorescence is less than expected, leading to a smaller value of σ_E than expected. We are presently attempting to extend our analysis to a transient formulation using the theory of Courtens and Szöke.[34]

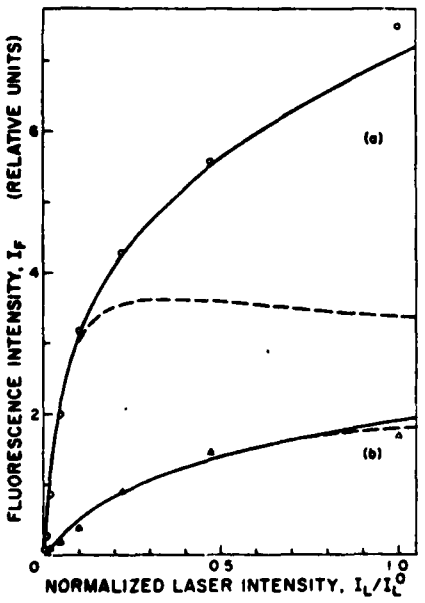

FIG. 17. Resonance fluorescence (spectrally integrated) versus laser intensity for a detuning of 0.17 nm on the red side (a) and the blue side (b) of resonance. Saturation on the red side is very pronounced. The theoretical curves were obtained from Eq. (24) assuming a rectangular profile (broken curve) and using the measured spatial profile given by Eq. (27) (solid curve). See Sec. IV C 4 for discussion.

We also have calculated the theoretical predictions for the fluorescence component without spatial averaging and using an incident laser power of 35 MW/cm^2 determined by the fit to the Rayleigh saturation data presented in Fig. 15. The resultant theoretical curves are shown in Fig. 17 by the broken lines. All other variables are the same as for the theory shown by the solid lines. Without spatial averaging, the theory predicts that the fluorescence at $\Delta = +0.17$ nm will saturate heavily. However, when we take the spatial average, the effect of extreme saturation is washed out by the spatial wings as seen by the solid curve. The reason that the effect of the wings is so much more important in the fluorescence than in the Rayleigh emission is that the slope of the fluorescence at low intensities is larger so that the wings are heavily weighted in the average.

We have also studied the fluorescence as a function of the intensity of the laser at larger detunings, where there is less saturation and the dependence is more linear. Good theoretical fits could be obtained using Eq. (24), but again all values of $\sigma_E(\Delta)$ determined from these fits were less than the values expected from the low intensity data shown in Fig. 11. As discussed above, we feel these differences are due to the steady-state assumption coupled with the effects of radiative trapping.

V. SUMMARY AND DISCUSSION

Our studies[1,2] were the first ones that actually observed the collisional redistribution of scattered radiation. The knowledge of this function is important to the theory of radiative transport and line formation in stellar atmospheres. It has been calculated from first principles in the impact region, but no firm theory exists in the static region. Our experiments for low incident intensities can be summarized in terms of an empirical redistribution function that is similar to Eq. (9):

$$I(\omega)\,d\omega = \left(\frac{\omega}{\omega_0}\right)^3 N \frac{(\gamma_N/2)\Omega^2\,d\omega}{\Delta^2+\gamma^2} \times \left(\delta(\omega-\omega_L)+\frac{\gamma_E(\Delta)}{\gamma_N+\gamma_I}f(\omega)\right). \quad (28)$$

where $\gamma_E(\Delta)$ can be obtained from Fig. 11. Here $f(\omega)$ is the emission line shape, normalized to $\int f(\omega)\,d\omega = 1$. We actually measured only pieces of this formula, i.e., $I_F \propto \gamma_E(\Delta)/\Delta^2$, $I_R \propto 1/\Delta^2$, and in a separate experiment $f(\omega)$, where we also found $f(\Delta) \propto \gamma_E(\Delta)/\Delta^2$ within our experimental range and error. We have also shown that experiments with variable perturber density can establish the inelastic collision rate γ_I, though we have done no experiments to determine the actual cause of quenching.

Radiation trapping, one of the major obstacles in our experiments, is an interesting subject by itself. We conducted enough experiments to convince ourselves that we can account for the influence of trapping consistently. It is interesting to note that experiments similar to ours can be conducted to study details of the space-time behavior of radiative trapping.[82] By measuring the space-, time-, and spectrally-resolved scattered light after a small cylindrical region is excited by a pulsed laser, the most fundamental quantity in radiative transfer, the Green's function, can be measured experimentally.

The high-field behavior of the Rayleigh and three-photon scattering has been studied and agreement was obtained with Mollow's steady-state theory. While the integrated Rayleigh component was found to be "collisionless," the third component was found to have a weak collisional dependence. The fluorescence component was also found to fit the steady-state theory quite well, but the cross section for the elastic collision was smaller than that predicted by our low intensity measurements. We feel that this discrepancy is due in part to the transient nature of the laser excitation because (a) there is not enough time for collisional equilibration, and (b) during the strong laser pulse the fluorescence is ac Stark shifted and therefore escapes, but after the pulse is over the rest of the fluorescence is trapped and partly lost to the detection system. It is interesting to note that according to recent studies[30-32] it is expected that the elastic collision rate should have some intensity dependence. We continue our studies in this direction.

Note added in proof. Recently Nienhuis and Schuller (private communication) have extended the theory of collisional redistribution into the far wing where the impact limit is invalid. They find that their predictions are in qualitative agreement with our observations of the asymmetry in the collisional redistribution.

ACKNOWLEDGMENTS

The authors wish to thank B. R. Mollow for making available his results prior to their publication, and also A. Gallagher for several very useful discussions on line broadining. In addition the authors acknowledge the helpful comments and suggestions of J. Cooper, W. C. Lineberger, and S. J. Smith.

*Research supported by the Office of Naval Research under Contract No. N00014-76-C-0611 and by the National Science Foundation under Grant No. MPS72-05169.

†Present address: Lawrence Livermore Laboratory, University of California, Livermore, California, 94550.

‡Department of Chemistry, University of Colorado, Boulder, Colorado 80309.

[1]J. L. Carlsten and A. Szöke, Phys. Rev. Lett. 36, 667 (1976).

[2]J. L. Carlsten and A. Szöke, J. Phys. B 9, L231 (1976).

[3]W. Heitler, *The Quantum Theory of Radiation* (Clarendon, Oxford, 1957), 3rd ed.

[4]D. Mihalas, *Stellar Atmospheres* (Freeman, San Francisco, 1970).

[5]N. M. Kroll, in *Quantum Optics and Electronics, Les Houches Lectures 1964*, edited by C. DeWitt, A. Blandin, and C. Cohen-Tannoudji (Gordon and Breach, New York, 1965).

[6]A. P. Kazantsev, Zh. Eksp. Teor. Fiz. 66, 1229 (1974) [Sov. Phys.-JETP 39, 601 (1974)].

[7]B. R. Mollow, Phys. Rev. A 13, 758 (1976).

[8]A. Omont, E. W. Smith, and J. Cooper, Astrophys. J. 175, 185 (1972); 182, 283 (1973).

[9]D. L. Huber, Phys. Rev. 178, 93 (1969).

[10]See, for example, J. L. Kohl and W. H. Parkinson, Astrophys. J. 205, 599 (1976); T. R. Ayres and J. L. Linsky, Astrophys. J. 205, 874 (1976).

[11]For extensive review, see e.g., A. Ben-Reuven, Adv. Chem. Phys. 33, 235 (1975); F. Schuller and W. Behmenburg, Phys. Rev. 12, 273 (1974).

[12]For reviews see, e.g., J. Cooper, Comments on the theory of satellite bands, JILA Report No. 111, Univ. of Colorado, Boulder, Colo. 80309 (1973); also Refs. 10 and 70.

[13]J. Szudy and W. E. Baylis, J. Quant. Spectrosc. Radiat. Transfer 15, 641 (1975).

[14]C. L. Chen and A. V. Phelps, Phys. Rev. A 7, 470 (1973).

[15]A. Gallagher, in *Atomic Physics*, Vol. 4, edited by G. zu Putlitz, E. W. Weber, and A. Winnacher (Plenum, New York, 1975).

[16]B. R. Mollow, Phys. Rev. A 188, 1969 (1969).

[17]S. S. Hassan and R. K. Bullough, J. Phys. B 8, L147 (1975).

[18]H. T. Carmichael and D. F. Walls, J. Phys. B 9, 1199 (1976).

[19]M. E. Smithers and H. S. Freedhoff, J. Phys. B 8, 2911

(1975).
[20]B. R. Mollow, Phys. Rev. A 12, 1919 (1975).
[21]H. J. Kimble and L. Mandel, Phys. Rev. A 13, 2123 (1976).
[22]C. Cohen-Tannoudji, in *Lecture Notes in Physics 43, Laser Spectroscopy*, Proceedings of the Second International Conference, Megeve, 1975, edited by S. Haroche, J. C. Pebay-Peyoula, T. W. Hänsch, and S. E. Harris (Springer, Berlin, 1975).
[23]F. Schuda, C. R. Stroud, Jr., and M. Hercher, J. Phys. B 7, L198 (1974).
[24]F. Y. Wu, R. E. Grove, and S. Ezekiel, Phys. Rev. Lett. 35, 1426 (1975).
[25]W. Hartig, W. Rasmussen, R. Schieder, and H. Walther, Z. Phys. A278, 205 (1976).
[26]B. R. Mollow, Phys. Rev. A 2, 76 (1970)
[27]B. R. Mollow, preceding paper, Phys. Rev. A 15, 1023 (1977).
[28]L. I. Gudzenko and S. I. Yakovlenko, Zh. Eksp. Teor. Fiz. 62, 1686 (1972) [Sov. Phys.-JETP 35, 877 (1972)].
[29]V. S. Lisitsa and S. I. Yakovlenko, Zh. Eksp. Teor. Fiz. 66, 759 (1974) [Sov. Phys.-JETP 39, 759 (1974)].
[30]V. S. Lisitsa and S. I. Yakovlenko, Zh. Eksp. Teor. Fiz. 68, 479 (1975) [Sov. Phys.-JETP 41, 233 (1975)].
[31]N. M. Kroll and K. M. Watson, Phys. Rev. A 13, 1018 (1976).
[32]A. M. F. Lau, Phys. Rev. A 13, 139 (1976); 14, 279 (1976).
[33]See, e.g., review by C. Cohen-Tannoudji, in *Cargèse Lectures in Physics*, Vol. 2 (Gordon and Breach, New York, 1968).
[34]E. Courtens and A. Szöke, Phys. Rev. A (to be published).
[35]S. E. Harris and D. B. Lidow, Phys. Rev. Lett. 33, 674 (1974).
[36]D. B. Lidow, R. W. Falcone, J. F. Young, and S. E. Harris, Phys. Rev. Lett. 36, 462 (1974).
[37]P. F. Williams, D. L. Rousseau, and S. H. Dworetsky, Phys. Rev. Lett. 32, 196 (1974).
[38]D. L. Rousseau, A. D. Patterson, and P. F. Williams, Phys. Rev. Lett. 34, 1306 (1975). See also a critique by P. A. Hackett, Phys. Rev. Lett. 36, 1403 (1976), and the authors' reply, Phys. Rev. Lett. 37, 1441 (1976).
[39]D. L. Rousseau and P. F. Williams, J. Chem. Phys. 64, 3519 (1976).
[40]S. Mukamel, A. Ben-Reuven, and J. Jortner, Phys. Rev. A 12, 947 (1975).
[41]S. Mukamel, A. Ben-Reuven, and J. Jortner, Chem. Phys. Lett. 38, 394 (1976).
[42]A. Szöke and E. Courtens, Phys. Rev. Lett. 34, 1053 (1975).
[43]Y. Liran, private communication, and unpublished.
[44]R. D. Driver and J. L. Snider, Center for Astrophysics Preprint No. 551 (unpublished).
[45]L. Vriens and M. Adriaansz, Appl. Phys. 11, 253 (1976).
[46]K. Sakurai, A. Adams, M. Lambropoulos, and H. P. Broida, Bull. Am. Phys. Soc. 21, 1245 (1976).
[47]R. T. M. Su, J. W. Bevan, and R. F. Curl, Jr. (unpublished).
[48]D. Grischkowsky, Phys. Rev. A 14, 802 (1976).
[49]R. E. Drullinger, M. M. Hessel, and E. W. Smith, NBS Monograph 143 (1975), and unpublished.
[50]R. J. Ballagh and J. Cooper, Astrophys. J. (to be published).
[51]H. M. Gibbs and T. N. C. Venkatesan, IEEE J. Quantum Electron. 11, 91D (1975).
[52]J. D. Jackson, *Classical Electrodynamics* (Wiley, New York, 1967), p. 603.
[53]A. M. Bonch-Bruevich and V. A. Khodovoi, Usp. Fiz. Nauk. 93, 71 (1967) [Sov. Phys. Usp. 10, 637 (1968)].
[54]This is an appealing, but *not* an accurate description of the process. In particular, the coherent component completely disappears when the incident field is strongly saturating.
[55]S. A. Rautian and I. I. Sobel'man, Zh. Eksp. Teor. Fiz. 41, 456 (1961) [Sov. Phys.-JETP 14, 328 (1962)].
[56]A. Javan, Phys. Rev. 107, 1579 (1957).
[57]P. P. Sorokin, N. S. Shiren, J. R. Lankard, E. C. Hammond, and T. G. Kazyaka, Appl. Phys. Lett. 10, 44 (1967).
[58]B. R. Mollow, Phys. Rev. A 5, 2217 (1974).
[59]S. L. McCall, Phys. Rev. A 9, 1515 (1974).
[60]N. N. Badalyan, V. A. Iradyan, and M. E. Movsesyan, Zh. Eksp. Teor. Fiz. Pis. Red. 8, 518 (1968) [JETP Lett. 8, 316 (1968)].
[61]V. M. Arutyunian, T. A. Papazyan, Yu. S. Chilingaryan, A. V. Karmenyan, and S. M. Sarkisyan, Zh. Eksp. Teor. Fiz. 66, 509 (1974) [Sov. Phys.-JETP 39, 243 (1974)].
[62]D. B. Aleksandrov, A. M. Bonch-Bruevich, V. A. Khodovoi, and N. A. Chigir, Zh. Eksp. Teor. Fiz. Pis. Red. [JETP Lett. 18, 58 (1973)].
[63]A. M. Bonch-Bruevich, V. A. Khodovoi and N. A. Chigir, Zh. Eksp. Teor. Fiz. 67, 2069 (1974) [Sov. Phys.-JETP 40, 1027 (1975)].
[64]See, e.g., Y. R. Shen, Rev. Mod. Phys. 48, 1 (1976) for a recent review and extensive list of references.
[65]T. J. McIlrath and J. L. Carlsten, Phys. Rev. A 6, 1091 (1972).
[66]F. M. Kelly, T. K. Koh, and M. S. Mathur, Can. J. Phys. 52, 795 (1974).
[67]B. W. Woodward, V. J. Ehlers, and W. C. Linberger, Rev. Sci. Instrum. 44, 882 (1973).
[68]R. E. Drullinger (private communication).
[69]P. F. Liao and J. E. Bjorkholm, Phys. Rev. Lett. 34, 1 (1975); Opt. Commun. 16, 392 (1976), and references therein.
[70]D. Prosnitz, D. W. Wildman, and E. V. George, Phys. Rev. A 13, 891 (1976).
[71]R. E. Honig and D. A. Kramer, RCA Rev. 285 (1969).
[72]N. P. Penkin and L. N. Shabanova, Opt. Spectrosc. 25, 446 (1968).
[73]J. M. Farr and W. R. Hindmarsh, J. Phys. B 4, 568 (1971).
[74]N. P. Penkin and L. N. Shabanova, Opt. Spectrosc. 26, 191 (1969).
[75]S. Mukamel and J. Jortner, J. Chem. Phys. 62, 3609 (1974).
[76]J. M. Friedman and R. M. Hochstrasser, Chem. Phys. 6, 155 (1974).
[77]J. O. Berg, C. A. Langhoff, and A. W. Robinson, Chem. Phys. Lett. 29, 305 (1974).
[78]H. Metiu, J. Ross and A. Nitzan, J. Chem. Phys. 63, 1289 (1975).
[79]P. A. Hackett and R. A. Black, Chem. Phys. Lett. 37, 339 (1976).
[80]J. L. Carlsten, J. Phys. B 7, 1620 (1974).
[81]R. Courant and D. Hilbert, *Methods of Mathematical Physics* (Interrcience, New York, 1953), Vol. I, Chap. III.
[82]A. V. Phelps (private communication).

Simultaneous Observations of Stimulated Raman Scattering and Stimulated Collision-Induced Fluorescence

M. G. Raymer[a] and J. L. Carlsten
Joint Institute for Laboratory Astrophysics, University of Colorado and National Bureau of Standards, Boulder, Colorado 80309
(Received 22 August 1977)

We have observed collisional redistribution of laser light scattered by a three-level atom, thallium, in the presence of argon. The two observed spectral components correspond to Raman scattering and collision-induced fluorescence. We have seen the growth of both components from spontaneous to stimulated scattering as the laser intensity is increased. While the gain for the Raman component agrees with theory, the observed gain of the collision-induced fluorescence is over an order of magnitude lower than predicted.

Since the experimental study by Rousseau, Patterson, and Williams,[1] there has been considerable theoretical and experimental interest in the collisional redistribution of near-resonant scattered light.[2-6] For a two-level atom in the presence of collisions, the spectrum of the scattered light at low intensities consists of two components; elastic scattering at the frequency of the incident light, referred to as Rayleigh scattering, and inelastic scattering at the frequency separation of the two levels, which is called collision-induced fluorescence. For a folded three-level system, as shown in Fig. 1, there will also be two emission components near the 2–3 frequency: Raman Stokes scattering at ω_s as well as collision-induced fluorescence at ω_{23}. Mollow[7] has predicted that both of these latter components can have gain. Therefore the possibility exists for simultaneous generation of stimulated emission at both frequencies, ω_s and ω_{23}. In an experiment by Wynne and Sorokin,[8] there are indications that these two processes were occurring but the two components could not be well resolved and the population mechanism for the fluorescence was not determined.

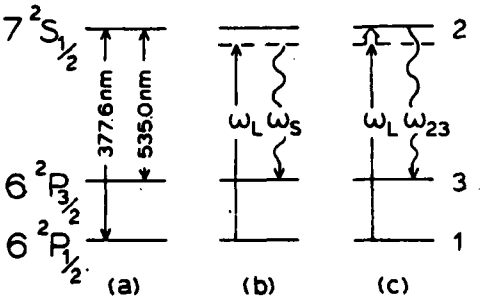

FIG. 1. (a) First three energy levels of thallium. With the laser tuned near the 377.6-nm resonance line, we observed scattered light near the 535.0-nm line. (b) Schematic representation of electron Raman scattering at the Stokes frequency ω_s from an incident laser at frequency ω_L. (c) Schematic representation of collision-induced fluorescence. Collisions (which in our case were Tl-Ar collisions) transferred Tl atoms from the laser-induced virtual level to level 2, resulting in fluorescence at ω_{23}. When level 3 is initially unpopulated, both of these components can become stimulated.

This Letter reports on the spectrally resolved observation of the simultaneous generation of stimulated Raman scattering (SRS) and stimulated collision-induced fluorescence (SCF). Using a dye laser tuned near the 377.6-nm ($6^1P_{1/2}$-$7^2S_{1/2}$) resonance line of Tl, we observed the growth of both of these components (near the 535.0-nm emission line) from the linear (with pump laser) regime, where the scattering is spontaneous, to the exponential regime, where the scattering becomes stimulated. In addition, we have studied the collisional dependence of the SCF and SRS. Recently SRS in vapors and gases has been used by a number of researchers as an efficient means of down-conversion.[9] This study is an effort to understand the effects of collisions on such stimulated scattering.

For a low-intensity monochromatic laser at frequency ω_L, detuned far from resonance, the spontaneous Raman scattering at ω_s has a steady-state intensity (in photons cm^{-3} sec^{-1}) given by[10]

$$I_R = \tfrac{1}{2}N\gamma_N^{23}(\Omega/\Delta)^2, \quad (1)$$

where N is the number density of scattering atoms (in our case Tl atoms), γ_N^{23} is the spontaneous decay rate from level 2 to level 3, $\Delta = \omega_{21} - \omega_L$ is the detuning, $\Omega = \mu E/\hbar$ is the Rabi frequency associated with the incident laser field E, and μ is the dipole matrix element between states 1 and 2. Similarly, the collision-induced fluorescence at ω_{23} has a steady-state intensity

given by[10]

$$I_F = \tfrac{1}{2} N \gamma_B(\Delta)(\Omega/\Delta)^2 \gamma_N^{23}/\gamma_N, \tag{2}$$

where $\gamma_B(\Delta)$ is the rate of quasielastic collisions (in our case Tl-Ar collisions) which make up the energy difference Δ needed to produce an atom in level 2 and $\gamma_N = \gamma_N^{21} + \gamma_N^{23}$. We have written the collision rate as a function of the detuning to account for the non-Lorentzian dependence outside the impact regime.[11] Effects of spatial degeneracy have not been included in Eqs. (1) and (2).

Mollow[7] has predicted that both I_R and I_F will have gain when level 3 is initially unpopulated. For laser intensities where $\Omega^2 < \Delta^2$, we expect the gain of the Raman scattering at ω_s to be

$$g_{SRS} = \frac{\pi}{2} N \frac{c^2}{\omega_{23}^2} \frac{\gamma_N^{23}}{\gamma_R} \frac{\Omega^2}{\Delta^2}, \tag{3}$$

where γ_R is a measure of the Raman linewidth (to be discussed later). For the collision-induced fluorescence at ω_{23}, the gain is expected to be

$$g_{SCF} = \frac{\pi}{2} N \frac{c^2}{\omega_{23}^2} \frac{\gamma_B(\Delta)}{[\gamma_D/\pi U]} \frac{\Omega^2}{\Delta^2}. \tag{4}$$

Here γ_D is the Doppler linewidth and U is the peak height of the normalized Voight profile,[12] both for the 2–3 transition. One can think of $\gamma_D/\pi U$ as an effective width for the Doppler-plus-collision-broadened transition, 2–3.

Expressions (1) and (2) for the spontaneous emission and Eqs. (3) and (4) for the gain can be used with simple photon propagation equations[13] to solve for the single-pass stimulated outputs (in photons $\sec^{-1}$) of the SRS and SCF collected by a solid angle α_2:

$$I_{SRS} = (I_R A \alpha_1/4\pi g_{SRS})[\exp(g_{SRS} L) - 1] + I_R A(\alpha_2 - \alpha_1)L/4\pi \tag{5}$$

and

$$I_{SCF} = (I_F A \alpha_1/4\pi g_{SCF})[\exp(g_{SCF} L) - 1] + I_F A(\alpha_2 - \alpha_1)L/4\pi, \tag{6}$$

where A and L are the area and length of the excitation region, α_1 is the solid angle formed by the excitation region, and it is assumed that $\alpha_2 \cdot \alpha_1$. In both equations, the second term accounts for the spontaneous emission which exits from the sample outside of the gain region, but which still enters our collection angle α_2. We note that Eqs. (5) and (6) predict that both the SRS and SCF will initially have a linear dependence on laser intensity when spontaneous scattering is dominant, but will eventually grow exponentially when the scattering becomes stimulated. Effects of saturation or population depletion have not been included.

The apparatus used in this experiment is similar to that described in detail by Carlsten, Szöke, and Raymer.[2] A tunable dye laser, pumped by an N_2 laser, was tuned near the $6^2P_{1/2}$-$7^2S_{1/2}$ resonance line of Tl at 377.6 nm. The dye laser had a pulse duration of 10 nsec, a spectral width of 0.03 nm, and an energy of 50 μJ inside the excitation region. The beam was focused to 330 μm diam giving a power density of 2 MW/cm^2 inside an oven containing 0.1 Torr of Tl vapor and 5 to 80 Torr of Ar buffer gas. The oven input and output windows were put at an angle to avoid back-reflections, which would affect the growth of the stimulated emission. The length of the Tl vapor region was ~2.5 cm. The emission region was then imaged onto the slit of a monochromator of 0.06 nm resolution with an $f/10$ optical system that was capable of viewing the emission at right angles to the laser beam or along the laser beam direction.

When the incident laser is tuned on resonance, only one spectral component, centered at ω_{23}, is observed in the emission. We have studied this emission at 535 nm in both the side and forward directions when the laser was tuned to the 377.6-nm resonance line of Tl. At low laser intensities we observed that both the side and forward emissions were linear in laser intensity. Above ~10 kW/cm^2, the forward emission became stimulated and eventually saturated, allowing a maximum photon conversion efficiency of 60%.

In order to study the collisional effects upon this stimulated scattering, we tuned the laser 0.14 nm to the red side of resonance. We were then able to resolve spectrally the Raman emission at ω_s and the collision-induced fluorescence at ω_{23}. The dependence of these two resolved components on laser intensity is shown in Fig. 2. The Ar pressure for these data was 20 Torr.

In the side direction [Fig. 2(b)] both the Raman scattering I_R and collision-induced fluorescence I_F were linear in laser intensity. By measuring the ratio I_F/I_R, we obtained an absolute measure of the collisional redistribution function. From Eqs. (1) and (2), this ratio is expected to be

$$I_F/I_R = \gamma_B(\Delta)/\gamma_N. \tag{7}$$

Using[14] $\gamma_N = 6.7 \times 10^7$ rad $\sec^{-1}$ and our measured value for I_F/I_R we obtain γ_B(0.14 nm to red) = 7.4

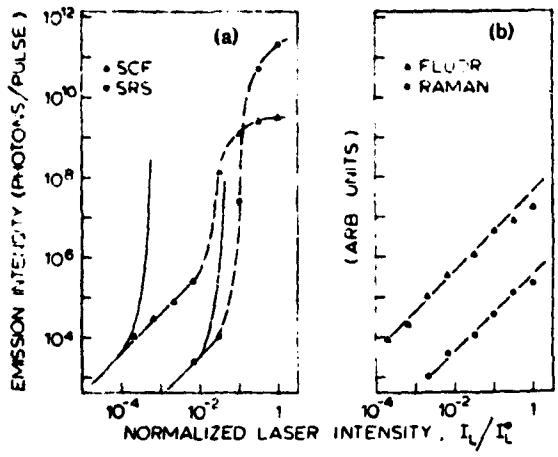

FIG. 2. Dependence of Raman scattering and collision-induced fluorescence on laser intensity when the laser was tuned off resonance (0.14 nm to the red side of the 377.6-nm resonance line). (a) Growth of the stimulated Raman scattering (SRS) and stimulated collision-induced fluorescence (SCF) from spontaneous, linear scattering in the forward direction. The solid curves are theoretical curves obtained from Eqs. (5) and (6) for the SRS and SCF, respectively. (b) Spontaneous, linear scattering in the side direction for comparison. The laser intensity I_L^0 was 2 MW/cm^2.

$\times 10^9$ rad sec^{-1}. This is a factor of 3 larger than the value determined by the emission line-shape measurements of Cheron, Scheps, and Gallagher.[15] According to recent results of Nienhuis and Schuller,[11] we expect the two experiments (collisional redistribution and collisional line broadening) to give the same value for $\gamma_R(\Delta)$ over the experimental range that we studied. The existing discrepancy may be due to the transient nature of our experiment as well as neglect of degeneracy in Eq. (7).

In the forward direction, as in the side direction, the emission is initially linear at low intensities. However, eventually both the Raman emission and the collision-induced fluorescence grow exponentially when the scattering becomes stimulated, and at still higher intensity saturation occurs. Using Eqs. (5) and (6) multiplied by the pulse duration we calculated the expected exponential growth for the Raman scattering and collision-induced fluorescence. The results are shown as the solid curves in Fig. 2(a). The vertical scale was considered a free parameter, but agreed to within a factor of 4 with an absolute-calibration estimate. The laser profile was taken to be uniform in intensity over the 300-μm diam of the excitation region. It is important to note that in calculating the SRS gain we have used the result of Akhmanov, D'yakov, and Pavlov[16] that, for forward SRS in a dispersionless medium, a broad-band laser has the same gain as a monochromatic laser. This is because the intensity variations of the Stokes emission follow those of the pump laser as the two pulses travel with the same velocity through the medium. Thus for γ_R we have used the Raman linewidth (which is predominantly the Doppler width for the 1–3 separation). This results in an SRS gain which is 240 times larger than that calculated by taking γ_R equal to the laser linewidth. We see that while the predicted initial exponential growth of the Raman scattering is quite close to our experimental results, the gain for the collision-induced fluorescence is more than an order of magnitude less than predicted by Eq. (6). We do not know the reason for the discrepancy, but problems may arise from use of the steady-state theory as well as from the assumption of a constant spatial profile.

In order to study further the predictions of Eqs. (5) and (6), we measured the dependence of both the SRS and SCF as a function of Ar pressure. Profiles similar to those in Fig. 2(a) were taken at 5, 20, and 80 Torr of Ar buffer gas, at both ± 0.14 nm detuning. While the SRS showed no pressure dependence, the SCF was highly pressure dependent, as expected from the theoretical discussion. In particular, the collision-induced fluorescence was linear in Ar pressure at low intensities, while the high-intensity behavior is described by noting that the SCF gain was roughly linear in Ar pressure. Thus, curves calculated from Eq. (6), but with the gain decreased by an overall factor of 30, were in good agreement with these data. These results show that the experimental dependence of the SRS and SCF on the collision rate was in accord with theory.

The authors wish to thank N. Bloembergen, Y.-R. Shen, P. P. Sorokin, and A. Szöke for useful discussions on stimulated Raman scattering. In addition the authors acknowledge the helpful comments and suggestions of J. Cooper and W. C. Lineberger.

This work was supported by the Office of Naval Research under Contract No. N00014-76-C-0611 and by the National Science Foundation under Grant No. MPS72-05169, both through the University of Colorado, and by the Lawrence Livermore Laboratory under P. O. 4353803 through the University of California.

[a]Also at the Department of Chemistry, University of Colorado, Boulder, Colo. 80309.

[1]D. L. Rousseau, A. D. Patterson, and P. F. Williams, Phys. Rev. Lett. 34, 1306 (1975).

[2]J. L. Carlsten, A. Szöke, and M. G. Raymer, Phys. Rev. A 15, 1029 (1977), and references therein.

[3]E. Courtens and A. Szöke, Phys. Rev. A 15, 1588 (1977).

[4]C. Cohen-Tannoudji and S. Reynaud, J. Phys. B 10, 345, 365 (1977).

[5]J. Liran, L. A. Levin, G. Erez, and J. Jortner, Phys. Rev. Lett. 38, 390 (1977).

[6]L. Vriens, J. Appl. Phys. 48, 653 (1977).

[7]B. M. Mollow, Phys. Rev. A 8, 1949 (1973).

[8]J. J. Wynne and P. P. Sorokin, J. Phys. B 8, L37 (1975).

[9]See for instance, N. Djeu and R. Burnham, Appl. Phys. Lett. 30, 473 (1977).

[10]A. Omont, E. W. Smith, and J. Cooper, Astrophys. J. 175, 185 (1972).

[11]D. L. Huber, Phys. Rev. 187, 392 (1969); G. Nienhuis and F. Schuller, to be published.

[12]D. Mihalas, *Stellar Atmospheres* (Freeman, San Francisco, 1970).

[13]J. J. Wynne and P. P. Sorokin, in *Topics in Applied Physics*, edited by Y.-R. Shen (Springer, Berlin, 1977), Vol. 16.

[14]M. Norton and A. Gallagher, Phys. Rev. A 3, 915 (1971).

[15]B. Cheron, R. Scheps, and A. Gallagher, Phys. Rev. A 15, 651 (1977).

[16]S. A. Akhamanov, Yu. E. D'yakov, and L. I. Pavlov, Zh. Eksp. Teor. Fiz. 66, 520 (1974) [Sov. Phys. JETP 39, 249 (1974)].

J. Phys. B: Atom. Molec. Phys., Vol. 11, No. 16, 1978. Printed in Great Britain

LETTER TO THE EDITOR

Self-broadening of the Tl 377·6 nm resonance line

Goran Pichler† and J L Carlsten
Joint Institute for Laboratory Astrophysics, University of Colorado and National Bureau of Standards, Boulder, Colorado 80309, USA

Received 19 June 1978

Abstract. We report preliminary studies on the self-broadening of the 377·6 nm thallium line. In the short wavelength wing we observe asymmetries and a satellite at about 377·1 nm. In the long wavelength quasi-static wing we clearly observe the transition from the Lorentzian to the van der Waals type wing.

In recent studies of self-broadening of the quasi-static wings of the resonance lines in the alkali elements, satisfactory agreement has been obtained between experiment (Niemax and Pichler 1975) and theory (Movre and Pichler 1977). In this letter we describe an extension of these studies to thallium, a group three element which is essentially also a one-electron system. Some early studies of the spectra of thallium vapour in emission were made by Hamada (1931). Since the ground state of Tl is a p level and the first excited state is an s level (see figure 1), we expected similarities with the alkalis in the self-broadening of the resonance lines. In particular, in studying the $6^2P_{1/2}$–$7^2S_{1/2}$ transition at 377·6 nm in thallium we expected that the main results from the study of the alkali resonance lines could be applied. The similarity arises since the interaction potential curves emerging from the $6^2P_{1/2} + 7^2S_{1/2}$ level are similar to the potential curves for the $ns\ ^2S_{1/2} + np\ ^2P_{1/2}$ resonance levels of the alkalis. However, one essential difference is very apparent—the very large spin–orbit interaction in the ground levels of thallium. Initially we expected that the inner wing satellites, observed near the heavy alkali resonance line doublets, would occur very far into the line wings, based on figure 3 in the paper of Movre and Pichler (1977). However, no satellite in the far blue wing spectrum of the 377·6 nm line of thallium was observed. Analysis has shown that this is due to the fact that the oscillator strength of the 377·6 nm line is very small ($f = 0{\cdot}14$), which together with the short wavelength, results in a smaller interaction constant for the resonance interaction expected by analogy to the alkalis ($C_3 \propto f\lambda$). Instead we observed the blue satellite structure much closer to the centre of the line. This letter reports our preliminary findings.

In our experiment we used a cw tungsten–halogen lamp with current stabilisation to study the absorption profile of the 3776 Å line of Tl. The light beam was collimated and sent through a heat-pipe oven having an approximate 10 cm column of pure thallium vapour. Argon was used as a buffer gas to protect the quartz windows from the hot thallium vapour. The working temperature range was in the interval

† Visiting Fellow, 1977–8. Permanent address: Institute of Physics, PO Box 304, 41001 Zagreb, Yugoslavia.

0022-3700/78/0016-9483 $01.00

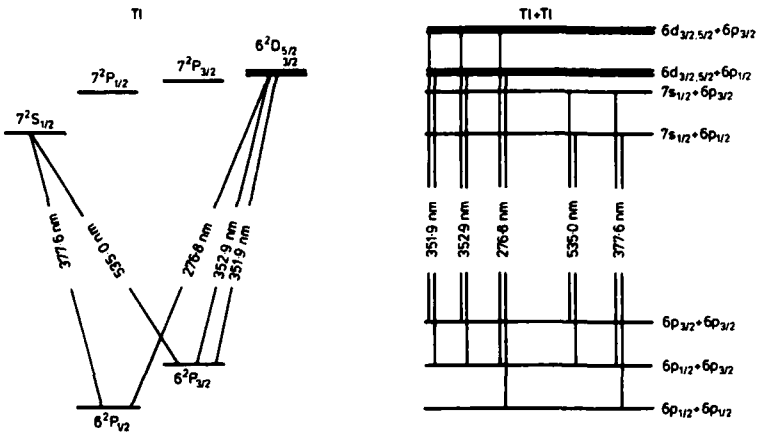

Figure 1. Partial term diagram for (*a*) Tl atom and (*b*) for Tl–Tl collisional molecule.

between 900 and 1100°C, in which the thallium vapour pressure was changed by means of changing the argon pressure in the interval of 1 and 20 Torr. In order to determine the centre of the strongly absorbed 377·6 nm line, we used a low current Tl emission lamp. During a spectral scan of the 377·6 nm line, the absorption in the heat-pipe oven was saturated within the region of about 0·05 nm around the line centre. In this spectral region a folding mirror was turned to allow the light from the Tl emission lamp to enter the monochromator and mark the centre of the resonance line. The light coming out from the absorption vessel and the Tl emission lamp was focused on the entrance slit of a scanning monochromator (McPherson, Model EU-700) with resolution of 0·05 nm. A photomultiplier with an S-20 photocathode was used for the light detection. The signal was amplified by means of the lock-in amplifier and recorded on an XY recorder.

In the preliminary results reported here we have not measured the length of the thallium vapour column, which varied when we changed the electrical power into the oven or the argon pressure. Hence the data have been analysed in terms of optical depth $\tau = kL$ and therefore have no absolute values of the absorption coefficient†. A typical absorption profile is shown in figure 2 for 6·3 Torr of thallium pressure. About 0·5 nm from the line centre, toward shorter wavelengths, a broad shoulder appears, beyond which there is a sharp decrease of absorption. We believe this satellite is formed by the 0_g^+ state as discussed below. Even closer to the line centre the red wing is more absorbed than the blue wing. However, our instrumental width precluded any detailed measurements within the region of the line centre. In order to verify that the oven was running in a heat-pipe mode and that the broadening was due to Tl-Tl collisions, and not Tl-Ar collisions we increased the argon pressure to the point where the effect of the Tl-Ar collisions could be seen. We found that the absorption lineshape was then consistent with a previous study by Cheron *et al* (1976, 1977).

We have analysed our data by plotting the logarithm of optical depth τ against the logarithm of the wavelength separation $\Delta\lambda$ from the line centre. Different sets

† In order to obtain k N^2 (cm^{-1}) values (absorption coefficient divided by the square of the particle density) it is necessary to multiply our relative τ values given in figure 3 by a factor of $(1{\cdot}6 \pm 0{\cdot}5) \times 10^{-35}$, which was obtained by a rough estimate of $L = 10$ cm.

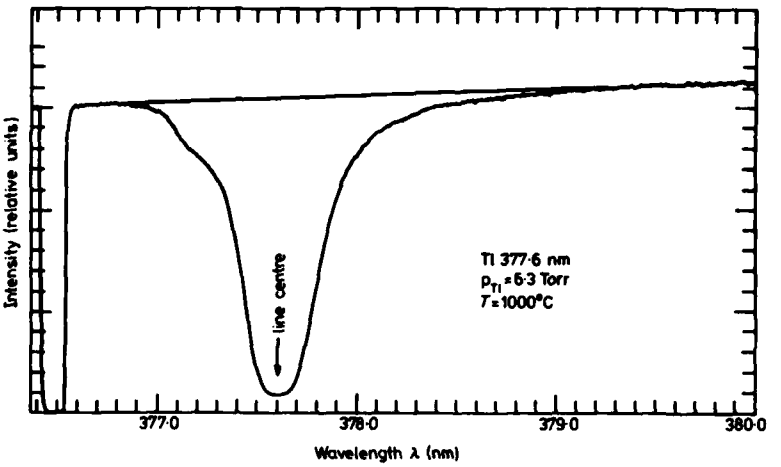

Figure 2. Typical absorption profile of the Tl 377·6 nm line. Arrow shows the line centre determined by the emission line. The temperature was 1000°C and the pressure of the thallium vapour was 6·3 Torr.

of data were put together by sliding along the log τ axis. Figure 3 shows the resulting diagram. The satellite in the blue wing at 0·5 nm is clearly seen. Since an exponential fall-off is expected after a satellite (Sando and Wormhoudt 1973, Szudy and Baylis 1975, Carrington and Gallagher 1974) we also analysed the optical depth beyond

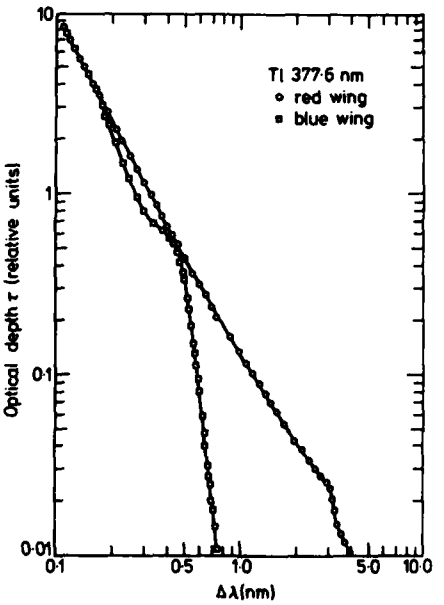

Figure 3. Absorption lineshape in terms of the logarithm of the optical depth versus the logarithm of the wavelength separation from the line centre of the 377·6 nm thallium line.

the satellite at 0·5 nm in terms of a semi-logarithmic plot (log τ, $\Delta\lambda$). Exponential behaviour was verified up to 0·8 nm at a thallium pressure of 20 Torr.

Careful study of figure 3 reveals that the red wing in the region from 0·1 to 0·5 nm from the line centre is approximately Lorentzian [$\tau \sim (\Delta\lambda)^{-2}$] and then it continuously converges to a van der Waals type wing ($\tau \sim (\Delta\lambda)^{-1.5}$, see e.g. Mihalas 1978) up to 381 nm where a red satellite appears. This change from Lorentzian to van der Waals dependence is indicative of the importance of the van der Waals type interaction in the shape of the resonance potential curves. As will be discussed below this van der Waals interaction is also of great importance in the formation of the satellite in the blue wing.

In figure 4 we have reproduced the resonance interaction potential curves (broken curves) emerging from the $7^2S_{1/2} + 6^2P_{1/2}$ level in a thallium collision-induced molecule (Fontana 1962, Movre and Pichler 1977) with the following C_3 interaction constants:

$$C_3(0_g^+) = -C_3(0_u^+) = \frac{4C}{9} \tag{1}$$

$$C_3(1_u) = -C_3(1_g) = \frac{2C}{9} \tag{2}$$

$$C_3(0_g^-) = C_3(0_u^-) = 0 \tag{3}$$

where $C = e^2|\langle 0|r|1\rangle|^2$ and

$$|\langle 0|r|1\rangle|^2 = \frac{9hf\lambda}{8\pi^2 mc}. \tag{4}$$

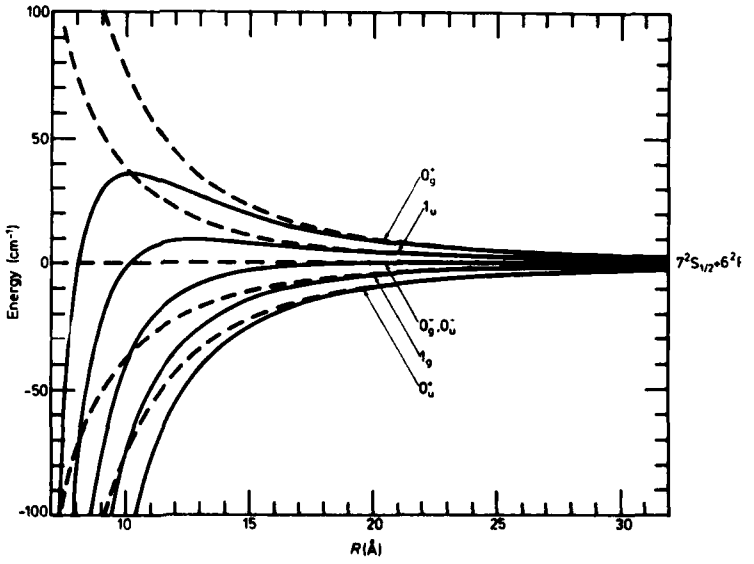

Figure 4. Resonance interaction curves emerging from the $7^2S_{1/2} + 6^2P_{1/2}$ molecular level (broken curves) and the bending of these curves caused by the van der Waals interaction (full curves).

Using an *f*-value of 0·14 (Gallagher and Lurio 1964, Penkin *et al* 1973) for the Tl 377·6 nm line we obtain interaction constants (in rad s^{-1} cm^3) for the repulsive states as follows

$$C_3(0_g^+) = 14{\cdot}2 \times 10^{-9} \tag{5}$$

and

$$C_3(1_u) = 7{\cdot}1 \times 10^{-9}. \tag{6}$$

The full curves in figure 4 show how the resonance potential curves bend down under the influence of the attractive van der Waals interaction. In this way the two maxima $H(0_g^+)$ and $H(1_u)$ are formed. We took the wavelength separation of $0{\cdot}5 \pm 0{\cdot}2$ nm as a position where the satellite has approximately 65% of its peak intensity (Carrington and Gallagher 1974, and references therein), which corresponds to the maximum H in the 0_g^+ potential curve. We assume that this maximum is formed by the competition of the R^{-3} and R^{-6} terms in the potential expansion (we also assume implicitly that the ground state is flat in this long-range region):

$$\Delta\omega(0_g^+) = \frac{C_3}{R^3} - \frac{C_6}{R^6}. \tag{7}$$

By means of the condition for an extremum

$$\frac{d(\Delta\omega)}{dR} = 0 \tag{8}$$

we can obtain both the C_6 constant and the internuclear separation, where the extremum occurs, by means of the following relations:

$$\Delta\omega_{max} = H = C_3^2/4C_6 \tag{9}$$

and

$$R_{max} = (2C_6/C_3)^{1/3}. \tag{10}$$

From (9), using the C_3 constant from (5) and $\Delta\lambda_{sat} = 0{\cdot}5 \pm 0{\cdot}02$ nm for the maximum, we obtain (in rad s^{-1} cm^6)

$$C_6 = (7{\cdot}6 \pm 0{\cdot}3) \times 10^{-30}$$

and from (10),

$$R_{max}(0_g^+) = 10{\cdot}2 \text{ Å}.$$

We have used the same C_6 constant in order to estimate the position of the maximum $H(1_u)$. The analysis indicates that it should appear at $\Delta\lambda = 0{\cdot}12$ nm in the blue wing (with $R_{max} = 12{\cdot}8$ Å).

Unfortunately, the resolution of our monochromator did not allow us to resolve the spectral region where this satellite should appear, but we have observed the red asymmetry in the wings outside this region, which would occur due to the exponential fall-off beyond the satellite.

We have estimated the limit between the quasi-static and impact approximations using both the C_3 and C_6 constants. We found that the region around $\Delta\lambda = 0{\cdot}1$ nm is still close to the edge of the impact region, a fact which will broaden the satellite related to the maximum $H(1_u)$. An additional broadening of the satellite could come from the mixing among near-by states in the $7^2S_{1/2} + 6^2P_{1/2}$ manifold.

Using the same continuum background source and quartz optics we have also made several scans across the Tl 276·8 nm line ($6^2D_{3/2}$–$6^2P_{1/2}$ transition) and we have observed one blue satellite even closer to the line centre at about $\Delta\lambda = 0{\cdot}18$ nm. Beyond this satellite the steep decrease of the absorption was observed and a very extended red wing. We have not studied this line in detail since there is no analogous line in the resonance lines of the alkali atoms. We intend to extend calculations of the potential curves for this line in the future.

We would like to point out one major difficulty encountered here in the thallium self-broadened resonance lines, which is not present in alkali cases. In figure 1 we have reproduced a partial term diagram of atomic thallium and a diatomic thallium collisional molecule. All strong resonance lines are marked in both diagrams. However we immediately see that all atomic lines can be generated in the diatomic molecule from two distinctively different molecular levels. If both transitions could occur at the same time then one spectral line would bear information about the splitting structure of all four levels involved. In absorption measurements this ambiguity is easily avoidable since thermal population of the $6^2P_{3/2}$ level at temperatures of about 1000°C is still relatively low. Nevertheless we have observed all five resonance lines in absorption, but the 535·0 nm, 351·9 nm, and 352·9 nm lines have not been absorbed enough to allow broadening studies in the quasi-static wings.

The authors acknowledge the helpful comments of A Gallagher. This work was partially supported by National Science Foundation Grant No PHY76-04761 and Office of Naval Research Contract No N00014-76-C-0611, both through the University of Colorado.

References

Carrington C G and Gallagher A 1974 *Phys. Rev.* A **10** 1464–73
Cheron B, Scheps R and Gallagher A 1976 *J. Chem. Phys.* **65** 326–35
——1977 *Phys. Rev.* A **15** 651–60
Fontana P P 1962 *Phys. Rev.* **125** 1597–602
Gallagher A and Lurio A 1964 *Phys. Rev.* **136** A87–105
Hamada H 1931 *Phil. Mag.* **12** 50–67
Mihalas D 1978 *Stellar Atmospheres* (San Francisco: Freeman) p 291
Movre M and Pichler G 1977 *J. Phys. B: Atom. Molec. Phys.* **10** 2631–8
Niemax K and Pichler G 1975 *J. Phys. B: Atom. Molec. Phys.* **8** 179–84
Penkin N P, Ruzov V P and Shabanova L N 1973 *Opt. Spektrosk.* **34** 1017–9 (1973 *Opt. Spectrosc.* **34** 588–9)
Sando K M and Wormhoudt J C 1973 *Phys. Rev.* A **7** 1889–98
Szudy J and Baylis W E 1975 *J. Quant. Spectrosc. Radiat. Transfer* **15** 641–68

J. Phys. B: Atom. Molec. Phys., Vol. 12, No. 4, 1979. Printed in Great Britain

LETTER TO THE EDITOR

Comparison of collisional redistribution and emission line shapes

M G Raymer†, J L Carlsten‡ and G Pichler§

Joint Institute for Laboratory Astrophysics, National Bureau of Standards and University of Colorado, Boulder, Colorado 80309, USA

Received 29 November 1978

Abstract. We have studied collisional redistribution of near-resonance radiation in thallium vapour caused by collisions with argon buffer gas. We spectrally resolved electronic Raman scattering and collision-induced fluorescence, both to the weakly populated metastable $6^2P_{3/2}$ level in thallium. Thus we partially avoided the problem with radiative trapping encountered in previous experiments. By measuring the total collision-induced fluorescence as a function of the incident laser frequency, we obtained the absolute collisional redistribution line shape. We have compared this line shape with the emission line shape measured by Cheron, Scheps and Gallagher.

The combined effect of collisional interaction and radiative interaction upon an atom in a vapour continues to be a subject of interest (Nayfeh *et al* 1977, Ballagh and Cooper 1977, Raymer and Carlsten 1977, Voslamber and Yelnik 1978). A question of basic importance is: what is the spectrum of the scattered radiation when monochromatic light from a laser is incident upon a vapour in which collisions are present? Although it is intuitively expected that this spectrum, known as the redistribution function, is related in some manner to the absorption and emission profiles obtained from conventional studies, it is not known what the explicit relationship is in the general case. At present there are several theoretical treatments which address this problem (Cooper 1978, Voslamber and Yelnik 1978, Nienhuis and Schuller 1977, Huber 1969). In this letter we present the results of a redistribution experiment and compare them to those of an emission experiment by Cheron *et al* (1977).

To describe the redistribution process we refer to figure 1, which shows the three lowest energy levels of atomic thallium. A low-intensity laser is incident at frequency ω_L, near the $^2P_{1/2}$–$^2S_{1/2}$ resonance line and emission occurs at four frequencies: Rayleigh scattering at ω_{RAY}, electronic Raman scattering at ω_{RAM} and collision-induced fluorescence at both ω_{21} and ω_{23}. The collisions can be thought of as providing the energy needed to transfer population from the laser-induced virtual level (broken line) to the real level 2. The process can also be viewed in a molecular picture as in figure 2, which shows the potential curves for a Tl–Ar collision (Cheron *et al* 1977). The

† Also at the Department of Chemistry, University of Colorado, Boulder, Colorado 80309, USA.
‡ Present address: Los Alamos Scientific Laboratory, University of California, Los Alamos, New Mexico 87545, USA.
§ Visiting Fellow, 1977–78. Permanent address: Institute of Physics, PO Box 304, 41001 Zagreb, Yugoslavia.

0022-3700/79/040119+06$01.00

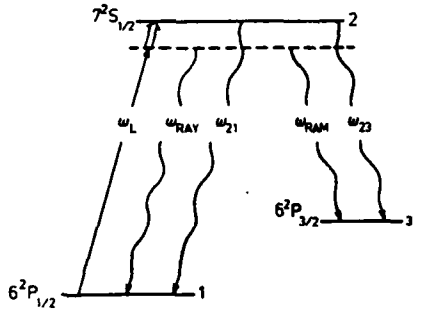

Figure 1. The three lowest levels of atomic thallium. A low-intensity laser of frequency ω_L incident on a vapour of three-level atoms generally produces four components in the scattered spectrum: Rayleigh scattering at $\omega_{RAY}(=\omega_L)$, electronic Raman scattering at $\omega_{RAM}(=\omega_L-\omega_{31})$ and collision-induced fluorescence at both ω_{21} and ω_{23}.

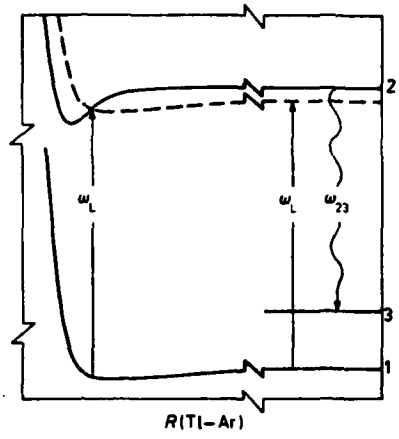

Figure 2. Potential curves for Tl–Ar (Cheron *et al* 1977), showing collisional redistribution, viewed as absorption by the quasi-molecule formed during the collision. The excited Tl atom then radiates at ω_{21} or ω_{23} after the collision is completed.

interaction with an Ar perturber causes the $Tl^2S_{1/2}$ level to come into resonance with the laser frequency (for the red detuning shown) at some internuclear separation, allowing absorption of a photon and creating an excited quasi-molecule. Usually the quasi-molecule has enough internal kinetic energy to fly apart into a ground-state Ar and an excited Tl atom, which can then emit a photon of frequency ω_{23} or ω_{21}. This type of collision has been called a dephasing collision or an elastic (or quasi-elastic) collision (Omont *et al* 1972, Mollow 1977).

The theory of light scattering, in the presence of collisions, is well understood at low intensities when the incident and scattered light have frequencies very close to the line centre (in the impact region). In this region the line shape is Lorentzian, regardless of the form of the interaction potentials. Referring to figure 1, the normalised absorption or emission profile for the 1–2 transition is given by Omont *et al* (1972) as

$$f(\Delta_1)=\frac{(\gamma_E+\gamma_N)/\pi}{\Delta_1^2+(\gamma_E+\gamma_N)^2} \tag{1}$$

where $2\gamma_N=2\gamma_N^{21}+2\gamma_N^{23}$ is the sum of the spontaneous decay rates from level 2 to levels 1 and 3, $2\gamma_E$ is the rate of elastic collisions, and $\Delta_1=\omega_1-\omega_{21}$ is the detuning of the incident light from resonance.

In a redistribution experiment, the differential cross section (in units $cm^2\ rad^{-1}\ s$) for absorbing a photon with frequency ω_1 and emitting one with frequency ω_2 (integrated over outgoing direction and polarisation) can be written as (Omont *et al* 1972, Ballagh and Cooper 1977):

$$\frac{d}{d\omega_2}\sigma(\omega_1,\omega_2)=(2\pi^2e^2f/mc)f(\omega_1-\omega_{21})P(\omega_1,\omega_2) \tag{2}$$

where

$$P(\omega_1,\omega_2)=\frac{\gamma_N^{21}}{\gamma_N}\left(\frac{\gamma_N}{\gamma_E+\gamma_N}\delta(\omega_2-\omega_1)+\frac{\gamma_E}{\gamma_E+\gamma_N}f(\omega_2-\omega_{21})\right)$$
$$+\frac{\gamma_N^{23}}{\gamma_N}\left(\frac{\gamma_N}{\gamma_E+\gamma_N}\delta(\omega_2-\omega_1+\omega_{31})+\frac{\gamma_E}{\gamma_E+\gamma_N}f(\omega_2-\omega_{23})\right) \tag{3}$$

and $f(\omega)$ is always the function in equation (1). Here $P(\omega_1,\omega_2)$ is the redistribution function. Given that a photon of frequency ω_1 has been absorbed, $P(\omega_1,\omega_2)$ gives the probability that one will be emitted at ω_2. Since we have ignored quenching collisions, we have $\int P(\omega_1,\omega_2)\,d\omega_2=1$.

The terms in equation (3) proportional to γ_N^{21} describe the emission near ω_{21}: the Rayleigh scattering is a delta function at $\omega_1(=\omega_L)$ while the collision-induced fluorescence is a Lorentzian centred at ω_{21}. Similarly, the terms proportional to γ_N^{23} describe the Raman scattering at ω_{RAM} and fluorescence centred at ω_{23}. If equation (2) is integrated over both the incident frequency ω_1 and the scattered frequency ω_2 one obtains the usual result for the total cross section $\sigma_{TOT}=2\pi^2e^2f/mc$, where f is the absorption oscillator strength for the 1–2 transition (Mihalas 1970). In order for equation (3) to be valid, the broadening of levels 1 and 3 must be negligible compared to that of level 2. When the incident light is far off resonance ($\Delta_1\gg\gamma_E+\gamma_N$), the four components can be spectrally resolved and integrated separately over ω_2 to give a cross section (in units of cm^2) for each process;

$$\sigma_{RAY}=\sigma_{TOT}(\gamma_N^{21}/\pi\Delta_1^2) \qquad \text{Rayleigh} \tag{4a}$$
$$\sigma_F^{21}=\sigma_{TOT}(\gamma_N^{21}/\gamma_N)(\gamma_E/\pi\Delta_1^2) \qquad \text{2–1 fluorescence} \tag{4b}$$
$$\sigma_{RAM}=\sigma_{TOT}(\gamma_N^{23}/\pi\Delta_1^2) \qquad \text{Raman} \tag{4c}$$
$$\sigma_F^{23}=\sigma_{TOT}(\gamma_N^{23}/\gamma_N)(\gamma_E/\pi\Delta_1^2) \qquad \text{2–3 fluorescence.} \tag{4d}$$

These cross sections can be used to calculate the scattered intensity; for example, the 2–3 fluorescence intensity I_F^{23} (in units of photons/cm^3/s) is equal to $N_{Tl}\sigma_F^{23}I_L$, where N_{Tl} is the atomic thallium density (cm^{-3}) and I_L is the incident laser intensity (in units of photons/cm^2/s). Thus the profile for collisionally redistributed fluorescence is Lorentzian in the impact region.

For larger detunings, outside the impact region, the situation is not completely understood. It is known that the absorption (emission) profile becomes non-Lorentzian, and Cooper (1978) has shown it can be obtained by replacing γ_E in equation (1) by $\gamma_E(\Delta_1)$

$$f(\Delta_1)=\frac{(\gamma_E(\Delta_1)+\gamma_N)/\pi}{\Delta_1^2+(\gamma_E(\Delta_1)+\gamma_N)^2} \tag{5}$$

where $\gamma_E(\Delta_1)$ is a frequency-dependent collision rate. It has been observed (Carlsten *et al* 1977) that the redistribution profile also becomes non-Lorentzian. Cooper (1978) has predicted that, when collisions dominate the spontaneous emission ($\gamma_E(\Delta_1)\gg\gamma_N$), the non-impact redistribution profile may also be obtained by replacing γ_E (in equation (4*d*)) by $\gamma_E(\Delta_1)$:

$$\sigma_F^{23}=\sigma_{TOT}\frac{\gamma_N^{23}}{\gamma_N}\frac{\gamma_E(\Delta_1)}{\pi\Delta_1^2}. \tag{6}$$

The condition $\gamma_E(\Delta_1) \gg \gamma_N$ ensures that the redistributed light comes from uncorrelated absorption and emission events and thus will be isotropic and unpolarised. When this condition is not upheld, the angle- and polarisation-resolved redistribution cross section should, in principle, contain more information about the mixing of the atomic states during the collision than the absorption cross section (Cooper 1978). When $\gamma_E(\Delta_1) \gg \gamma_N$, the absorption (emission) profile, equation (5), can be approximated in the line wing as

$$f(\Delta_1) \simeq \frac{\gamma_E(\Delta_1)}{\pi \Delta_1^2}. \tag{7}$$

Thus when collisions dominate spontaneous emission, the redistribution profile (6) and the absorption (emission) profile (7) are predicted to have the same shape.

To study the relation between emission and redistribution we chose the Tl–Ar system for two reasons: it has already been studied by Cheron *et al* (1977) using the emission technique, and it avoids some of the experimental problems associated with radiative trapping. In the experiment by Cheron *et al*, the Tl resonance line was excited at its line centre by a spectrally narrow light source and the spectrum of fluorescence in the line wings was measured. Since in that experiment collisions dominated spontaneous emission, the emission profile they observed was essentially that in equation (7). In a previous study (Carlsten *et al* 1977) we observed redistribution in a two-level atom Sr, but the fluorescence was heavily trapped, making an absolute measurement of $\gamma_E(\Delta_1)$ difficult. By detecting fluorescence at ω_{23} in Tl we avoid part of this problem (see later in the discussion), as the $^2P_{3/2}$ level is essentially unpopulated at our operating temperature.

The apparatus used in this experiment is shown in figure 3 and is similar to that described by Carlsten *et al* (1977). A dye laser, pumped by an N_2 laser, was tuned in the region of the $6^2P_{1/2}$–$7^2S_{1/2}$ Tl resonance line at 377·6 nm. Emission was observed near the $7^2S_{1/2}$–$6^2P_{3/2}$ line at 535·0 nm. The dye laser had a pulse duration of 10 ns, a spectral width of 0·03 nm and an energy of about 50 μJ. The beam was directed into an oven at 1000 K containing 0·1 Torr of Tl vapour and 20 Torr of Ar buffer gas. The column length of Tl was approximately 10 cm. As our present oven did not allow observation at right angles to the laser beam, we chose to detect back-scattered light by use of a dichroic mirror, which transmitted the UV laser light, but reflected the green fluorescence signal. A cut-off filter was also inserted to further reject laser light. The fluorescence was then focused onto the slits of a monochromator of 0·06 nm resolution with an *f*/10 optical system. The signal from a photomultiplier was boxcar averaged and the spectral profiles recorded on a chart recorder.

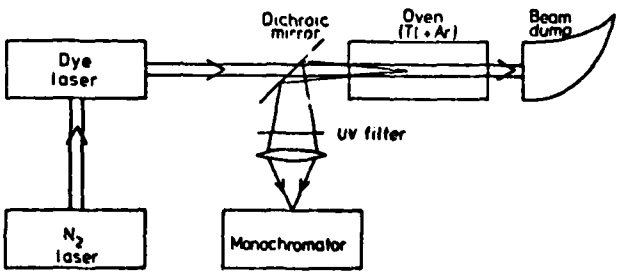

Figure 3. Experimental apparatus.

The ratio of fluorescence intensity, I_F^{23}, to Raman intensity, I_{RAM}, was measured at each incident laser frequency and the quantity $(I_F^{23}/I_{RAM})(\gamma_N/\pi\Delta_1^2)N^{-1}2\pi c$ is plotted as points in figure 4, where N is the number density of argon and γ_N is the half-width (in units of rad s^{-1}) due to natural broadening (Gallagher and Lurio 1964). From equations (4*c*) and (6) one can see that this quantity should have the same shape as $f(\Delta_1)$ in equation (7). The constant factors guarantee normalisation in units of cm^4. Because we measured only the ratio I_F^{23}/I_{RAM}, and not I_F^{23} separately, one can say that we used the Raman to monitor our dye laser intensity as we moved it through its tuning range. This procedure relies on the well founded assumption (Cooper 1978, Carlsten *et al* 1977) that the Raman is Lorentzian over the entire spectral range (i.e. equation (4*c*) holds even outside the impact region). The linearity of the signal with laser power was checked to verify that there were no saturation or stimulated effects present. This test is important because, at higher laser power, stimulated emission at both ω_{RAM} and ω_{23} has been observed to occur (Raymer and Carlsten 1977).

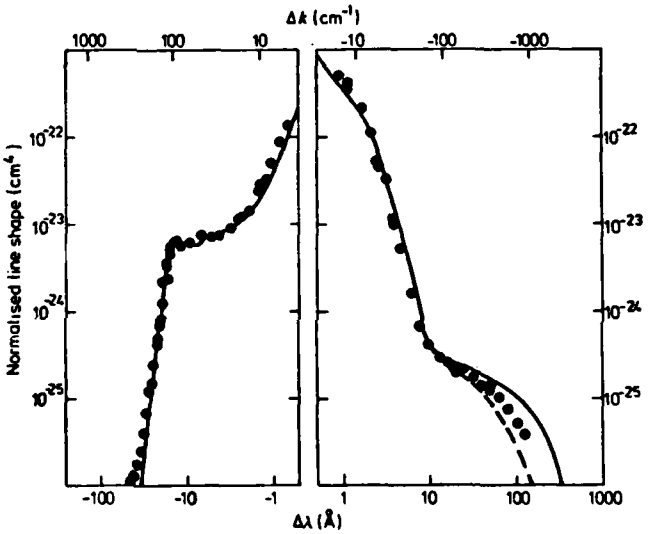

Figure 4. Line shape of the $^2P_{1/2}$–$^2S_{1/2}$ transition in Tl, broadened by Ar, obtained by two techniques: ●, collisional redistribution (present work); ——, emission spectroscopy (Cheron *et al* 1977). The broken curve is the absorption profile, obtained from the emission profile by multiplying by a Boltzmann factor (see text).

Also plotted in figure 4 as a full curve is the normalised emission profile of Cheron *et al* (1977). The agreement between this emission profile and our redistribution profile is striking. The difference at large detunings on the red side ($+\Delta\lambda$) is due to a temperature-dependent population effect, discussed by Hedges *et al* (1972). According to their discussion, we should really compare our data with an absorption profile, obtained by multiplying the emission profile by the factor $\exp(\Delta k/kT)$, where Δk is in cm^{-1} and $kT = 516\ cm^{-1}$ at 743 K, the temperature at which the emission experiment was done. This derived absorption profile is shown as a broken curve in figure 4. However, since our redistribution experiment was done at a higher temperature (1000 K), it is not surprising that our points lie above the derived absorption profile, because our

collisions at higher temperature should probe farther up the repulsive wall of the ground state (figure 2) than those at the lower temperature used in the other experiment. The effect on the blue side ($-\Delta\lambda$) is less pronounced (and not plotted) due to the steep fall-off in the line shape. The deviation beyond 30 Å on the blue side is believed to be caused by impurities in the oven, as these points do not scale linearly in argon pressure as the rest of the profile does. The present data were all taken outside the impact region (due to instrumental resolution) and so we never reached the limit, near line centre, where the red and blue sides of the line become symmetric. A complete discussion of the line shape in figure 4 is given by Cheron *et al* (1977) and will not be repeated here. Clearly, it is related to the detailed shapes of the potential curves shown in figure 2.

Although the line shapes agree very well, there is uncertainty in our experiment about the absolute scale in figure 4. We plotted our data as if the emission were coming from a single Tl atom which behaves in the way described by equation (3). That is, the branching ratios for the 2-3 and 2-1 transitions are γ_N^{23}/γ_N and γ_N^{21}/γ_N. However, when we look for emission at ω_{21} we find that it is trapped by the surrounding ground-state atoms. If all of this trapped radiation is subsequently emitted at ω_{23} then we should see a fluorescence signal at ω_{23} enhanced by the factor $(\gamma_N^{23}+\gamma_N^{21})/\gamma_N^{23} = 2{\cdot}01$. This interpretation would require us to lower all of our points by the factor $(2{\cdot}01)^{-1}$. This uncertainty must be resolved before the absolute cross sections from the two experiments can be compared more accurately.

In summary, we have demonstrated the relationship between collisional redistribution and emission line profiles. We found that in the Tl–Ar system these two profiles are essentially the same when collisions dominate spontaneous emission. When collisional and radiative rates are comparable, systems may exist in which a difference in the line shapes could be found, due to angular and polarisation effects in the redistribution process.

We would like to acknowledge helpful discussions with R J Ballagh, J Cooper, A Gallagher and A Szöke. This work was supported by Office of Naval Research Contract No N00014-76-C-0611 and National Science Foundation Grant No PHY76-04761, both through the University of Colorado.

References

Ballagh R J and Cooper J 1977 *Astrophys. J.* **213** 479
Carlsten J L, Szöke A and Raymer M G 1977 *Phys. Rev.* A **15** 1029
Cheron B, Scheps R and Gallagher A 1977 *Phys. Rev* A **15** 651
Cooper J 1978 *Astrophys. J.* in press
Gallagher A and Lurio A 1964 *Phys. Rev.* **136** A87
Hedges R, Drummond D and Gallagher A 1972 *Phys. Rev.* A **6** 1519
Huber D L 1969 *Phys. Rev.* **187** 392
Mihalas D 1970 *Stellar Atmospheres* (San Francisco: Freeman)
Mollow B R 1977 *Phys. Rev.* A **15** 1023
Nayfeh M H, Hurst G S, Payne M G and Young J P 1977 *Phys. Rev. Lett.* **39** 604
Nienhuis G and Schuller F 1977 *Physica* C **92** 397
Omont A, Smith E W and Cooper J 1972 *Astrophys. J.* **175** 185
Raymer M G and Carlsten J L 1977 *Phys. Rev. Lett.* **39** 1326
Voslamber D and Yelnik J-B 1978 *Phys. Rev. Lett.* **41** 1233

PHYSICAL REVIEW A VOLUME 19, NUMBER 6

Theory of stimulated Raman scattering with broad-band lasers

M. G. Raymer,* J. Mostowski,† and J. L. Carlsten‡
Joint Institute for Laboratory Astrophysics, University of Colorado and National Bureau of Standards, Boulder, Colorado 80309
(Received 18 December 1978)

The authors have extended the theory of stimulated Raman scattering to include the effects of laser bandwidths, in both the transient and steady-state regimes. The case of two interacting laser beams, a pump laser and a probe (Stokes) laser, is treated. Using the phase-diffusion model for laser bandwidth, the authors demonstrate that in the absence of dispersion, the forward Raman gain is essentially independent of the laser bandwidths in the high-gain limit, while in the low-gain limit the gain coefficient is inversely proportional to the sum of the bandwidths. It is further shown that when the pump-laser bandwidth is much larger than the linewidth of the Raman medium, the stimulated Stokes output assumes the same spectrum as the pump laser in the high-gain limit. A possible interpretation of these results is discussed assuming a "phase-locking" of the Stokes phase to the fluctuations in the pump-laser phase, due to the nonlinear interaction of the two beams through the Raman medium.

I. INTRODUCTION

The effects of finite laser bandwidth are being recognized as important in the study of nonlinear optical processes. Resonance fluorescence,[1-6] two-photon absorption,[7,8] second harmonic generation,[9] multiphoton ionization,[10-13] and stimulated Raman scattering are all areas in which key elements of understanding depend on the ability to model the laser, not as a monochromatic wave of definite phase and amplitude, but as a multimode broad-band wave with fluctuating phase and amplitude. The problem of stimulated Raman scattering (SRS) is especially timely in light of ongoing efforts to use it as method for developing new coherent light sources[14] as well as compressing high-energy laser pulses to achieve higher peak powers for use in laser fusion.[15] In applications of these types a detailed understanding of all the factors influencing the efficiencies of the processes is obviously desirable. However, one important factor, laser bandwidth, has not yet been fully explored.

Recently, two groups[15,16] have observed a large forward-backward asymmetry of the Raman gain, which they attribute to the broad-band nature of the pump laser used. These were in the absence of other effects, such as self-focusing or extraneous feedback, which are known to produce anomalous gains.[17] These asymmetries are consistent with several theoretical predictions[18,19] that in the backward direction (counterpropagating pump and Stokes waves) the gain coefficient is proportional to $(\Gamma+\Gamma_L)^{-1}$, where Γ and Γ_L are the spectral widths of the Raman medium and the pump laser, respectively; while, in the forward direction, in the absence of dispersion of the Stokes wave relative to the pump wave, the gain coefficient is proportional to Γ^{-1} alone. Carman *et al.*[18] refer to this as "the rather startling conclusion... that the Stokes gain is independent of the frequency spectrum of the (pump) laser... even if this spectrum is much broader than Γ." Thus when Γ_L is much larger than Γ the forward gain is much larger than the backward gain. These results go against intuition based on the idea that gain should depend on the number of photons per unit frequency in the pump beam. Apparently, the concept of photons as independent incoherent bundles is inadequate to describe the subtleties in the SRS problem.

The purpose of this paper is to further develop the theory of SRS, including the effects of finite laser bandwidths, in a way that allows explicit calculation of the gain and spectrum of the Stokes wave. We consider, as in Fig. 1, a medium of three-level atoms interacting with two classical

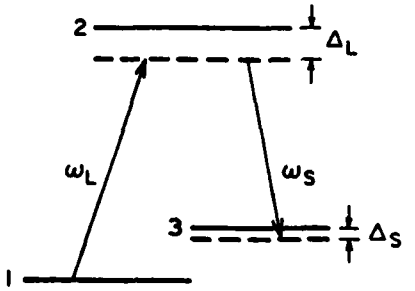

FIG. 1. Three-level atom interacting with a pump laser with frequency ω_L and a probe (Stokes) laser with frequency ω_S. The cumulative detunings are Δ_L and Δ_S.

electromagnetic waves; one a pump (laser) wave and the other a Stokes wave, differing in frequency by the Raman shift of the medium. Both waves have constant amplitudes, but phases which fluctuate randomly, giving rise to bandwidths Γ_L and Γ_S. This is the "phase-diffusion model," which has been used recently as a means to include bandwidth effects into the calculation of light-scattering spectra,[2-6] as well as multiphoton ionization.[10,11] The calculations are performed as statistical averages over the random phase variables of the two waves. Previous treatments[18,19] of SRS attempted to accommodate both fluctuating phases and amplitudes. We will discuss later why the inclusion of amplitude fluctuations in this problem is such a difficult task. Within the stated model, we verify the independence of the forward gain from the pump width Γ_L and the Stokes width Γ_S, in the high-gain limit. Further we will show that in the case that the width of the pump laser Γ_L is broader than the Raman linewidth Γ, the amplified Stokes signal assumes the spectral width of the pump laser, regardless of its initial width.

Akhmanov, D'yakov and Pavlov[19] have separated the problem into four regimes of interest: (i) $\Gamma_L \ll \Gamma$, with no dispersion; (ii) $\Gamma_L \ll \Gamma$, with dispersion; (iii) $\Gamma_L \gg \Gamma$, with no dispersion; (iv) $\Gamma_L \gg \Gamma$, with dispersion. Case (i) was considered by Bloembergen and Shen,[20] who predicted an enhancement of the forward gain for a multimode laser. In this paper we treat mainly case (iii), where the laser linewidth is broader than the atomic linewidth. Here there is no enhancement, but neither is there a significant suppression of the gain, compared to that calculated in case (i) in the limit $\Gamma_L = 0$. Carman *et al.*[18] have also treated case (iii), and they reached essentially the same conclusions by calculating numerical solutions to the problem. Cases (ii) and (iv) treat the effects of dispersion. There is a consensus[14,19,21] that broadening of the laser in the presence of dispersion does result in a lowering of the gain, due to the inability of the Stokes wave to stay correlated with the pump fluctuations as they propagate. However, Akhmanov *et al.*[19] have shown, further, that there is a critical pump intensity, above which the effects of dispersion are overcome and the gain coefficient increases again to nearly the narrow-band value.

Dzhotyan *et al.*[22] have treated the problem by assuming the pump and Stokes waves to be composed of many monochromatic modes, with uniform frequency spacings large compared to the Raman linewidth Γ. This results in significant interaction only between certain resonant pairs of modes (one pump and one Stokes). This approach can be thought of as complementary to the present approach, in which the energy in the waves is taken to be spread continuously over a small frequency interval. The multimode approach of Dzhotyan *et al.* is a generalization of an idea developed by Giordmaine and Kaiser[22] (and discussed by Byer and Herbst[22]), in which the pump and Stokes waves each consist of two modes. This treatment illustrates the relationship of SRS with four-wave parametric interactions. Another related discussion is that of Harris,[22] in which the threshold for parametric oscillation with multimode lasers is shown to depend only on the total power in the pump laser.

In Sec. II we derive the equations of motion for the Raman problem in a novel way by using the "two-photon vector model" of Takatsuji[24] and Grischkowsky *et al.*[25] In Sec. III we review the general solutions of the equations, following Carman *et al.*[18] and evaluate the gain with monochromatic pumping for both the transient and steady-state limits. Then we apply the phase-diffusion model to evaluate the gain under arbitrary broad-band pumping conditions, again in both the transient and steady-state limits. In Sec. IV we calculate the spectrum of the amplified Stokes wave by considering its autocorrelation function in the steady-state limit. In Sec. V we discuss a possible interpretation of the results obtained, and in Sec. VI we summarize the main results of the paper.

II. EQUATIONS OF MOTION

Here we give a novel derivation of the usual equations of motion for the Raman problem and a discussion of the physical model leading to them. For simplicity, we treat the case of near-resonance Raman Stokes scattering, in which only three atomic levels need to be considered. Thus we consider a vapor of atoms with energy levels shown in Fig. 1. A pump laser is tuned near (but not on) the 1-2 transition and a probe laser is tuned near (but not on) the 2-3 transition. It is sufficient to treat the pump laser as a prescribed field as long as it is not depleted. The probe laser will experience gain in a manner dependent on both the amplitude and phase structure of the pump laser.

Consider the fields $\vec{E}_L$ (pump laser) and $\vec{E}_S$ (Stokes, or probe laser) acting on the three-level atom of Fig. 1. Let

$$\vec{E}_L = \mathcal{E}_L \hat{x}_L \cos(\omega_L t - k_L z + \varphi_L) = \mathcal{E}_L \hat{x}_L \cos\phi_L , \quad (1a)$$

$$\vec{E}_S = \mathcal{E}_S \hat{x}_S \cos(\omega_S t \mp k_S z + \varphi_S) = \mathcal{E}_S \hat{x}_S \cos\phi_S , \quad (1b)$$

where $\mathcal{E}_L$ and $\mathcal{E}_S$ are the (real) amplitudes of the waves, with linear polarization vectors $\hat{x}_L$ and $\hat{x}_S$, carrier frequencies ω_L and ω_S, propagation vectors $\vec{k}_L = k_L\hat{z}$, $\vec{k}_S = k_S\hat{z}$, and slowly varying phases φ_L and φ_S. The state of the atom can be written

$$\psi = a_1 e^{-i\omega_1 t}\psi_1 + a_2 e^{-i(\omega_1+\omega_L)t}\psi_2 + a_3 e^{-i(\omega_1+\omega_L-\omega_S)t}\psi_3 , \tag{2}$$

where a_1, a_2, and a_3 are the slowly varying coefficients in a "doubly rotating frame,"[23] and ψ_1, ψ_2, and ψ_3 are the stationary eigenstates of the atomic Hamiltonian, with energies $\hbar\omega_1$, $\hbar\omega_2$, and $\hbar\omega_3$. At $t = 0$ the atom is in the ground state ($a_1 = 1$, $a_2 = a_3 = 0$) and afterwards the coefficients evolve according to Schrödinger's equation

$$i\dot{a}_1 = -\tfrac{1}{2}\Omega_L a_2 , \tag{3a}$$

$$i\dot{a}_2 = (\Delta_L - \dot{\varphi}_L)a_2 - \tfrac{1}{2}\Omega_L a_1 - \tfrac{1}{2}\Omega_S a_3 , \tag{3b}$$

$$i\dot{a}_3 = (\Delta_S - \dot{\varphi}_L + \dot{\varphi}_S)a_3 - \tfrac{1}{2}\Omega_S a_2 , \tag{3c}$$

where the detunings are $\Delta_L = \omega_{21} - \omega_L$ and $\Delta_S = \omega_{31} + \omega_S - \omega_L$. The Rabi frequencies for the two transitions are given by $\Omega_L = d_{12}\mathcal{E}_L/\hbar$ and $\Omega_S = d_{23}\mathcal{E}_S/\hbar$, where $d_{12} = \vec{d}_{12}\cdot\hat{x}_L$ and $d_{23} = \vec{d}_{23}\cdot\hat{x}_S$ are dipole matrix elements. The rotating-wave approximation[23] (RWA) has been invoked in writing Eq. (3). This is valid when the detunings are small enough ($\Delta_L \ll \omega_{21}$, $\Delta_S \ll \omega_{23}$).

Several authors[24-26] have discussed the case in which level 2 may be eliminated from the Eqs. (3a)–(3c). When Δ_L is much larger than Δ_S and the fields have no appreciable Fourier components at the atomic frequencies, we may set $\dot{a}_2 \approx 0$ in Eq. (3b) and get (neglecting $\dot{\varphi}_L$)

$$a_2 \approx (\tfrac{1}{2}\Omega_L a_1 + \tfrac{1}{2}\Omega_S a_3)/\Delta_L . \tag{4}$$

This approximation is the basis of the "two-photon vector model" of Takatsuji[24] and Grischkowsky *et al.*,[25] and is discussed more fully in Appendix A. Using this approximation in the Schrödinger equation [Eq. (3)], one may obtain two equations for a_1 and a_3, which are identical in form to those of a one-photon transition with effective Rabi frequency $\Omega_e = \frac{1}{2}\Omega_L\Omega_S/\Delta_L$ and effective detuning $\Delta_e = \Delta_S + \frac{1}{4}(\Omega_L^2 - \Omega_S^2)/\Delta_L$, which shows the effect of ac Stark shifting. We write the resulting equations in the convenient Bloch form,[23] using $U + iV = 2a_1 a_3^*$, and $W = a_3 a_3^* - a_1 a_1^*$,

$$\dot{U} = -(\Delta_e - \dot{\varphi}_L + \dot{\varphi}_S)V - \Gamma U , \tag{5a}$$

$$\dot{V} = (\Delta_e - \dot{\varphi}_L + \dot{\varphi}_S)U + \Omega_e W - \Gamma V , \tag{5b}$$

$$\dot{W} = -\Omega_e V . \tag{5c}$$

Here we have included the phenomenological collisional dephasing rate Γ, which is the halfwidth at half maximum (HWHM) in rad sec^{-1} for the (Raman) transition between levels 1 and 3.

To describe Raman amplification, one must solve the wave equation for the Stokes wave

$$\frac{\partial^2\vec{E}_S}{\partial z^2} - \frac{1}{v^2}\frac{\partial^2\vec{E}_S}{\partial t^2} = \frac{4\pi}{c^2}\frac{\partial^2\vec{P}}{\partial t^2} , \tag{6}$$

where v is the velocity in the medium, and $\vec{P}$ is the polarization of the medium. Considering only Fourier components close to the carrier frequency ω_S, and only the linear polarization $\hat{x}_S$, leads to a polarization

$$P = N\langle\psi|\vec{d}\cdot\hat{x}_S|\psi\rangle = 2Nd_{23}\,\mathrm{Re}(a_2 a_3^*)\cos\phi_S + 2Nd_{23}\,\mathrm{Im}(a_2 a_3^*)\sin\phi_S , \tag{7}$$

where N is the atomic number density. Making use of Eq. (7) for the polarization, Eq. (4) to again eliminate a_2, and the slowly varying envelope approximation,[23] one can write Eq. (6) in the form

$$\pm\frac{\partial\mathcal{E}_S}{\partial z} + \frac{1}{v}\frac{\partial\mathcal{E}_S}{\partial t} = -\kappa_2\mathcal{E}_L V , \tag{8a}$$

$$\mathcal{E}_S\left(\pm\frac{\partial\varphi_S}{\partial z} + \frac{1}{v}\frac{\partial\varphi_S}{\partial t}\right) = -\kappa_2\mathcal{E}_L U - \frac{d_{23}}{d_{12}}\kappa_2\mathcal{E}_S(W+1) , \tag{8b}$$

where $\kappa_2 = \pi N\omega_S v d_{12}d_{23}/c^2\hbar\Delta_L$ and the plus and minus signs are for copropagating and counterpropagating pump and probe beams, respectively. Equations (5) and (8), along with a similar one for the pump laser $\mathcal{E}_L$, completely describe the propagation and material response for the Raman problem, including the effects of phase modulation ($\dot{\varphi}_L, \dot{\varphi}_S$). They have been derived by Takatsuji[24] and by Courtens[26] in essentially the same form and used for considerations of optical transient phenomena.

In contrast, we are interested in the special case that the atoms are weakly excited and the pump laser is a prescribed, external field. Thus we take for the inversion $W = -1$, $W = 0$ in Eq. (5). We also assume exact resonance ($\Delta_e = 0$). The remaining four equations, (5a), (5b), (8a), and (8b), can be combined into two complex equations. Defining the quantities

$$E_L = \mathcal{E}_L e^{i\varphi_L};\quad E_S = \mathcal{E}_S e^{i\varphi_S};\quad Q = (U + iV)e^{i(\varphi_L - \varphi_S)} , \tag{9}$$

we obtain directly

$$\pm\frac{\partial E_S}{\partial z} + \frac{1}{v}\frac{\partial E_S}{\partial t} = -i\kappa_2 Q^* E_L , \tag{10a}$$

$$\frac{\partial Q^*}{\partial t} = -\Gamma Q^* + i\kappa_1 E_L^* E_S , \tag{10b}$$

where $\kappa_1 = d_{12}d_{23}/2\hbar^2\Delta_L$. These two coupled equations are the starting point for many theories of

stimulated Raman scattering. They have usually been derived in the coupled wave approach of nonlinear optics[27] for the case of molecular Raman scattering, where Q is the normal-mode coordinate of a molecular vibration and is often called an optical-phonon wave. In those treatments, perturbation theory was used from the beginning and the coupling constants κ_1 and κ_2 were given in terms of molecular polarizabilities. Here we have provided a connection between the "two-photon vector model" and the standard theories of Raman propagation. We have given the explicit relations, Eq. (9), between the variables used in the earlier nonlinear-optics theories and the more modern optical resonance or Bloch vector picture, which has been used here, and continues to give insight into many laser-related problems.

III. EVALUATION OF RAMAN GAIN

General solutions of Eq. (10) have been obtained in the case of copropagating waves by Carman *et al.*[18] In this case the prescribed undepleted pump-laser field E_L depends only on the local time variable $\tau = t - z/v$. It is assumed that the waves travel with equal velocity ($k_L = k_S$), i.e., there is no dispersion. Denoting by $E_S(0,\tau)$ the Stokes field at the input of the cell ($z = 0$), the solution for the Stokes output field is[18]

$$E_S(z,\tau) = E_S(0,\tau) + (\kappa_1\kappa_2 z)^{1/2}\int_0^\tau \frac{e^{-\Gamma(\tau-\tau')}}{[p(\tau)-p(\tau')]^{1/2}} \times I_1(\{4\kappa_1\kappa_2 z[p(\tau)-p(\tau')]\}^{1/2}) \times E_L(\tau)E_L^*(\tau')E_S(0,\tau')\,d\tau', \quad (11)$$

where $I_1(x)$ is the Bessel function of imaginary argument,[28] and

$$p(\tau) = \int_0^\tau |E_L(\tau'')|^2 d\tau''$$

is the integrated power in the pump laser up to time τ.

A. Stokes gain for monochromatic pump and input waves

It is instructive to review the properties of the solution (11) for the case that the pump wave and the input Stokes wave are constant and monochromatic. In this case we have $E_L(\tau) = E_L^*(\tau') = \mathcal{E}_L$ and $E_S(0,\tau') = \mathcal{E}_{S0}$. This leads to

$$E_S(z,\tau) = \mathcal{E}_{S0} + \mathcal{E}_{S0}\frac{(\alpha z)^{1/2}}{2} \times \int_0^\tau \frac{e^{-\Gamma x}}{\sqrt{x}} I_1[(\alpha z x)^{1/2}]\,dx, \quad (12)$$

where we have used $x = \tau - \tau'$, $p(\tau) = \mathcal{E}_L^2\tau$ and $\alpha = 4\kappa_1\kappa_2\mathcal{E}_L^2$. Following Wang[27] we present analytic approximations and numerical evaluations of the Stokes output, given by Eq. (12), for two different limits.

1. Transient limit

The transient limit occurs for times much shorter than the reciprocal of the Raman linewidth ($\Gamma\tau \ll 1$). After replacing $e^{-\Gamma x}$ by 1 in Eq. (12), the integral can be done to give $E_S(z,\tau) = \mathcal{E}_{S0} I_0[(\alpha z\tau)^{1/2}]$, which for large enough $\alpha z\tau$ leads to the asymptotic form for the output Stokes intensity

$$E_S^2(z,\tau) \simeq \frac{\mathcal{E}_{S0}^2}{2\pi}\frac{e^{2(\alpha z\tau)^{1/2}}}{(\alpha z\tau)^{1/2}} \quad \text{(high gain, } \Gamma\tau \ll 1\text{)}. \quad (13)$$

We have used the property $I_i(x) \sim e^x/(2\pi x)^{1/2}$, for $x \to \infty$, for any i.[28] Equation (13) is the usual result for the transient Raman effect.[27] It is interesting to note that, in the transient limit, the Raman gain given by Eq. (13) does not depend on the Raman linewidth Γ.

2. Steady-state limit

The steady-state limit occurs for times much larger than the reciprocal of the Raman linewidth ($\Gamma\tau \gg 1$). Extending the upper limit to infinity, the integral in Eq. (12) can be done exactly[29] to give for the Stokes intensity

$$E_S^2(z,\tau) = \mathcal{E}_{S0}^2 e^{gz} \quad \text{(arbitrary gain, } \Gamma\tau \gg 1\text{)}, \quad (14a)$$

where

$$g = \frac{\alpha}{2\Gamma} = \frac{\pi N\omega_S}{c^2}\frac{v d_{12}^2 d_{21}^2}{\hbar^3\Delta_L^2}\frac{\mathcal{E}_L^2}{\Gamma}. \quad (14b)$$

The steady-state gain coefficient g is the usual one derived for stimulated electronic Raman scattering.[30] It does depend on the Raman linewidth Γ, in contrast to the transient case.

Equations (13) and (14a) for the output Stokes intensity, along with numerical evaluation of Eq. (12), are plotted in Fig. 2, as a function of gz, or equivalently, pump laser intensity, for both a transient case ($\Gamma\tau = 10^{-2}$) and a steady-state case ($\Gamma\tau = 10^2$). Here we interpret τ as the pulse duration of the pump laser. Equation (13) for the transient gain ($\Gamma\tau = 10^{-2}$) is seen to agree well with the exact numerical results when $\log_{10}(E_S^2/\mathcal{E}_{S0}^2) > 1$, while Eq. (14a) for the steady-state gain ($\Gamma\tau = 10^2$) agrees everywhere. Note that the values below $\log_{10}(E_S^2/\mathcal{E}_{S0}^2) = 0$ are unphysical. The other four curves in Fig. 2 show the effects of laser bandwidth on the gain, as described in Sec. III B.

B. Raman gain for broad-band pump and/or input waves

We now evaluate the Raman gain in the case that the spectral width of either the pump laser or the

Stokes input wave (or both) is greater than the Raman linewidth ($\Gamma_L + \Gamma_S \gg \Gamma$). This can be accomplished by performing an average of the general solution, Eq. (11), over a statistical ensemble chosen to model the bandwidths. An especially useful model is that of phase diffusion,[2-6] in which the field amplitude $\mathcal{E}_L$ is constant, but the phase suffers abrupt changes at an average rate $2\Gamma_L$ (see Appendix B). The field autocorrelation functions are then

$$\langle\langle E_L(\tau)E_L^*(\tau')\rangle\rangle = \mathcal{E}_L^2 e^{-\Gamma_L|\tau-\tau'|} \tag{15a}$$

and

$$\langle\langle E_S(0,\tau)E_S^*(0,\tau')\rangle\rangle = \mathcal{E}_{S0}^2 e^{-\Gamma_S|\tau-\tau'|}, \tag{15b}$$

which lead directly to Lorentzian line shapes with halfwidths (HWHM) equal to Γ_L for the pump laser and Γ_S for the input Stokes wave. The brackets $\langle\langle\ \rangle\rangle$ indicate an ensemble average over the statistical fluctuations of the field.[31] This model describes a stabilized laser operating far above threshold, but it also proves to be very convenient mathematically.

The intensity of the output Stokes wave is given by $\langle\langle|E_S(z,\tau)|^2\rangle\rangle$. To evaluate the intensity of the Stokes wave we first introduce some notation:

$$f(x) = (e^{-\Gamma x}/\sqrt{x})I_1[(\alpha z x)^{1/2}], \tag{16a}$$

$$F(\tau) = \int_0^\tau f(\tau-\tau')\frac{E_L(\tau)E_L^*(\tau')}{\mathcal{E}_L^2}\,\frac{E_S(0,\tau')}{\mathcal{E}_{S0}}\,d\tau'. \tag{16b}$$

Then from Eq. (11), using $p(\tau) = \mathcal{E}_L^2\tau$ in accordance with the phase diffusion model for the pump laser, we have

$$E_S(z,\tau) = E_S(0,\tau) + \mathcal{E}_{S0}\{\tfrac{1}{2}[(\alpha z)^{1/2}]\}F(\tau), \tag{17a}$$

$$\begin{aligned}\langle\langle|E_S(z,\tau)|^2\rangle\rangle &= \mathcal{E}_{S0}^2 + \mathcal{E}_{S0}(\alpha z)^{1/2}\\ &\quad\times\langle\langle E_S^*(0,\tau)F(\tau)\rangle\rangle\\ &\quad+\mathcal{E}_{S0}^2\{\tfrac{1}{4}(\alpha z)\}\langle\langle|F(\tau)|^2\rangle\rangle.\end{aligned} \tag{17b}$$

The second term in Eq. (17b) can be easily evaluated using Eq. (15),

$$\begin{aligned}\langle\langle E_S^*(0,\tau)F(\tau)\rangle\rangle &= \mathcal{E}_{S0}\int_0^\tau f(\tau-\tau')\\ &\quad\times e^{-\Gamma_L(\tau-\tau')}e^{-\Gamma_S(\tau-\tau')}\,d\tau',\end{aligned} \tag{18}$$

where we have assumed statistical independent of the waves at $z = 0$; that is

$$\begin{aligned}&\langle\langle E_L(\tau)E_L^*(\tau')E_S(0,\tau')E_S^*(0,\tau)\rangle\rangle\\ &= \langle\langle E_L(\tau)E_L^*(\tau')\rangle\rangle\langle\langle E_S(0,\tau')E_S^*(0,\tau)\rangle\rangle\end{aligned}$$

(see Ref. 32). This integral is identical to the integral in Eq. (12), but with Γ replaced by $\Gamma + \Gamma_L + \Gamma_S$. Thus when $\Gamma_L + \Gamma_S \gg \Gamma$, this term grows with a very small gain coefficient. This is in contrast to the third term in Eq. (17b), which, as we will see, grows with essentially the narrowband gain given in Eq. (14a). Thus we expect the third term of Eq. (17b) to be dominant in the high-gain limit. Using the correlation functions given by Eq. (15), one can evaluate this third term as

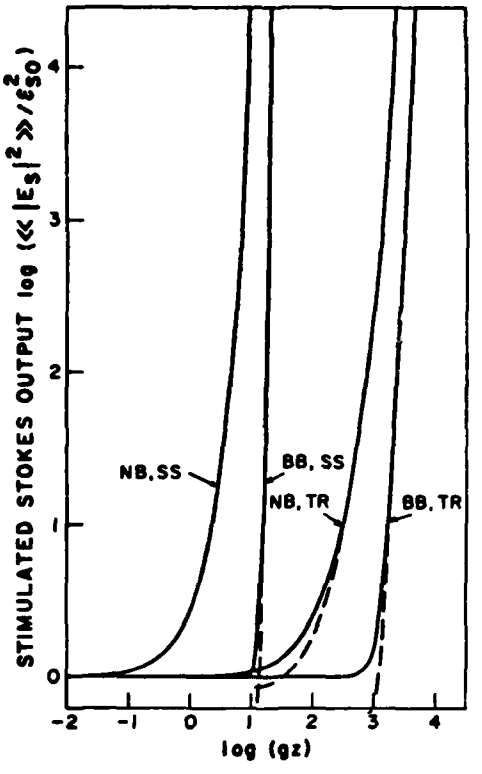

FIG. 2. Normalized Stokes output intensity as a function of gain coefficient gz (or equivalently, pump laser intensity) under various physical conditions and differing levels of approximation. The curve labeled "NB, SS" is the narrow-band steady-state result obtained from Eq. (14a), or Eq. (12) with $\Gamma\tau = 10^2$, where Γ is the Raman linewidth and τ is the laser pulse length. The "NB, TR" curves are the narrow-band transient results, obtained exactly from Eq. (12) with $\Gamma\tau = 10^{-2}$ (solid curve), or approximately from Eq. (13) (dashed curve). The curves labeled "BB, SS" are the broad-band steady-state results obtained exactly from Eqs. (17b), (18), and (20b) with $\Gamma\tau = 10^2$ (solid curve), or approximately from Eq. (25) (dashed curve). The "BB, TR" curves are the broad-band transient results obtained exactly from Eqs. (17b), (18), and (20b) with $\Gamma\tau = 10^{-2}$ (solid curve), or approximately from Eq. (22) (dashed curve). The broad-band curves are for a bandwidth ratio $(\Gamma_L + \Gamma_S)/\Gamma = 10^5$, where Γ_L and Γ_S are the bandwidths of the pump and probe (Stokes) lasers.

$$\langle\langle|F(\tau)|^2\rangle\rangle = \int_0^\tau \int_0^\tau f(\tau-\tau')f(\tau-\tau'')\frac{\langle\langle E_L^*(\tau')E_L(\tau'')\rangle\rangle}{\mathcal{E}_L^2}\frac{\langle\langle E_S(0,\tau')E_S^*(0,\tau'')\rangle\rangle}{\mathcal{E}_{S0}^2}d\tau'\,d\tau'' \tag{19a}$$

$$= \int_0^\tau \int_0^\tau f(\tau-\tau')f(\tau-\tau'')e^{-(\Gamma_L+\Gamma_S)|\tau'-\tau''|}\,d\tau'\,d\tau'', \tag{19b}$$

where we used the fact that $E_L(\tau)E_L^*(\tau)=\mathcal{E}_L^2$ is independent of the statistical averaging. To evaluate the double integral in Eq. (19b), we note that the exponential factor is much different from zero only near the line $\tau'=\tau''$. In the limit that $f(x)$ changes very slowly in a time $(\Gamma_L+\Gamma_S)^{-1}$ (i.e., $\Gamma,\ \alpha z \ll \Gamma_L+\Gamma_S$), we can replace the exponential factor by the properly normalized δ function $2(\Gamma_L+\Gamma_S)^{-1}\,\delta(\tau'-\tau'')$. We then get

$$\langle\langle|F(\tau)|^2\rangle\rangle \cong \frac{2}{\Gamma_L+\Gamma_S}\int_0^\tau f^2(\tau-\tau')\,d\tau' \tag{20a}$$

$$= \frac{2}{\Gamma_L+\Gamma_S}\int_0^\tau \frac{e^{-\Gamma x}}{x} I_1^2[(\alpha z x)^{1/2}]\,dx. \tag{20b}$$

In similar fashion to the integral in Eq. (12), this integral can be evaluated analytically as well as numerically, in the two limits:

1. Transient limit

As before, for $\Gamma\tau \ll 1$, the exponential can be replaced by 1 and the integral done (in this case asymptotically, using the asymptotic form for I_1) to give

$$\langle\langle|F(\tau)|^2\rangle\rangle = \frac{1}{\pi(\Gamma_L+\Gamma_S)}\frac{e^{2(\alpha z\tau)^{1/2}}}{\alpha z\tau}. \tag{21}$$

Thus, in the high-gain limit where Eq. (17b) is dominated by the last term, we find that the Stokes output intensity in the transient limit is

$$\langle\langle|E_S(z,\tau)|^2\rangle\rangle = \frac{\mathcal{E}_{S0}^2}{2\pi}\frac{e^{2(\alpha z\tau)^{1/2}}}{2(\Gamma_L+\Gamma_S)}$$

$$\text{(high gain, } \Gamma\tau \ll 1\text{)}. \tag{22}$$

Because of the form of the exponential, this result for the broad-band transient will be nearly indistinguishable from the result, Eq. (13), for the narrowband transient.

2. Steady-state limit

To evaluate the steady-state limit of Eq. (20b), we extend the upper limit of the integration to infinity, and do the integral to give[33]

$$\langle\langle|F(\infty)|^2\rangle\rangle = \frac{\alpha z}{4\Gamma(\Gamma_L+\Gamma_S)}\,{}_2F_2\left(\tfrac{3}{2},1;2,3,\frac{\alpha z}{2\Gamma}\right), \tag{23}$$

where ${}_2F_2$ is the generalized hypergeometric function, which can be evaluated asymptotically for large argument as[34]

$${}_2F_2(\tfrac{1}{2},1;2,3,x) \sim (4/\sqrt{\pi})\,e^x/x^{5/2}. \tag{24}$$

This leads to an asymptotic form for the Stokes intensity under broad-band steady-state high-gain conditions:

$$\langle\langle|E_S(z,\infty)|^2\rangle\rangle = \mathcal{E}_{S0}^2\frac{\Gamma}{\Gamma_L+\Gamma_S}\frac{e^{gz}}{(\pi gz)^{1/2}}$$

$$\text{(high gain, } \Gamma\tau \gg 1\text{)}. \tag{25}$$

It can be seen by comparing the Stokes intensities given by Eqs. (25) and (14a) that under the conditions assumed (copropagating waves, no dispersion), the growth of a Stokes wave, in the steady-state high-gain limit, is virtually unaffected by either its input bandwidth or that of the pump laser. We can demonstrate this result by writing the output Stokes intensity as

$$\langle\langle|E_S(z,\infty)|^{22}\rangle\rangle = \mathcal{E}_{S0}^2 e^G, \tag{26}$$

$$G = G_{NB} - \ln\{[(\Gamma_L+\Gamma_S)/\Gamma](\pi G_{NB})^{1/2}\}, \tag{27}$$

where $G_{NB}=gz$ is the narrow-band gain coefficient from Eq. (14b). Thus for large gain the difference between G and G_{NB} becomes relatively insignificant. We will present a possible interpretation for this result in Sec. V. Equation (27) is similar to the result, conjectured by Carman *et al.*,[18] that $G = G_{NB} - \ln[(\Gamma_L/\Gamma)G_{NB}]$. The difference between our result and theirs (when $\Gamma_S = 0$) may be due to the fact that they allowed also for amplitude fluctuations of the pump laser, whereas we have restricted ourselves to phase modulation alone, in order to make an explicit calculation tractible. The calculation becomes intractible when amplitude fluctuations are present because, then, $p(\tau)$ in Eq. (11) is a random variable which makes the statistical average difficult to perform.

As in the narrow-band case, we plot the broad-band Stokes intensities, Eqs. (22) and (25), in Fig. 2, along with numerical evaluation of the Stokes intensity from $\langle\langle|E_S(z,\tau)|^2\rangle\rangle$, defined by Eqs. (17b), (18), and (20b). Since Eq. (20b) is valid only for $\Gamma_L+\Gamma_S \gg \Gamma, \alpha z$, we have plotted the extreme case that $(\Gamma_L+\Gamma_S)/\Gamma = 10^5$, in order to demonstrate the validity of the asymptotic forms Eqs. (22) and (25). Again we have plotted the transient and steady-state cases: $\Gamma\tau = 10^{-2}$ and 10^2. Again we see agreement of the asymptotic forms with the exact numerical results when $\log\langle\langle|E_S(z,\tau)|^2\rangle\rangle/\mathcal{E}_{S0}^2 > 1$.

We may now compare the narrow-band and broad-band results. For this extreme steady-state case, $(\Gamma_L+\Gamma_S)/\Gamma = 10^5$, we see a significant sup-

pression of the gain in the turn-on region for both transient and steady-state limits. However, according to Eq. (27), at very high gains the difference between the narrow- and broad-band stimulated outputs becomes less and less, relative to their absolute magnitudes. It is interesting that the broad-band output exhibits a threshold-type behavior, in contrast to the exponential behavior of the narrow-band output.

Although the principal interest here is in the high-gain limit, some comments can also be made about the low-gain steady-state limit, important to such experimental techniques as CARS (coherent anti-Stokes Raman scattering). Thus we will find the terms in Eq. (17b) which are of lowest order (linear) in αz. It can be shown[34] that the third term, containing $\langle\langle|F(\tau)|^2\rangle\rangle$, is quadratic in αz as $\alpha z \to 0$ and can thus be neglected. The first and second terms in Eq. (17b) are evaluated, using Eq. (18) with the upper limit τ taken to infinity, to give[29]

$$\langle\langle|E_S(z,\infty)|^2\rangle\rangle = \mathcal{E}_{S0}^2(2e^{g_{BB}z/2}-1), \tag{28}$$

$$g_{BB} = \alpha/2(\Gamma+\Gamma_L+\Gamma_S). \tag{29}$$

In the limit $\alpha z \to 0$, this reduces to

$$\langle\langle|E_S(z,\infty)|^2\rangle\rangle = \mathcal{E}_{S0}^2(1+g_{BB}z) \quad \text{(low gain, } \Gamma\tau \gg 1\text{)}. \tag{30}$$

We see that in the low-gain steady-state limit, the SRS grows linearly with the ("broad-band") gain coefficient g_{BB}. This is the result that would naively be predicted on the basis of photons per mode, as discussed in Sec. I.

C. Raman gain for arbitrary bandwidths

Here we analyze, numerically, the properties of the stimulated output when the condition $\Gamma_L+\Gamma_S \gg \Gamma, \alpha z$ is *not* necessarily upheld, as was assumed in Sec. III B. First note that if we take $(\Gamma_L+\Gamma_S)/\Gamma = 10^2$, rather than 10^5 as used in Fig. 2, the analysis of Sec. III B is valid only for $gz < 10^2$, making prediction of the broad-band transient above $gz = 10^2$ impossible by those methods. However, also note that the solution in Eq. (19b), before approximation to obtain Eq. (20), contains the information we are seeking in the general case. Thus we evaluated Eq. (19b), by a numerical method discussed in Appendix C, and obtained the output Stokes intensity $\langle\langle|E_S(z,\tau)|^2\rangle\rangle$ defined by Eqs. (17b), (18), and (19b). These results are shown in Fig. 3, where we have covered a large region of the interesting parameters: $\Gamma\tau$ and $(\Gamma_L+\Gamma_S)/\Gamma$ both vary between 10^{-2} and 10^2.

Beginning with Fig. 3(a), we see that the laser bandwidth has little effect on the gain in the transient limit ($\Gamma\tau = 10^{-2}$). This is not surprising, as a short laser pulse of duration $\tau = 10^{-2}/\Gamma$ has a spectral width of $10^2\Gamma$ without phase diffusion ($\Gamma_L = 0$). Thus we see no effect of additional broadening by phase diffusion until $\Gamma_L+\Gamma_S \geq 10^2\Gamma$, at which point the gain becomes slightly depressed. Progressing in Figs. 3(b) and 3(c) to longer pulse duration τ, we see the general result that no effect of phase diffusion broadening is apparent until $\Gamma_L+\Gamma_S \geq 1/\tau$. The steady-state limit occurs in Fig. 3(d), where no difference is seen between $\Gamma\tau = 10$ and $\Gamma\tau = 10^2$.

IV. SPECTRUM OF THE STOKES OUTPUT IN STEADY STATE

In Secs. I–III the input Stokes wave has been taken to have a width Γ_S. But because all of the power in the broad-band pump laser is effective for amplifying the Stokes wave, it is interesting to ask what becomes of the spectral distribution of the Stokes wave after it has been amplified. In this section we calculate the spectrum of the Stokes wave in the steady-state high-gain limit, in two different cases: $\Gamma_L = 0$ and $\Gamma_L \gg \Gamma$.

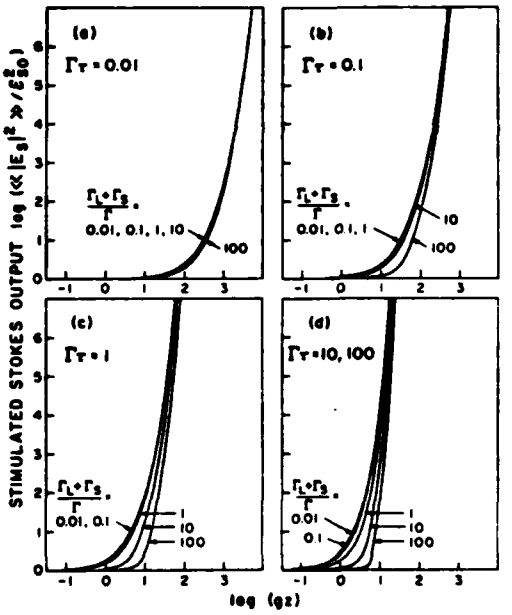

FIG. 3. Normalized Stokes output intensity as a function of gz (or pump-laser intensity), evaluated numerically using Eqs. (17b), (18), and (19b), for various values of the bandwidth ratio $(\Gamma_L+\Gamma_S)/\Gamma$, where Γ is the Raman linewidth, and Γ_L and Γ_S are the bandwidths, due to phase diffusion broadening, of the pump and probe (Stokes) lasers. Four different pulse lengths τ are shown: (a) $\Gamma\tau = 10^{-2}$, transient limit; (b) $\Gamma\tau = 10^{-1}$; (c) $\Gamma\tau = 1$; (d) $\Gamma\tau = 10$ and 10^2, steady-state limit. In all cases the effect of the laser bandwidths becomes relatively unimportant at high gains.

For a stationary wave $E(\tau)$, the definition of the power spectrum $P(\omega)$ is

$$P(\omega)=\frac{1}{2\pi}\int_{-\infty}^{\infty}e^{-i\omega s}K(s)\,ds\,, \tag{31}$$

where ω is the frequency as measured from the frequency of the carrier wave and $P(\omega)$ is the Fourier transform of the electric field autocorrelation function $K(s)$,

$$K(s)=\langle\langle E(\tau)E^{*}(\tau+s)\rangle\rangle\,. \tag{32}$$

It is easy to show from Eq. (31) that $P(\omega)$ is normalized as follows:

$$\int_{-\infty}^{\infty}P(\omega)\,d\omega=K(0)=\langle\langle|E(\tau)|^{2}\rangle\rangle\,. \tag{33}$$

As an example, when Eq. (31) is used to calculate the laser spectrum $P_L(\omega)$, from the correlation function Eq. (15), one finds

$$P_L(\omega)=\frac{\Gamma_L/\pi}{\omega^2+\Gamma_L^2}\mathcal{E}_L^2\,, \tag{34}$$

a Lorentzian, as stated in Sec. III. We can use the general solution, Eq. (11), to determine $K(s)$ for the Stokes wave

$$K(s)\simeq\mathcal{E}_{S0}^2[\tfrac{1}{4}(\alpha z)]\langle\langle F(\tau)F^{*}(\tau+s)\rangle\rangle\,, \tag{35}$$

where we have again kept only the term which dominates in the high-gain limit. In steady state ($\tau\to\infty$) we expect that $K(s)$ will depend only on s and not τ. $K(s)$ can be evaluated as

$$K(s)=\mathcal{E}_{S0}^2\frac{\alpha z}{4}\int_0^{\tau}d\tau'\int_0^{\tau+s}d\tau''f(\tau-\tau')f(\tau+s-\tau'')\frac{\langle\langle E_L(\tau)E_L^{*}(\tau')E_L^{*}(\tau+s)E_L(\tau'')\rangle\rangle}{\mathcal{E}_L^4}\frac{\langle\langle E_S(0,\tau')E_S^{*}(0,\tau'')\rangle\rangle}{\mathcal{E}_{S0}^2} \tag{36a}$$

$$=\mathcal{E}_{S0}^2\frac{\alpha z}{4}\int_0^{\tau}dx\int_0^{\tau+s}dy\,f(x)f(y)G(x,y,s)e^{-\Gamma_S|s-y+x|}\,, \tag{36b}$$

where

$$G(x,y,s)=\exp[\Gamma_L(|s+x|+|s-y|-|s-y+x|-|x|-|y|-|s|)]\,. \tag{36c}$$

Here $G(x,y,s)$ is the four-time correlation function of the pump-laser field, assuming the phase diffusion model, and is evaluated in Appendix B. In deriving Eq. (36b) we have used $x=\tau-\tau'$ and $y=\tau+s-\tau''$. In steady state the upper integration limits are extended to infinity and $K(s)$ becomes independent of τ. In order to simplify the absolute values, the integral is transformed to the triangular region above the $y=x$ line by use of the property $G(y,x,s)=G(x,y,-s)$. Then for the Stokes spectrum we have

$$P_S(\omega)=\frac{1}{2\pi}\mathcal{E}_{S0}^2\frac{\alpha z}{4}\times\int_0^{\infty}dy\int_0^{y}dx\,f(x)f(y)\mathcal{L}(x,y,\omega)\,, \tag{37a}$$

where

$$\mathcal{L}(x,y,\omega)=2\,\mathrm{Re}e^{-\Gamma_L(y+x)}\int_{-\infty}^{\infty}ds\,e^{-i\omega s}\times\exp[\Gamma_L(|s+x|+|s-y|-|s-y+x|-|s|)-\Gamma_S|s-y+x|]\,. \tag{37b}$$

The transform $\mathcal{L}$ can be calculated under the condition $x<y$. We write $\mathcal{L}$ as the sum of two parts $\mathcal{L}=\mathcal{L}_1+\mathcal{L}_2$. Defining

$$A_{\pm}=\frac{i\omega+(2\Gamma_L+\Gamma_S)}{\omega^2+(2\Gamma_L+\Gamma_S)^2}\pm\frac{i\omega+\Gamma_S}{\omega^2+\Gamma_S^2}\,, \tag{38a}$$

we can write

$$\mathcal{L}_1=2\,\mathrm{Re}A_{-}e^{-(\Gamma_L+\Gamma_S)(y-x)}+2\,\mathrm{Re}A_{+}e^{-\Gamma_L(y-x)}\cos\omega(y-x)-2\,\mathrm{Im}A_{-}e^{-\Gamma_L(y-x)}\sin\omega(y-x)\,, \tag{38b}$$

$$\mathcal{L}_2=2(-\mathrm{Re}A_{-}\cos\omega x+\mathrm{Im}A_{-}\sin\omega x)\times e^{-\Gamma_L(y+x)-\Gamma_S y}-2(\mathrm{Re}A_{-}\cos\omega y+\mathrm{Im}A_{-}\sin\omega y)\times e^{-\Gamma_L(y+x)-\Gamma_S x}\,. \tag{38c}$$

Equations (37) and (38) are now used to evaluate the Stokes output spectrum in two different cases.

A. Stokes output spectrum for a monochromatic pump laser

Here we treat the case that the pump laser is monochromatic ($\Gamma_L=0$) and the spectral width of the input Stokes is allowed to assume two different limits: $\Gamma_S=0$ or $\Gamma_S\gg\Gamma$. The steady-state gain for these two limits has already been given in Eqs. (14) and (25).

The spectrum is easily obtained by setting $\Gamma_L=0$ in Eq. (38). Then, because $A_{-}=0$, we have $\mathcal{L}_2=0$ and

$$\mathcal{L}_1=4[\Gamma_S/(\omega^2+\Gamma_S^2)]\cos\omega(y-x)\,. \tag{39}$$

Transforming back to the full x,y quadrant gives for the spectrum of the Stokes output

$$P_S(\omega) = \frac{1}{2\pi}\mathcal{E}_{S0}^2 \frac{\alpha z}{4} \frac{4\Gamma_S}{\omega^2+\Gamma_S^2} \times \frac{1}{2}\int_0^\infty dy \int_0^\infty dx f(x) f(y) \cos\omega(y-x) \tag{40a}$$

$$= \mathcal{E}_{S0}^2 \frac{\alpha z}{4} \frac{\Gamma_S/\pi}{\omega^2+\Gamma_S^2} |I|^2, \tag{40b}$$

where[29]

$$I = \int_0^\infty e^{i\omega x} f(x)\, dx = \frac{2}{(\alpha z)^{1/2}} \left[\exp\left(\frac{gz}{2}\frac{\Gamma}{\Gamma - i\omega}\right) - 1\right]. \tag{40c}$$

In the high-gain limit the Stokes output spectrum is

$$P_S(\omega) = \mathcal{E}_{S0}^2 \frac{\Gamma_S/\pi}{\omega^2+\Gamma_S^2} \exp\left(gz\frac{\Gamma^2}{\omega^2+\Gamma^2}\right). \tag{41}$$

To put this result into proper form we must assume one of the two above-mentioned limits.

The first limit is that of a monochromatic input Stokes wave ($\Gamma_S = 0$). Here we can use Eq. (14a) for the output Stokes intensity: $\langle\langle |E_S(z,\infty)|^2\rangle\rangle = \mathcal{E}_{S0}^2 e^{gz}$. Then Eq. (41) can be rewritten, in the limit $\Gamma_S \to 0$,

$$P_S(\omega) = \delta(\omega)\langle\langle |E_S(z,\infty)|^2\rangle\rangle. \tag{42}$$

Thus we see that the output Stokes wave is monochromatic when the input Stokes wave and the pump laser are monochromatic, as expected.

The second limit is $\Gamma_S \gg \Gamma$. Here we again consider a monochromatic pump laser ($\Gamma_L = 0$) and use Eq. (25) for the Stokes output $\langle\langle |E_S(z,\infty)|^2\rangle\rangle$ to rewrite Eq. (41) for the Stokes output spectrum as

$$P_S(\omega) = \frac{\Gamma_S^2}{\omega^2+\Gamma_S^2}\left(\frac{gz}{\pi\Gamma^2}\right)^{1/2} \exp\left(-gz\frac{\omega^2}{\omega^2+\Gamma^2}\right) \times \langle\langle |E_S(z,\infty)|^2\rangle\rangle, \tag{43a}$$

$$P_S(\omega) \cong \left(\frac{gz}{\pi\Gamma^2}\right)^{1/2} \exp\left(-\frac{gz}{\Gamma^2}\omega^2\right) \langle\langle |E_S(z,\infty)|^2\rangle\rangle, \tag{43b}$$

where the last step is valid because the halfwidth $[(\ln 2)\Gamma^2/gz]^{1/2}$ of the exponential factor is much less than Γ and Γ_S. Note that Eq. (43b) is normalized as in Eq. (33). Equation (43) describes a Lorentzian-shaped atomic line of width Γ that has been gain narrowed. The ideal that the center of the line will experience more gain than the wings is a familiar idea in laser theory. A comparison of the atomic line and the gain-narrowed Stokes line is shown in Fig. 4 for the case $gz = 15$.

B. Stokes output spectrum for a broad-band pump laser

Here we treat the case that the pump laser width is larger than the atomic width ($\Gamma_L \gg \Gamma$) and the input Stokes width Γ_S is arbitrary. The spectrum is obtained by applying several approximations to Eq. (38). First note that in the high-gain limit, only $\mathcal{L}_1$ will give a significant contribution to the spectrum because its exponentials damp as $(y-x)$, rather than $(y+x)$. Thus along the line $y = x$, $\mathcal{L}_1$ is large, while $\mathcal{L}_2$ becomes negligible. Second, note that because $\Gamma_L + \Gamma_S$ is assumed large ($\Gamma_L + \Gamma_S \gg \Gamma, \alpha z$), we may replace the exponential factors by properly normalized delta functions, as in the argument leading to Eq. (20);

$$e^{-(\Gamma_L+\Gamma_S)(y-x)} \to (\Gamma_L+\Gamma_S)^{-1}\delta(y-x), \tag{44a}$$

$$e^{-\Gamma_L(y-x)}\cos\omega(y-x) \to [\Gamma_L/(\omega^2+\Gamma_L^2)]\delta(y-x), \tag{44b}$$

$$e^{-\Gamma_L(y-x)}\sin\omega(y-x) \to [\omega/(\omega^2+\Gamma_L^2)]\delta(y-x). \tag{44c}$$

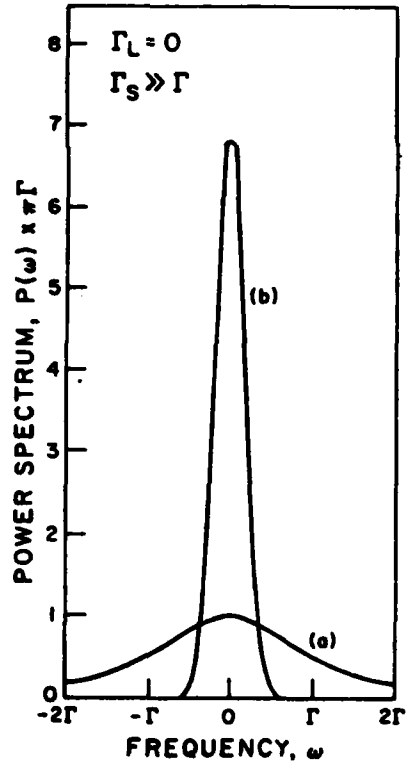

FIG. 4. Comparison of the Lorentzian Raman line shape [curve (a)] with atomic halfwidth Γ, and the gain-narrowed output Stokes spectrum [curve (b)] with halfwidth $(\ln 2\Gamma^2/gz)^{1/2}$ for $gz = 15$, plotted from Eq. (43b). This Stokes spectrum narrowing results when the pump laser is monochromatic and the input Stokes laser is broad band.

Combining these results gives

$$\mathcal{L}_1 - [4/(\Gamma_L+\Gamma_S)][\Gamma_L/(\omega^2+\Gamma_L^2)]\delta(y-x). \quad (45)$$

Now the spectrum of the output Stokes intensity $P_S(\omega)$ is easily evaluated from Eq. (37a):

$$P_S(\omega) = \frac{1}{2\pi}\mathcal{E}_{S0}^2\frac{\alpha z}{4}\frac{4}{\Gamma_L+\Gamma_S}\frac{\Gamma_L}{\omega^2+\Gamma_L^2} \times\int_0^\infty f^2(y)\,dy, \quad (46a)$$

$$P_S(\omega) = \frac{\Gamma_L/\pi}{\omega^2+\Gamma_L^2}\langle\langle|E_S(z,\infty)|^2\rangle\rangle, \quad (46b)$$

where we used Eqs. (17b) and (20a) to define the output Stokes intensity $\langle\langle|E_S(z,\infty)|^2\rangle\rangle$. Note that $P_S(\omega)$ is normalized as required by Eq. (33). This indicates that our neglect of $\mathcal{L}_2$ is justified.

Comparing Eqs. (46b) and (34) shows that the Stokes wave assumes *exactly* the same spectrum as the pump laser during the amplification process, regardless of the spectral width of the input Stokes wave.

V. DISCUSSION

In the case just treated, that the pump laser width is greater than the atomic width ($\Gamma_L \gg \Gamma$), our interpretation is that the fluctuations in the phase of the pump laser dominate the time behavior of the amplification process. Indeed, Carman *et al.*[18] found numerically, in the case of a quadratic phase sweep in the pump laser, that the Stokes phase closely followed this sweep after a brief initial period. Our result for the Stokes spectrum [Eq. (46)] is *consistent* with the conjecture of Carman *et al.* that, when $\Gamma_L \gg \Gamma$, the Stokes phase always follows the pump phase in the high-gain limit, regardless of the phase structure of the input Stokes wave. If correct, this effect, which we will call "phase locking," also explains the fact that the gain is unaffected by the phase fluctuations which lead to the bandwidth. As Carman *et al.* pointed out, if the phases φ_S and φ_L differ at all points by a constant [$\varphi_S(z,t) = \varphi_L(z,t) + \varphi_0$], the phases drop out entirely from Eq. (11), leading to the narrow-band gain result, Eq. (14). Thus, the idea of "phase locking" leads to results consistent with our results for $\Gamma_L \gg \Gamma$. When both Γ_L and Γ_S are larger than Γ, we can say that the amplified Stokes wave builds up from the broad-band input noise in a way which automatically satisfies $\varphi_S = \varphi_L + \varphi_0$. That is, only that part of the noise which satisfies this relation will experience large gain.

To illustrate the idea of phase locking we have compared, in Fig. 5, several steady-state gain curves. We have reproduced curves from Fig. 3(d), calculated from the exact equations (labeled "phase locked"). We have also plotted curves using Eq. (14a) (labeled "narrow band"), and also using Eq. (14a) with g replaced by g_{BB} of Eq. (29) (labeled "unlocked"). We see that at low gains the exact curve follows the "unlocked" curve, consistent with the idea that there is no correlation between the output Stokes and pump laser waves. This low-gain behavior was predicted at the end of Sec. III B. However, at high gains the exact curve approaches the "narrow-band" curves, consistent with the idea that it has become "phase locked," resulting in an enhanced gain. We thus see that phase locking appears to occur only above a certain (threshold) gain. In contrast to the behavior found in the present treatment, Dzhotyan *et al.*[22] found in the multimode approach (see Sec. I) that the "narrow-band" gain was appropriate even at low gains. This is a major difference between the two models.

Finally, we point out that we have treated only the case of Raman amplification, and not SRS which grows from the initial Stokes photons spontaneously emitted with frequencies near ω_S, in the absence of an external input Stokes wave at that frequency. Here we wish to make some conjectures on the outcome in the latter case. We may consider the spontaneous photons as making up the source term $E_S(0,\tau)$. Although here we certainly cannot make the decorrelation of the pump wave $E_L(\tau)$ and source term $E_S(0,\tau)$ that we made in connection with Eq. (18), we still expect that, at high gains, the major results we have obtained do apply to spontaneously generated SRS. That is, we expect the gain to be essentially in-

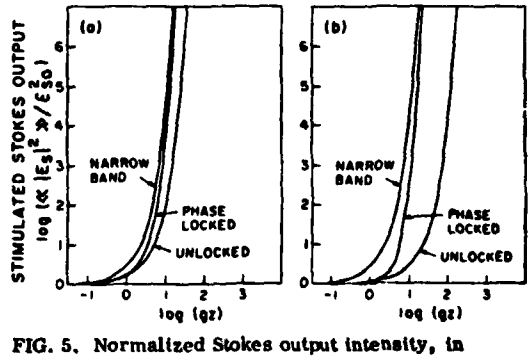

FIG. 5. Normalized Stokes output intensity, in steady-state, as a function of gz (or pump-laser intensity), for two different laser bandwidth ratios: (a) $(\Gamma_L+\Gamma_S)/\Gamma = 1$ and (b) $(\Gamma_L+\Gamma_S)/\Gamma = 10$. In both cases, the exact results (labeled "phase locked") are seen to agree, at low gains, with the results one would expect in the absence of phase locking (labeled "unlocked"), which were obtained by replacing Γ by $\Gamma+\Gamma_L+\Gamma_S$ in the expression [Eq. (14b)] for the gain coefficient g. However, at higher gains, the exact results approach the narrow-band curve [Eqs. (14a) and (14b)].

dependent of pump-laser bandwidth, and when the pump bandwidth is greater than the atomic width we expect the output SRS to assume the spectrum of the pump.

VI. SUMMARY

Using the phase diffusion model, we have extended the theory of stimulated Raman scattering, in the case of two interacting classical waves (pump and input Stokes), to allow for arbitrary bandwidth of either wave. In the forward direction if there is no dispersion, we showed that, in the high-gain limit, the gain of the Stokes wave is essentially independent of the input bandwidth of either wave. In the low-gain limit the gain coefficient was found to be inversely proportional to the sum of the bandwidths. We also calculated the spectrum of the output Stokes wave, in the high-gain limit, under various conditions. We found that when the pump bandwidth Γ_L is greater than the atomic width Γ, the Stokes wave assumes exactly the spectrum of the pump laser, regardless of the spectral width Γ_S of the input Stokes wave. When both input waves are monochromatic ($\Gamma_L, \Gamma_S = 0$), we found that the Stokes spectrum is unchanged by the amplification process. Finally, when $\Gamma_L = 0$ and $\Gamma_S \gg \Gamma$, we found that the output Stokes wave has a spectrum which is a gain-narrowed atomic profile; that is, the Stokes width becomes much narrower than the atomic width.

Note added in proof. A recent preprint by W. R. Trutna, Y. K. Park, and R. L. Byer [to appear in IEEE J. Quant. Electron. (July 1979)] has come to our attention. Broad-band SRS was treated using the coupled-wave approach (similar to that in Ref. 22) and qualitative agreement was found with our work in the high-gain limit. At low gains, however, their treatment indicates no suppression of the gain, in contrast to our results [Eq. (30)].

ACKNOWLEDGMENTS

We would like to acknowledge the interest and helpful comments of C. R. Holt, J. H. Eberly, A. Szöke, and J. Cooper, as well as the assistance of C. V. Kunasz with the numerical work. This work was supported by Office of Naval Research Contract No. N00014-76-C-0611 and National Science Foundation Grant No. PHY76-04761, both through the University of Colorado. One of us (J.M.) was supported by a Fulbright-Hays Fellowship.

APPENDIX A

Here we discuss more carefully the elimination of a_2 from Eq. (3). We first neglect $\dot{\phi}_L$ in Eq. (3b), as Δ_L is assumed to be much larger than the pump laser bandwidth. The formal solution of Eq. (3b) can then be written

$$a_2(t) = \int_0^t e^{-i\Delta_L(t-t')} g(t')\,dt', \tag{A1}$$

$$g(t) = i[\tfrac{1}{2}\Omega_L a_1(t) + \tfrac{1}{2}\Omega_S a_3(t)]. \tag{A2}$$

Repeated integration by parts gives

$$a_2(t) = \frac{g(t) - e^{-i\Delta_L t} g(0)}{i\Delta_L} - \frac{\dot{g}(t) - e^{-i\Delta_L t}\dot{g}(0)}{(i\Delta_L)^2} + \frac{\ddot{g}(t) - e^{-i\Delta_L t}\ddot{g}(0)}{(i\Delta_L)^3} - \cdots . \tag{A3}$$

Note that since $a_1(0) = 1$ and $a_2(0) = 0$, $g(0) = i(\frac{1}{2})\Omega_L$. When one assumes $\Delta_L \gg \Delta_S, \dot{\phi}_L, \dot{\phi}_S, \Omega_L, \Omega_S$, it can be shown from Eq. (3) that $\dot{g}(t) \ll \Delta_L g(t)$. Thus when Δ_L is large, one is left with

$$a_2(t) \cong [g(t) - i\tfrac{1}{2}\Omega_L e^{-i\Delta_L t}]/i\Delta_L . \tag{A4}$$

However, because Δ_L is large, the exponential term oscillates rapidly compared to $g(t)$. Hence, in the spirit of the RWA, we neglect the rapidly oscillating part and retain only the slowly varying part:

$$a_2(t) \cong g(t)/i\Delta_L = (\tfrac{1}{2}\Omega_L a_1(t)\,\tfrac{1}{2}\Omega_S a_3(t))/\Delta_L . \tag{A5}$$

It is interesting that the same result is obtained by merely setting $\dot{a}_2 = 0$ in Eq. (3b).

APPENDIX B: PHASE-DIFFUSION MODEL

The phase-diffusion model for laser bandwidth describes, to good approximation, a cw laser operating well above threshold, where the intensity, $I(t) = I_0 + I'(t)$, is nearly constant, with average value I_0 and small fluctuations $I'(t)$.[35] However, well above threshold the phase $\varphi(t)$ fluctuates randomly, in a way reminiscent of a diffusing Brownian particle. Simple laser theory gives the equations for the intensity and phase as[36]

$$\dot{I}'(t) = -\lambda I'(t) + F_I(t), \tag{B1}$$

$$\dot{\phi}(t) = F_\phi(t), \tag{B2}$$

where $F_I(t)$ and $F_\phi(t)$ are random Langevin forces with correlation functions

$$\langle\langle F_I(t_1)F_I(t_2)\rangle\rangle = 2D\delta(t_1 - t_2),$$

$$\langle\langle F_\phi(t_1)F_\phi(t_2)\rangle\rangle = 2\Gamma\delta(t_1 - t_2),$$

and

$$\langle\langle F_I(t_1)F_\phi(t_2)\rangle\rangle = 0.$$

Here $1/\lambda$ is the correlation time of the intensity fluctuations, with mean value D/λ, and Γ is the bandwidth of the light. These δ correlations simply imply that the forces fluctuate on a time scale shorter than any other interesting time scale.

The phase-diffusion model is based on the assumption that the intensity exhibits no fluctuations, $I'(t) = 0$, and that the phase fluctuates according to Eq. (B2). The correlation function for the phase

can be derived from Eq. (B2) as

$$\langle\langle \varphi(t_1)\varphi(t_2)\rangle\rangle = \int_0^{t_1} dt \int_0^{t_2} dt' \langle\langle F_\varphi(t)F_\varphi(t')\rangle\rangle$$
$$= \Gamma(t_1 + t_2 - |t_1 - t_2|), \tag{B3}$$

where we have taken $\varphi(0) = 0$, since the results calculated later cannot depend on $\varphi(0)$ for a stationary process. In the present context, the aim of the model is to calculate correlation functions for the field $E(t) = \mathcal{E} e^{i\varphi(t)}$, where we are using the notation of Eq. (9). Here we have assumed that the field amplitude $\mathcal{E}$ (and thus the intensity) is a constant. So the correlation functions can be written

$$\langle\langle E(t_1)\cdots E(t_m)E^*(t_{m+1})\cdots E^*(t_n)\rangle\rangle$$
$$= \mathcal{E}^n \langle\langle \exp[i\varphi(t_1) + \cdots + i\varphi(t_m)$$
$$- i\varphi(t_{m+1}) - \cdots - i\varphi(t_n)]\rangle\rangle. \tag{B4}$$

In order to calculate these correlations it is expedient to further assume that the phase $\varphi(t)$ is a Gaussian stochastic quantity, that is, correlation functions of any order can be expressed in terms of the two-time correlation function of the phase $\langle\langle \varphi(t_1)\varphi(t_2)\rangle\rangle$. Specifically,[37] we have

$$\langle\langle \varphi(t_1)\cdots\varphi(t_{2m+1})\rangle\rangle = 0,$$
$$\langle\langle \varphi(t_1)\cdots\varphi(t_{2m})\rangle\rangle = \sum_{\text{perm}} \langle\langle \varphi(t_{i_1})\varphi(t_{i_2})\rangle\rangle \cdots$$
$$\times \langle\langle \varphi(t_{i_{2m-1}})\varphi(t_{i_{2m}})\rangle\rangle, \tag{B5}$$

where the summation is taken over all unique permutations of $t_1, \ldots, t_{2m}$. A useful relation can be derived from Eq. (B5), which makes it easy to calculate the correlation functions in Eq. (B4). This is

$$\left\langle\left\langle \exp\left(i\int_{-\infty}^{\infty} dt' J(t')\varphi(t')\right)\right\rangle\right\rangle$$
$$= \exp\left(-\frac{1}{2}\int_{-\infty}^{\infty} dt' \int_{-\infty}^{\infty} dt'' J(t')J(t'')\right.$$
$$\left.\times \langle\langle \varphi(t')\varphi(t'')\rangle\rangle\right), \tag{B6}$$

where $J(t')$ is an arbitrary function.[38] This relation can be proven, term by term, after expanding the exponentials and using the property Eq. (B5).

We can now calculate the desired correlation functions. By letting $J(t') = \delta(t' - t_1)$ in Eq. (B6) we get

$$\langle\langle E(t_1)\rangle\rangle = \mathcal{E}\langle\langle \exp[i\varphi(t_1)]\rangle\rangle$$
$$= \mathcal{E} \exp(-\Gamma t_1) \to 0, \tag{B7}$$

where we have taken the stationary limit $\Gamma t_1 \to \infty$, where the initial transients have died out. Thus the average field is zero, as expected for a fluctuating field. By letting $J(t') = \delta(t' - t_1) - \delta(t' - t_2)$ in Eq. (B6) we get

$$\langle\langle E(t_1)E^*(t_2)\rangle\rangle = \mathcal{E}^2\langle\langle \exp[i\varphi(t_1) - i\varphi(t_2)]\rangle\rangle$$
$$= \mathcal{E}^2 \exp(-\Gamma|t_1 - t_2|). \tag{B8}$$

The power spectrum of the field, given by the Fourier transform of the two-time correlation function in Eq. (B8), is thus a Lorentzian with halfwidth Γ. The four-time correlation function used in Sec. IV can be calculated by letting

$$J(t') = \delta(t' - t_1) + \delta(t' - t_2)$$
$$- \delta(t' - t_3) - \delta(t' - t_4),$$

which gives

$$\langle\langle E(t_1)E(t_2)E^*(t_3)E^*(t_4)\rangle\rangle$$
$$= \mathcal{E}^4 \exp\{\Gamma(|t_1 - t_2| + |t_3 - t_4| - |t_1 - t_3|$$
$$- |t_1 - t_4| - |t_2 - t_3| - |t_2 - t_4|)\}. \tag{B9}$$

This result can be used to illustrate one of the basic assumptions of the phase-diffusion model. By letting $t_3 = t_1$ and $t_4 = t_2$, and defining the intensity as $I(t) = |E(t)|^2$, we can see from Eq. (B9) that the intensity correlation function is given by

$$\langle\langle I(t_1)I(t_2)\rangle\rangle = \mathcal{E}^4 = I_0^2, \tag{B10}$$

i.e., the intensity is always perfectly correlated with itself in the phase-diffusion model, because it does not fluctuate.

APPENDIX C

Here we describe the numerical technique used to evaluate the double integral in Eq. (19b). Let $r = (\tau - \tau')^{1/2}$, $s = (\tau - \tau'')^{1/2}$, and $a = (\alpha z)^{1/2}$. Then, we have

$$\langle\langle |F(\tau)|^2\rangle\rangle = 4\int_0^{\tau^{1/2}} dr \int_0^{\tau^{1/2}} ds\, e^{-\Gamma r^2} I_1(ar)$$
$$\times e^{-\Gamma s^2} I_1(as)\, e^{-(\Gamma_L + \Gamma_S)|s^2 - r^2|} \tag{C1}$$
$$= 8\int_0^{\tau^{1/2}} dr \int_0^{r} ds\, e^{-\Gamma r^2} I_1(ar)$$
$$\times e^{-\Gamma s^2} I_1(as)\, e^{-(\Gamma_L + \Gamma_S)(r^2 - s^2)}, \tag{C2}$$

where we used the symmetry of the integrand in Eq. (C1) with respect to interchange of r and s. Now defining

$$u(x) = \tfrac{1}{4}\langle\langle |F(x^2)|^2\rangle\rangle \tag{C3}$$

and

$$v(x) = e^{-(\Gamma + \Gamma_L + \Gamma_S)x^2} \int_0^x ds\, e^{(\Gamma - \Gamma_L - \Gamma_S)s^2} I_1(as), \tag{C4}$$

we have

$$u(x)=\int_0^x dr\, I_1(ar)v(r), \tag{C5}$$

from which we can obtain

$$u'(x)=I_1(ax)v(x), \tag{C6}$$

$$v'(x)=-2(\Gamma+\Gamma_L+\Gamma_S)xv(x)+e^{-2\Gamma x^2}I_1(ax). \tag{C7}$$

Thus we have transformed the double integral into a set of two coupled ordinary differential equations, Eqs. (C6) and (C7), which can be solved readily by standard numerical techniques.

---

*Also at the Dept. of Chemistry, University of Colorado, Boulder, Colo.
†Permanent address: Institute of Physics, Polish Academy of Sciences, 02-668 Warsaw, Poland.
‡Present address: Los Alamos Scientific Laboratory, University of California, Los Alamos, N. M. 87545.

[1]P. Zoller, J. Phys. B 11, 2825 (1978).
[2]P. L. Knight, W. A. Molander, and C. R. Stroud, Jr., Phys. Rev. A 17, 1547 (1978).
[3]H. J. Kimble and L. Mandel, Phys. Rev. A 15, 689 (1977).
[4]G. S. Agarwal, Phys. Rev. Lett. 37, 1383 (1976).
[5]J. H. Eberly, Phys. Rev. Lett. 37, 1387 (1976).
[6]P. Avan and C. Cohen-Tannoudji, J. Phys. B 10, 155 (1977).
[7]N. C. Wong and J. H. Eberly, Opt. Lett. 1, 211 (1977); J. H. Eberly, J. Phys. B 11, L611 (1978).
[8]B. R. Marx, J. Simons, and L. Allen, J. Phys. B 11, L273 (1978).
[9]J. Ducuing and N. Bloembergen, Phys. Rev. 133, A1493 (1964).
[10]A. T. Georges and P. Lambropoulos, Phys. Rev. A 18, 587 (1978).
[11]J. L. F. de Meijere and J. H. Eberly, Phys. Rev. A 17, 1416 (1978).
[12]L. A. Armstrong, Jr., P. Lambropoulos, and N. K. Rahman, Phys. Rev. Lett. 36, 952 (1976).
[13]G. Mainfray, in *Multiphoton Processes*, edited by J. H. Eberly and P. Lambropoulos (Wiley, New York, 1978).
[14]See, for example, D. Cotter, and W. Zapka, Opt. Commun. 26, 251 (1978); and N. Djeu and R. Burnham, Appl. Phys. Lett. 30, 473 (1977).
[15]J. R. Murray, J. Goldhar, and A. Szöke, Appl. Phys. Lett. 32, 551 (1978).
[16]M. G. Raymer and J. L. Carlsten, Bull. Am. Phys. Soc. 22, 1318 (1977); 23, 1106 (1978); and unpublished.
[17]Y. R. Shen, Rev. Mod. Phys. 48, 1 (1976); J. B. Grun, A. K. McQuillan, and B. P. Stoicheff, Phys. Rev. 180, 61 (1969).
[18]R. L. Carman, F. Shimizu, C. S. Wang, and N. Bloembergen, Phys. Rev. A 2, 60 (1970).
[19]S. A. Akhmanov, Yu. E. D'yakov, and L. I. Pavlov, Sov. Phys. JETP 39, 249 (1974).
[20]N. Bloembergen and Y. R. Shen, Phys. Rev. Lett. 13, 720 (1964).
[21]R. G. Brewer, J. R. Lifsitz, E. Garmire, R. Y. Chiao, and C. H. Townes, Phys. Rev. 166, 326 (1968).
[22]G. P. Dzhotyan, Yu. E. D'yakov, I. G. Zubarev, A. B. Mironov, and S. I. Mikhailov, Sov. Phys. JETP 46, 431 (1977); Sov. J. Quantum Electron. 7, 783 (1977); J. A. Giordmaine and W. Kaiser, Phys. Rev. 144, 676 (1966); R. L. Byer and R. L. Herbst, in *Nonlinear Infrared Generation*, edited by Y. R. Shen (Springer-Verlag, Berlin, 1977); S. E. Harris, IEEE J. Quant. Electron. 2, 701 (1966); 3, 205 (1967).
[23]For discussions of the rotating frame, the Bloch equations, and the slowly varying envelope approximation, see L. Allen and J. H. Eberly, *Optical Resonance and Two-Level Atoms* (Wiley, New York, 1975); J. D. Macomber, *The Dynamics of Spectroscopic Transitions* (Wiley, New York, 1976).
[24]M. Takatsuji, Phys. Rev. A 11, 619 (1975).
[25]D. Grischkowsky, M. M. T. Loy, and P. F. Liao, Phys. Rev. A 12, 2514 (1975).
[26]E. Courtens, in *Laser Handbook*, edited by F. T. Arecchi and E. O. Schulz-Dubois (North-Holland, Amsterdam, 1972).
[27]C. S. Wang, Phys. Rev. 182, 482 (1969); and in *Quantum Electronics: A Treatise*, edited by H. Rabin and C. L. Tang (Academic, New York, 1975).
[28]*Handbook of Mathematical Functions*, edited by M. Abramowitz and I. Stegun (U.S. GPO, Washington, 1964).
[29]I. S. Gradshteyn and I. M. Ryzik, *Table of Integrals, Series, and Products* (Academic, New York, 1965), see Sec. 6.618, Eq. (4), Sec. 8.407, Eq. (3), and Sec. 8.464, Eq. (1).
[30]J. J. Wynne and P. P. Sorokin, in *Topics in Applied Physics, Vol. 16: Nonlinear Infrared Generation*, edited by Y.-R. Shen (Springer-Verlag, Berlin, 1977), see Eq. (5.14).
[31]One might also imagine the brackets to indicate a time average. Apparently, in the present context, the relationship of ensemble and time averages is somewhat debatable [J. H. Eberly (private communication, 1978)].
[32]For discussion of a case where this type of decorrelation is *not* assumed, see the first paper in Ref. 7.
[33]See Ref. 29, Sec. 6.633, Eq. (5), and Ref. 34 for properties of the hypergeometric functions.
[34]Y. L. Luke, *The Special Functions and Their Approximations* (Academic, New York, 1969), Vol. 1, see Sec. 5.11.
[35]H. Haken, in Ref. 26.
[36]See Ref. 1 and discussion following Eq. (22) of Ref. 35.
[37]See Ref. 35 and M. C. Wang and G. E. Uhlenbeck, in *Selected Papers on Noise and Stochastic Processes*, edited by N. Wax (Dover, New York, 1954), see Eq. (42).
[38]J. R. Klauder and E. C. G. Sudarshan, *Fundamentals of Quantum Optics* (Benjamin, New York, 1968), p. 33.

Resonance fluorescence in a weak radiation field with arbitrary spectral distribution

M. G. Raymer* and J. Cooper
Joint Institute for Laboratory Astrophysics, University of Colorado and National Bureau of Standards, Boulder, Colorado 80309
(Received 16 July 1979)

The authors show that the laser bandwidth effects in resonance fluorescence at low intensities can be treated most readily in terms of simple convolutions, and further that this approach allows one to consider an incident field with an arbitrary spectral distribution, with or without the presence of atomic (line-broadening) collisions.

I. INTRODUCTION

In a recent paper by Knight, Molander, and Stroud[1] (KMS) an interesting pedagogical discussion was given of the effects of laser bandwidth on atomic resonance fluorescence spectra at low intensities. Assuming a Lorentzian-shaped laser spectrum (phase-diffusion model[2,3]) they showed that the finite bandwidth gives rise to an asymmetry in the scattered spectrum when the incident field is detuned from the atomic resonance. They offered a physical explanation for the asymmetry, first found by Kimble and Mandel,[4] in terms of a continuing reinitiation of the transient response of the atom owing to the fluctuations in the laser field. While this explanation is most certainly correct, one point remained unclear, that concerning the role of the convolution in this problem, which is a particular case of linear response theory.

The purpose of this comment is twofold: to show that the laser bandwidth effects in resonance fluorescence at low intensities can be treated most readily in terms of a simple convolution and to show further that this approach allows one to consider an incident field with an arbitrary spectral distribution, with or without the presence of atomic (line-broadening) collisions.

II. EFFECT OF LASER LINE SHAPE

For ease of comparison we will follow KMS and use, where possible, their notation. We start with the low-intensity operator Bloch equation for the positive-frequency dipole operator $\hat{\sigma}_+$,

$$\dot{\hat{\sigma}}_+(t) = (i\omega_0 - \gamma_N)\hat{\sigma}_+(t) - (id/\hbar)\hat{E}^-(t), \tag{1}$$

where ω_0 is the atomic resonance frequency, γ_N is one-half the natural decay width, d is the transition dipole moment, and $\hat{E}^-(t)$ is the negative-frequency electric field operator for the driving field, which oscillates with frequency ω_L. The scattered spectrum $g(\omega,\omega_L)$ is given in steady state by the Fourier transform of the dipole autocorrelation function $\langle\langle\hat{\sigma}_+(t)\hat{\sigma}_-(t+\tau)\rangle\rangle$, which is obtained by formally solving Eq. (1). This yields

$$g(\omega,\omega_L) = \int_{-\infty}^{\infty} d\tau \exp(i\omega\tau)\frac{d^2}{\hbar^2}\int_{-\infty}^{t} dt' \int_{-\infty}^{t+\tau} dt'' \exp[(i\omega_0-\gamma_N)(t-t')]\exp[(-i\omega_0-\gamma_N)(t+\tau-t'')]\langle\langle\hat{E}^-(t')\hat{E}^+(t'')\rangle\rangle, \tag{2}$$

where ω is the frequency of the scattered light. The angular brackets $\langle\langle\ \rangle\rangle$ indicate both a quantum expectation value and an ensemble average over the statistics of the driving field.

For a monochromatic laser the field-correlation function is

$$\langle\langle\hat{E}^-(t')\hat{E}^+(t'')\rangle\rangle = |E_0|^2\exp[i\omega_L(t'-t'')], \tag{3}$$

giving for the narrow-band spectrum $g_{NB}(\omega,\omega_L)$

$$g_{NB}(\omega,\omega_L) = \int_{-\infty}^{\infty} d\tau \exp(i\omega\tau)\frac{d^2|E_0|^2}{\hbar^2}\int_{-\infty}^{t} dt' \int_{-\infty}^{t+\tau} dt'' \exp[(i\omega_0-\gamma_N)(t-t')]\exp[(-i\omega_0-\gamma_N)(t+\tau-t'')]\exp[i\omega_L(t'-t'')]. \tag{4}$$

This result can be evaluated to give

$$g_{NB}(\omega,\omega_L) = \frac{\pi}{2}\frac{\Omega^2}{(\omega_0-\omega_L)^2+\gamma_N^2}\delta(\omega-\omega_L), \tag{5}$$

which shows that only elastic scattering occurs for an isolated atom suffering no collisions.

KMS treat the broad-band laser by assuming the phase-diffusion model[2,3] for the field

$$\langle\langle\hat{E}^-(t')\hat{E}^+(t'')\rangle\rangle = |E_0|^2\exp[i\omega_L(t'-t'')]\exp(-\gamma_L|t'-t''|), \tag{6}$$

where γ_L is one-half the laser bandwidth. Using this in Eq. (2) leads directly to the main result of KMS[6]:

$$g(\omega,\omega_L)=\frac{\Omega^2\gamma_L/2}{[\Delta^2+(\gamma_N-\gamma_L)^2][\Delta^2+(\gamma_N+\gamma_L)^2]}\times\left(\frac{\Delta^2+2\Delta(\omega-\omega_L)+(\gamma_N^2-\gamma_L^2)}{(\omega-\omega_L)^2+\gamma_L^2}+\frac{\Delta^2-2\Delta(\omega-\omega_0)-(\gamma_N^2-\gamma_L^2)}{(\omega-\omega_0)^2+\gamma_N^2}\right), \quad (7)$$

where the detuning is $\Delta=\omega_0-\omega_L$ and the Rabi frequency is $\Omega=2d|E_0|/\hbar$. This spectrum clearly shows two maxima: elastic scattering centered at ω_L and fluorescence centered at ω_0. However, it also seems to contain interesting interference structure, e.g., $(\omega-\omega_L)$ in the numerator. It is stated by KMS that "the spectrum $[g(\omega,\omega_L)]$ is *not* the narrow-band response convolved with the spectral line shape of the incident field" (Lorentzian in this case). This statement is certainly correct for intense, saturating incident fields. However, we will show here that $g(\omega,\omega_L)$ in Eq. (7), valid for low fields, *is* obtainable by a simple convolution. This is as expected in linear response theory.

We will solve the problem in a different, more revealing, way. The power spectrum $P_L(\omega_L')$ of the incident field is generally given by[6]

$$P_L(\omega_L')=\frac{1}{2\pi}\int_{-\infty}^{\infty}d\tau\,\exp(i\omega_L'\tau)\,\langle\!\langle\hat{E}^-(t)\hat{E}^+(t+\tau)\rangle\!\rangle, \quad (8)$$

and the inverse can be written as

$$\langle\!\langle\hat{E}^-(t')\hat{E}^+(t'')\rangle\!\rangle=\int_{-\infty}^{\infty}d\omega_L'\exp[i\omega_L'(t'-t'')]P_L(\omega_L'). \quad (9)$$

Inserting this form for the correlation function into Eq. (2) for the spectrum $g(\omega,\omega_L)$, and comparing the resulting equation with the narrow-band spectrum $g_{NB}(\omega,\omega_L)$ in Eq. (4), it becomes apparent that the spectrum $g(\omega,\omega_L)$ can be written as

$$g(\omega,\omega_L)=|E_0|^{-2}\int_{-\infty}^{\infty}d\omega_L'\,g_{NB}(\omega,\omega_L')P_L(\omega_L'). \quad (10)$$

This is the main result of this paper and shows that, for an *arbitrary* laser spectrum $P_L(\omega_L')$, the scattered spectrum $g(\omega,\omega_L)$, at low intensity, is given by the narrow-band scattered spectrum $g_{NB}(\omega,\omega_L)$ convolved with the laser spectrum. Using the δ-function form of $g_{NB}(\omega,\omega_L)$ from Eq. (5) in Eq. (10) results in

$$g(\omega,\omega_L)=|E_0|^{-2}\frac{\pi}{2}\frac{\Omega^2}{(\omega-\omega_0)^2+\gamma_N^2}P_L(\omega), \quad (11)$$

which shows that the scattered light retains a distorted version of the incident light spectrum $P_L(\omega_L')$.

For the special case of the phase-diffusion model, used by KMS and described in Eq. (6), the laser spectrum becomes [by inserting Eq. (6) into Eq. (8)]

$$P_L(\omega_L')=|E_0|^2\frac{\gamma_L/\pi}{(\omega_L'-\omega_L)^2+\gamma_L^2}, \quad (12)$$

a Lorentzian, as stated earlier. This then gives, from Eq. (11), the scattered spectrum as

$$g(\omega,\omega_L)=\frac{\pi}{2}\frac{\Omega^2}{[(\omega-\omega_0)^2+\gamma_N^2]}\frac{\gamma_L/\pi}{[(\omega-\omega_L)^2+\gamma_L^2]}, \quad (13)$$

a result which is simple in form, but in fact (after some algebra) is identical to the more complex-looking expression given by KMS in Eq. (7). This shows that the scattered spectrum is the product of two Lorentzians, one peaked at the laser frequency ω_L and the other at the atomic resonance frequency ω_0.

III. COMMENTS

We have shown [Eq. (10)] that, for low-intensity resonance fluorescence in the absence of collisions, the scattered spectrum is given by that derived by assuming a monochromatic driving laser convolved with the spectrum of the actual driving laser. This result holds for *arbitrary* laser line shapes and, in particular, for the Lorentzian line shape derived from the phase-diffusion model[2,3] and used by KMS. The convolution is no longer valid when an intense, saturating driving laser is considered, as the response of the atom is then nonlinear.[4] The conclusion of KMS, that the inelastic component of the scattered light (centered on ω_0) is due to the continuing reinitiation of the transient response of the atom by fluctuations in the driving field, is strengthened by the present result. The conclusion holds regardless of the form of the power spectrum of the fluctuations.

As a further demonstration of the generality of the convolution result, we consider the effects of atomic line-broadening collisions on the scattered spectrum. These include dephasing (or elastic) collisions and quenching collisions, as well as alignment- and orientation-changing collisions. The effect of collisions has been studied in detail for the case of a low-intensity monochromatic driving field.[7-9] In particular, it is known that collisions redistribute the frequency of the scattered light and thus Eq. (5), for the scattered spectrum, is not appropriate in this case. However, denoting the appropriate narrow-band scattered spectrum[10] by $G_{NB}(\omega,\omega_L)$, the scattered spectrum $G(\omega,\omega_L)$ for broad-band excitation can be shown still to be a simple convolution

$$G(\omega,\omega_L)=|E_0|^{-2}\int_{-\infty}^{\infty}d\omega_L'\,G_{NB}(\omega,\omega_L')P_L(\omega_L'), \quad (14)$$

where again $P_L(\omega_L')$ is the (arbitrary) spectrum of the low-intensity driving field. This result can be verified by inspecting Eqs. (4) and (5) of Ref. 7, which give the scattered spectrum $G_{NB}(\omega,\omega_L)$ as an integral over several terms including the factor

$$I_1(\hat{\epsilon}_1^* \cdot \vec{\mu})(\hat{\epsilon}_1 \cdot \vec{\mu})\exp[-i\omega_L(t_1 - t_3)],$$

where I_1 is the intensity of the incident laser with polarization vector $\hat{\epsilon}_1$ and $\vec{\mu}$ is the atomic dipole operator. For an arbitrary driving field spectrum this factor should be replaced by

$$\langle\langle(\vec{E}_1^*(t_1)\cdot\vec{\mu})(\vec{E}_1(t_3)\cdot\vec{\mu})\rangle\rangle,$$

where $\vec{E}_1(t)$ is the electric field of the laser, and the field average has been performed. This field-correlation function is analogous to the one appearing in the integrand in Eq. (2) for $\mathcal{G}(\omega,\omega_L)$, where collisions were ignored. Thus the derivation of $G(\omega,\omega_L)$ in Eq. (14) follows identically to that of $\mathcal{G}(\omega,\omega_L)$ in Eq. (10). The convolution result Eq. (14) for the scattered spectrum $G(\omega,\omega_L)$ holds for arbitrary collisional line shapes, both inside and outside the impact region.

This research was supported by the Office of Naval Research and the National Science Foundation.

---

*Present address: The Institute of Optics, Univ. of Rochester, Rochester, N.Y. 14627.

[1]P. L. Knight, W. A. Molander, and C. R. Stroud, Jr., Phys. Rev. A 17, 1547 (1978).
[2]J. H. Eberly, Phys. Rev. Lett. 37, 1387 (1976).
[3]M. G. Raymer, J. Mostowski, and J. L. Carlsten, Phys. Rev. A 19, 2304 (1979).
[4]H. J. Kimble and L. Mandel, Phys. Rev. A 15, 689 (1977).
[5]The square on the Ω^2 was inadvertently left out of the equation in Ref. 1.
[6]See, for example, B. R. Mollow, Phys. Rev. A 188, 1969 (1969).
[7]A. Omont, E. W. Smith, and J. Cooper, Astrophys. J. 175, 185 (1972).
[8]J. Cooper, Astrophys. J. 228, 339 (1979).
[9]M. G. Raymer, J. L. Carlsten, and G. Pichler, J. Phys. B 12, L119 (1979); J. L. Carlsten, A. Szöke, and M. G. Raymer, Phys. Rev. A 15, 1029 (1977), and references therein.
[10]See, for example, Eq. (63) of Ref. 7 and Eq. (88) of Ref. 8.

OBSERVATION OF ZEEMAN DEGENERACY EFFECTS IN COLLISIONAL INTENSE FIELD RESONANCE FLUORESCENCE

P.D. KLEIBER, K. BURNETT and J. COOPER

Joint Institute for Laboratory Astrophysics, University of Colorado and National Bureau of Standards, and Department of Physics, University of Colorado, Boulder, CO 80309, USA

Received 11 May 1981

We report observation of the scattered spectrum from a Zeeman degenerate atom at high laser intensities. For a $J = 0$ to $J = 1$ transition in the presence of collisions we observe an asymmetric triplet in the polarization parallel to the incident laser and an asymmetric doublet in the polarization perpendicular to the incident laser.

1. Introduction. In recent years there has been widespread interest in high-intensity near-resonant light scattering in the presence of collisions [1–6]. Mollow [1,2] has developed the theory for a simple two-state atom, including the effects of collisions by introducing phenomenological relaxation terms to the equations of a strongly driven two-state system. This approximation, which is equivalent to the Markoff approximation, leads to equations which are valid in the impact region of the spectrum. The theory predicts the well-known asymmetric triplet structure in the scattered spectrum. These effects have been observed by Carlsten, Szöke and Raymer (CSR) [4] in nonlinear light scattering from strontium perturbed by argon.

Recently, Copper, Ballagh and Burnett (CBB) [5], and Fiutak and Van Kranendonk [6] have calculated the expected polarized scattering spectrum at high intensities when Zeeman degeneracy effects are included. CBB predict, for the case of a $J = 0$ to $J = 1$ transition and a linearly polarized incident laser, an asymmetric triplet scattered in π polarization, and an asymmetric doublet in σ polarization. The predictions for the π-polarized scattering spectrum agree with ref. [6], however, Fiutak and Van Kranendonk do not quote results for the σ-polarized spectrum. In this letter we report the observation of these spectral features in the case of strontium perturbed by argon. The qualitative agreement with the results of CBB [5] is quite good.

2. Theoretical considerations. The theory for intense field scattering from a Zeeman degenerate atom in a collisional environment has been given by CBB [5] in the impact approximation and steady-state limit. We use the notation of CBB throughout. The impact approximation restricts the validity of their results to pressures low enough such that the duration of a collision (τ_c) is small compared to the time between collisions (T_c). In addition the results are applicable for detunings from line center ($\omega_L - \omega_0 = \Delta$) small compared to the inverse of a collision duration, $\Delta < 1/\tau_c$. For the case of van der Waals broadening $1/\tau_c \approx 10^{12}\ \mathrm{s}^{-1}$, thus their results should be valid for detunings $\Delta \lesssim 5\ \mathrm{cm}^{-1}$. The theory, furthermore, is valid in the regime where the collision rates are independent of laser intensity, i.e., when $\Omega\tau_c \ll 1$, where Ω is the Rabi frequency.

Similarly the steady-state assumption restricts their results to laser pulse lengths (τ_p) large compared to the time scales associated with the system relaxation rates ($\tau_p \gg T_c, \tau_N$ where τ_N is the radiative lifetime). For buffer gas pressures of $\approx$10 Torr and again assuming a van der Waals interaction $T_c \approx \tau_N \approx 5$ ns.

For the case of interest here, a linearly polarized laser tuned near the Sr resonance line (a $J = 0$ to $J = 1$ transition) and perturbed by Ar (van der Waals broadening) CBB [5] predict a triplet in the scattered spectrum polarized parallel to the incident laser and a doublet in the scattered spectrum polarized perpendic-

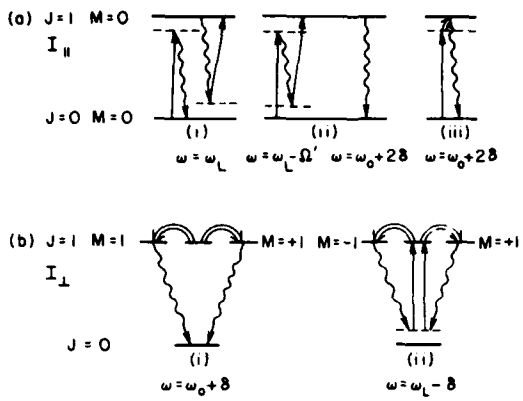

Fig. 1. Processes involved in the formation of the spectrum (the straight arrows represent absorption of a laser photon, the wavy arrows represent an emitted photon, and the double arrows represent a collisional process).

ular to the incident laser. In the parallel polarization (fig. 1a) the three peaks correspond to (i) Rayleigh scattering off the ground or $m_J = 0$ sublevel of the excited state, (ii) "three-photon" scattering followed by fluorescence, and (iii) collision-induced fluorescence from the excited $m_J = 0$ state. These features are exactly those associated with nonlinear scattering from an idealized two-state atom in the presence of collisions.

In the perpendicular polarization the two peaks correspond to collisional excitation of the $m_J = \pm 1$ sublevels of the excited state (fig. 1b) followed by (i) fluorescence to the ground state or (ii) an inverse Raman excitation of the $m_J = 0$ excited state.

In the experimental results reported here, neither the impact approximation nor the steady-state approximation is strictly valid. Thus detailed quantitative comparisons with the theory are not possible. However, the experimental results are in agreement with the qualitative conclusions of CBB [5].

3. Experimental apparatus. The experimental apparatus is basically the same as that used by CSR [4]. The apparatus consists of an N_2-pumped Hänsch-type dye laser tuned near the strontium resonance line ($6s^2\ {}^1S_0 - 6s6p\ {}^1P_1$ at 460.7 nm) and tightly focused into a stainless-steel crossed oven containing strontium vapor at ≈500°C–600°C and an argon buffer gas at pressures of ≈2 to 500 Torr. The laser power at the center of the oven was estimated to be ≈1 GW/cm^2. The scattered light was detected at 90° through the side arm of the oven, and focused onto the entrance slit of the monochromator. The signal was detected by a photomultiplier, fed into an rf shielded, gated, analog integrate and hold circuit and recorded on a chart recorder with a 2.2 s time constant. Further details of the apparatus can be found in CSR [4]. The major difference in our experiment was the addition of a glan-prism polarizer on the dye-laser output, an analyzing polarizer at the side window output of the oven, and a reference polarizer oriented at 45° and positioned before the entrance slit of the monochromator to remove the polarizing influence of the grating.

4. Experimental results; spectrum. Typical spectra are shown in fig. 2. These spectra were taken at a temperature of ≈600°C and argon pressures of 5, 50 and 500 Torr, respectively. The Sr density, as mea-

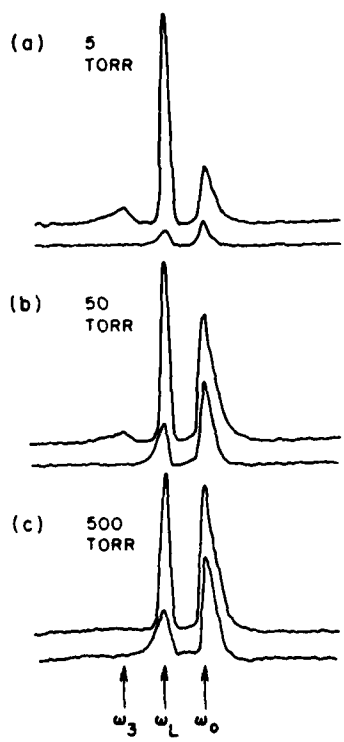

Fig. 2. Typical scattered light spectra (red detuning), at (a) 5 Torr, (b) 50 Torr and (c) 500 Torr. In each case the upper curve is the parallel polarization and the lower curve the perpendicular polarization. The arrows indicate the unshifted positions of the peaks.